



Electrochemical Kinetics and Sensing of Conjugated Dienes in Acetonitrile

A full thesis submitted in fulfillment of the requirements of the degree of
Magister Scientiae in the Department of Chemistry
University of the Western Cape.



Noluthando Myedi

Supervisor: Professor Emmanuel I Iwuoha

Co-Supervisor: Dr Tesfaye T Waryo

Keywords

Sensing

Conjugated dienes electrochemistry

Electrode kinetics

Organic phase

Gasoline

1.3-Cyclooctadiene

1.3-Cyclohexadiene

2-Methyl-1.3-butadiene

Trans-1.3-pentadiene

Platinum electrode

Glassy carbon electrode



Abstract

This thesis focuses on the electroanalysis of some dienes (2-methyl-1,3-butadiene (MBD), *trans*-1,3-pentadiene (PD), 1,3-cyclohexadiene (CHD) and 3-cyclooctadiene (COD)) found in gasoline and the development of simple electrochemical diene sensors. The detection of dienes in fuels is important as they readily polymerise and form gum in fuel tanks. The electroactivity of the dienes was studied with glassy carbon electrode (GCE) and Pt electrode in tetrabutylammonium perchlorate (TBAP)/acetonitrile solution. Polyaniline-polystyrene sulfonic acid (PANi-PSSA) composite films were electro-deposited or drop-coated on GCE, with and without gold nanoparticles (AuNPs) and characterized by cyclic voltammetry (CV), high resolution transmission electron microscopy (HRTEM) and ultraviolet-visible (UV-vis) spectroscopy. Both composite polymers were found to be of nanofibrillar structure, and the spherical gold nanoparticles were dispersed uniformly within the polymer. The dienes exhibited no redox peaks on GCE/PANi-PSSA and GCE/PANi-PSSA/AuNPs electrode systems from -1.0 V to +1.5 V, beyond which PANi would overoxidize and lose its electroactivity. Therefore, cyclic voltammetry and steady state amperometry of the four dienes (MBD, PD, CHD and COD) were studied with unmodified Pt and GCE electrodes. Subtractively normalised interfacial-fourier transform infra-red (SNIFTIR) spectroscopic studies of the dienes were performed with Pt electrode. SNIFTIR data showed that there was a definite electro-oxidation of 1,3-cyclohexadiene as electrode potential was changed from $E = 770$ mV to $E = 1638$ mV. Severe electrode fouling was observed when steady state amperometric detection of CHD, as a representative diene, was performed on Pt electrode. Randel-Sevcik analysis of the CVs of the dienes on Pt electrode gave diffusion coefficient (D_{ox}) values of 10.65 cm²/s, 9.55 cm²/s, 3.20 cm²/s and 3.96 cm²/s for CHD, COD, PD, and MBD, respectively. The corresponding detection limits ($3\sigma_{n-1}$) were 0.0106 M, 0.0111 M, 0.0109 M, and 0.0107 M.

Acknowledgements

First of all I would like to thank the all mighty for giving me the strength throughout my studies. I wish to express my earnest appreciation for my supervisor Professor Emmanuel I Iwuoha for his guidance and encouraging words, for believing in me while I was an undergraduate student and recognising that I possess a potential to go as far as PhD. My co-supervisor Dr Tesfaye Waryo with whom I have worked very closely has helped me to develop further my expertise in electrochemistry in particular and scientific thinking in general.

I would like to appreciate members of sensor lab research group for their valuable input and suggestion throughout my research. My friends who have shown interest in my studies and engaged me with useful conversations that add valuable input to my research are in no particular order Fanelwa, Busi, Babes, Njomo, Peter, Wale, Sibusiso and Billy. I would also like to thank my sister Zandile Myedi for the support and love she has shown me. My two little sisters Zinziswa and Nomthandazo Myedi for constantly showing me the love and patiently behind me in every step that I take. My two older brothers Mxolisi and Lwandile Myedi for always telling me there is no limit to reach your dreams while alive only death is the limit, I can be what I want to be.

Most of all I will like to acknowledge my late mother Thembeke Myedi who passed on 2006 before I could even obtain my bsc. She was a strong believer of education and knew that one day I will be educated. I want to thank her for her teachings and giving me necessary tools for survival in life. To thank my sister who passed away 2006 for showing me what is the meaning of education and opening doors for me to come to university, I will be forever grateful. I wish to thank my husband Mziwoxolo Mayedwa for his support in my academics and life in general, this has been possible because of him. He believes so much in me even if

I don't believe; he has been a positive role model in my life. I love you so much baby for being a breath of fresh air. Last but not least my beautiful daughter Buhle Mayedwa for being the reason I wake up each and every moment. She inspires me to be more than what I am and to also be a better mother on a daily basis. Finally I would like to acknowledge South African Nuclear Human Asset and Research Program /Department of Science and Technology for financial support.



Dedication

This Thesis is dedicated

To

My late mother and sister

Thembeke Julia Myedi and Nomaledi Myedi.



Declaration

I declare that *Electrochemical Kinetics and Sensing of Conjugated Dienes in Acetonitrile*

Is my own work that it has not been submitted for any degree or examination in any other university, and all sources I have used or quoted have been indicated and acknowledged by means of complete reference.



Noluthando Myedi

November 2011

Signed.....

List of abbreviations

CHD	- 1.3-Cyclohexadiene
COD	- 1.3-Cyclooctadiene
MDB	-2-Methyl-1.3-Butadiene
PD	-Trans-1.3-Pentadiene
AuNP	-Gold Nanoparticles
PANi	-Polyaniline
PANi/PSSA	-Polyaniline and Poly-Styrene Sulfonic Acid composite
PANi/PSSA/AuNPs	-Polyaniline, Poly-Styrene Sulfonic Acid and Gold Nanoparticles composite
CV	-Cyclic Voltammetry
UV/Vis	-Ultra-Violet Visible Spectroscopy
TEM	-Transmission Electron Microscopy
GCE	-Glassy Carbon Electrode
SNIFTIR	-Subtractive Normalized Interfacial Fourier Transmission Infra-Red

List of Figures

Figure	Title	Page
Figure 1:	Ultra-violet visible spectroscopy of gold nanoparticles.	58
Figure 2:	HRTEM for gold nanoparticles at 5 nm.	59
Figure 3:	EDX for gold nanoparticles.	60
Figure 4:	Interfacial polymerization of PANi, PANi/PSSA and PANi/PSSA/AuNP.	60
Figure 5:	10-cycle CV's of GCE modified with (a) PANi, (b) PANi/PSSA, (c) PANi/PSSA/AuNP recorded in acetonitrile containing 0.1 M TBAP at 100 mV/s.	61
Figure 6:	HRTEM for PANi nanofibers at 100 nm.	64
Figure 7:	HRTEM of PANi/PSSA at 50 nm.	64
Figure 8:	HRTEM of PANi/PSSA/AuNP at 100 nm.	65
Figure 9:	UV-vis absorption spectra of PANi, PANi/PSSA and PANi/PSSA/AuNP.	66
Figure 10:	10-cycle CV of electropolymerised PANi on GCE in 0.1 M H ₂ SO ₄ at 100 mV/s.	67
Figure 11:	10-cycle CV of electropolymerised PANi on GCE in acetonitrile containing 0.1 M TBAP at 100 mV/s.	68
Figure 12:	CV of 0.001 M ferrocene in acetonitrile containing 0.1 M TBAP on GCE.	69
Figure 13:	i_{p_a} and i_{p_c} versus $v^{1/2}$ of ferrocene.	70
Figure 14:	E_{p_a} , E_{p_c} , E^0 and $E_{p_a}-E_{p_c}$ versus the log scan rate of ferrocene.	70
Figure 15:	(a) Cyclic voltammogram of 1,3-cyclohexadiene in acetonitrile containing 0.1 M TBAP at 100 mV/s. (b) A plot of current versus	72

concentration of CHD.

- Figure 16:** (a) Cyclic voltammogram of 1.3-cyclooctadiene in acetonitrile containing 0.1 M TBAP at 100 mV/s. (b) A plot of current versus concentration of COD. 73
- Figure 17:** (a) Cyclic voltammogram of trans-1.3-pentadiene in acetonitrile and 0.1 M TBAP at 100 mV/s. (b) A plot of current versus concentration of PD. 74
- Figure 18:** (a) Cyclic voltammogram of 2-methyl-1.3-butadiene in acetonitrile containing 0.1 M TBAP at 100 mV/s. (b) A plot of current versus concentration of MBD. 75
- Figure 19:** Cyclic voltammogram of 1.3-cyclohexadiene on Pt working electrode in acetonitrile containing 0.1 M TBAP with variation of scan rate from 1000, 750, 500, 400, 300, 200, 150, 100, 75, 50, 25 and 20 mV/s. 77
- Figure 20:** (a) A plot of anodic peak potential versus log of scan rate of CHD. (b) A linear plot of anodic peak potential versus log scan rate for CHD. 78
- Figure 21:** (a) A plot of log of anodic peak current versus log scan rate for CHD. (b) A linear plot of log of anodic current versus log of scan rate for CHD. 79
- Figure 22:** (a) A plot of anodic peak current versus square root of scan rate of CHD. (b) A linear plot of anodic current versus square root of scan rate of CHD. 80
- Figure 23:** Cyclic voltammogram of 1.3-cyclooctadiene with Pt working electrode in acetonitrile containing 0.1 M TBAP with variation of scan rate from 1000, 750, 500, 400, 300, 200, 150, 100, 75, 50, 25 and 20 mV/s. 81
- Figure 24** (a) A plot of anodic peak potential versus log of scan rate of COD. 82

- (b) A linear plot of anodic peak potential versus log of scan rate of COD.
- Figure 25:** (a) A plot of log anodic peak current versus log of scan rate of COD. 83
(b) A linear plot of log anodic peak current versus log of scan rate of COD.
- Figure 26:** (a) A plot of anodic peak current versus square root of scan rate of COD. 84
(b) A linear plot of anodic peak current versus square root of scan rate of COD.
- Figure 27:** (a) Cyclic voltammogram of trans-1.3-pentadiene with a Pt working electrode in acetonitrile containing 0.1 M TBAP with variation of scan rate from 1000, 750, 500, 400, 300, 200, 150, 100, 75, 50, 25 and 20 mV/s. 85
- Figure 28:** (a) A plot of anodic peak potential versus log of scan rate of PD. (b) 86
A linear plot of anodic peak current versus log of scan rate of PD.
- Figure 29:** (a) A plot of log of anodic peak current versus log of scan rate of PD. 87
(b) A linear plot of log of anodic peak current versus log of scan rate of PD.
- Figure 30:** (a) A plot of anodic peak current versus square root of scan rate of PD. 88
(b) A linear plot of anodic peak current versus square root of scan rate of PD.
- Figure 31:** Cyclic voltammogram of 2-methyl-1.3-butadiene with a Pt working electrode in acetonitrile containing 0.1 M TBAP with variation of scan rate from 1000, 750, 500, 400, 300, 200, 150, 100, 75, 50, 25 and 20 mV/s. 89
- Figure 32:** (a) A plot of anodic peak potential versus log of scan rate of MBD. 90
(b) A linear plot of anodic peak potential versus log of scan rate of MBD.
- Figure 33:** (a) A plot of log of anodic peak current versus log of scan rate of 91

MBD. (b) A linear plot of log of anodic peak current versus log of scan rate of MBD.

Figure 34: (a) A plot of anodic peak current versus square root of scan rate of MBD. (b) A linear plot of anodic peak current versus square root of scan rate of MBD. 92

Figure 35 SNIFTIR of acetonitrile containing 0.1 M TBAP electrolyte with positive potential steps starting at $E_{\text{ref}2} = 0$ mV, $E_2 = 770$ mV; $E_{\text{ref}3} = 0$ mV, $E_3 = 1120$ mV; $E_{\text{ref}4} = 0$ mV, $E_4 = 1300$ mV; $E_{\text{ref}5} = 0$ mV, $E_5 = 1425$ mV; $E_{\text{ref}6} = 0$ mV, $E_6 = 1532$ mV; $E_{\text{ref}7} = 0$ mV, and $E_7 = 1638$ mV. 94

Figure 36: : SNIFTIR of 0.1M 1.3-cyclohexadiene in acetonitrile containing 0.1 M TBAP electrolyte with positive potential steps starting at $E_{\text{ref}2} = 0$ mV, $E_2 = 770$ mV; $E_{\text{ref}3} = 0$ mV, $E_3 = 1120$ mV; $E_{\text{ref}4} = 0$ mV, $E_4 = 1300$ mV; $E_{\text{ref}5} = 0$ mV, $E_5 = 1425$ mV; $E_{\text{ref}6} = 0$ mV, $E_6 = 1532$ mV; $E_{\text{ref}7} = 0$ mV and $E_7 = 1638$ mV. 95

Figure 37: (a) UV-vis spectroscopy of 1.3-cyclohexadiene variation of period. (b) UV-vis spectroscopy of 1.3-cyclooctadiene variation of period. (c) UV-vis spectroscopy of trans-1.3-pentadiene variation of period. (d) UV-vis spectroscopy 2- methyl-1.3-butadiene variation of period. 97

Figure 38: (a) CHD, (b) COD, (c) PD and (d) MBD cyclic voltammogram of 0.0025 M of conjugated dienes in acetonitrile containing 0.1 M TBAP at room temperature for interference studies with water in increments of 10, 20 and 50 μL . 99

Figure 39: A plot of current versus time response of organic sensor of 1.3-cyclohexadiene in acetonitrile containing 0.1 M TBAP. 101

List of schemes

Scheme 1 Fractional distillation of crude oil and end products.

Scheme 2: Research frame work.

Scheme 3: General representation of a sensor.

Scheme 4: Colour and size representation of gold nanoparticles.

Scheme 5: Polyaniline structure.

Scheme 6: Cyclic voltammogram where I_{p_c} and I_{p_a} show the cathodic and anodic peak current and E_{p_c} and E_{p_a} show cathodic and anodic peak potential for a reversible reaction.



List of Tables

Table 1: Theoretical yield characterization of PANi/PSSA/AuNP.

Table 2: Comparison of linear regression of GCE and Pt electrode of conjugated dienes.

Table 3: GCE kinetics of conjugated dienes (CHD, COD, PD and MBD).



Table of Contents

Keywords.....	ii
Abstract	iii
Acknowledgements.....	iv
Dedication.....	vi
Declaration.....	vii
List of abbreviations.....	viii
List of Figures.....	ix
List of schemes	xiii
List of Tables	xiv
CHAPTER ONE.....	1
INTRODUCTION	1
1 Introduction.....	2
1.1 Gasoline properties	2
1.2. Oil refinery operations.....	4
1.3. Mechanism of gum formation in cracked gasoline	5
1.4. Risks associated with conjugated dienes in gasoline	5
1.5. Rational and motivation	7
1.6. Objectives	8
1.7. Research frame work.....	9
1.8. References	10
CHAPTER TWO	12
LITERATURE REVIEW.....	12
2 Literature review.....	13
2.1 Introduction to sensors	13
2.1.1 Electrochemical sensor (liquid electrolyte)	13
2.1.2 Ion-selective electrodes	14
2.1.3 Solid electrode sensor.....	15
2.1.4 Piezoelectric sensors and optical sensors.....	15
2.1.5 Transducer	17
2.2. Conjugated dienes	17
2.2.1. Determination of conjugated dienes in gasoline	21

2.2.2. Voltammetric analysis of conjugated dienes in gasoline.....	23
2.3. Ferrocene.....	24
2.3.1. Ferrocene as an internal reference.....	25
2.4. Gold nanoparticles.....	27
2.5. Polyaniline.....	29
2.6.1. Reversible charge transfer.....	32
2.6.2. Irreversible charge transfer.....	33
2.6.3. Analytical techniques.....	34
2.6.4. Cyclic voltammetry.....	34
2.6.5. Subtractive normalized interfacial fourier transform infra-red spectroscopy.....	38
2.6.6. Ultra-violet visible spectroscopy.....	39
2.6.7. Transmission electron microscopy.....	40
8. References.....	42
CHAPTER THREE.....	50
EXPERIMENTAL METHODS.....	50
3. Experimental.....	51
3.1. Instrumentation.....	51
3.2. Reagents.....	51
3.3. Preliminary preparation of gold nanoparticles.....	52
3.4. First attempt synthesis of PANi, PANi/PSSA and PANi/PSSA/AuNP composites....	52
3.4.1. Interfacial chemical synthesis of PANi and its two composites.....	52
3.4.2. Voltammetric analysis.....	53
3.5. Second attempt electrosynthesis of PANi.....	53
3.5.1. Voltammetric analysis.....	53
3.6. Preparation of ferrocene.....	54
3.6.1. Voltammetric analysis.....	54
3.7. Preparation of COD, CHD, PD and MBD.....	55
3.7.1 Voltammetric analysis.....	55
3.7.1.1 Concentration variation.....	55
3.7.1.2 Scan rate variation.....	55
3.7.2 SNIFTIR.....	56
3.7.3. Ultra-violet visible spectroscopy.....	56

3.8. Interference studies.....	57
3.9. Steady state amperometry	57
CHAPTER FOUR.....	59
RESULTS AND DISCUSSION.....	59
4. Results and Discussion.....	60
4.1. Preliminary characterization of gold nanoparticles.....	60
4.1.1 Ultra-violet visible spectroscopy	60
4.1.2 High resolution transmission electron spectroscopy	61
4.2. Preliminary characterization of interfacial chemical synthesis of PANi/PSSA/AuNP....	63
4.2.1. Cyclic voltammetry	63
4.2.2. High resolution transmission electron spectroscopy	66
4.2.3. Ultra-violet visible spectroscopy.....	69
4.4. Preliminary electrosynthesised PANi.....	71
4.4.1. Cyclic voltammetry	71
4.5. Ferrocene	72
4.5.1 Cyclic voltammetry	73
4.6. Electrochemical characterization of conjugated dienes.....	76
4.6.1 Cyclic voltammetry.....	77
4.6.1.1 Concentration variation of conjugated dienes.....	77
4.6.1.2 Scan rate variation of conjugated dienes.	85
4.7. SNIFTIR	110
4.8. Ultra-violet visible spectroscopy.....	112
4.9. Interference studies.....	115
4.10 Steady state amperometry	118
4.11. References.....	120
CHAPTER FIVE	122
CONCLUSIONS AND RECOMMENDATIONS	122
5.1. Conclusions.....	123
5.2. Recommendation.....	125

CHAPTER ONE

INTRODUCTION



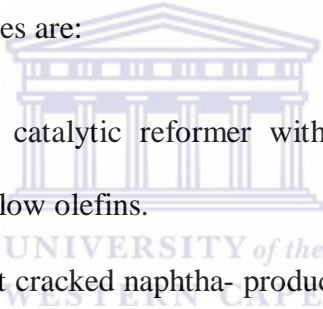
UNIVERSITY *of the*
WESTERN CAPE

1 Introduction

1.1 Gasoline properties

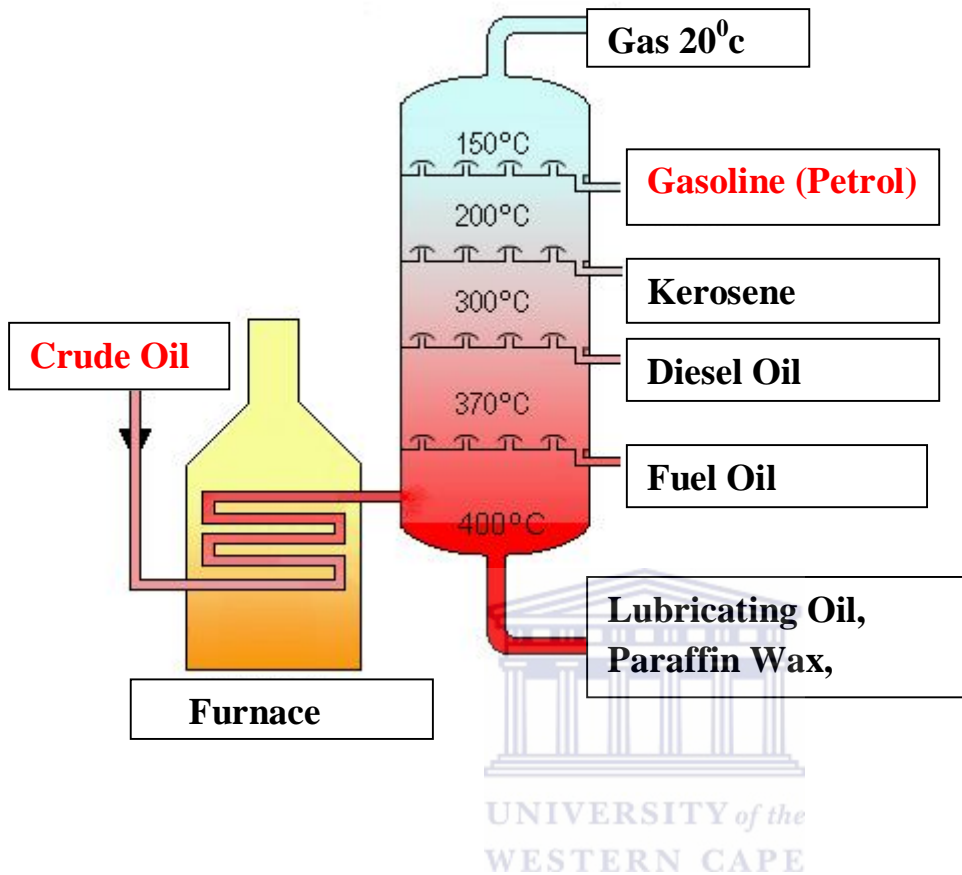
Gasoline or petrol is produced from crude oil via fractional distillation in a temperature range of 30-220 °C, which is primarily used as a fuel in internal combustion engines. The composition of gasoline varies widely depending on the crude oil used, refinery processes used, and overall balance of product demand and product specification. It is a volatile, inflammable mixture composed of paraffin, naphtha, olefins, di-olefins and aromatic hydrocarbons (C4-C12). Gasoline contains trace amounts of sulphur, atmospheric oxygen and traces of nitrogen [1].

There are refinery processes used to produce different commercial gasoline with different characteristics, some important ones are:

- 
- Reformate-produced in a catalytic reformer with a high octane rating and high aromatic content and very low olefins.
 - Cat cracked gasoline or cat cracked naphtha- produced from a catalytic cracker with a moderate octane rating, high olefins (alkene) content and moderate aromatic level.
 - Hydrocrackate (heavy, mid, and light) produced from a hydrocracker, with medium to low octane rating and moderate aromatic levels.
 - Virgin or straight-run naphtha, directly from crude oil with low octane rating, low aromatics (depending on the grade of crude oil), some naphthenes (cycloalkanes) and no olefins (alkenes).
 - Alkylate, produced in an alkylation unit, with a high octane rating and which is pure paraffin (alkane), mainly branched chains.
 - Isomerase (various names), which is obtained by isomerising the pentane and hexane in light virgin naphthas to yield their higher octane isomers [2].

Hydrocarbons present in gasoline react with atmospheric oxygen during storage, these results in promoting changes in their physical and chemical characteristics. The primary oxidation reaction products continue to react and form non-volatile molecules with high molar mass and are commonly called gum [3]. Stability of a gasoline is commonly understood to be the length of time a gasoline will remain stable in storage before it forms objectionable amounts of deterioration products such as gum and peroxides. Cracked gasoline is much more stable than other gasoline obtained by other refinery processes. Studies were made on cracked gasoline and pure hydrocarbons by measuring the rate of gum formation and peroxide formation on aging gasoline gum appears to originate from oxidation of both reactive hydrocarbons and gasoline impurities (non-hydrocarbons). Products that formed gum were found to be more difficult to inhibit against oxidation than those formed by peroxides. The gum stability of cracked gasoline was improved by treatment, inhibition or dilution with straight-run components, boiling range was found to be important. Metal catalysts reduced gum stability but were found capable of complete inactivation by metal deactivators. Factors influencing antioxidant and deactivator behaviour are of importance. Activation energies of gum-formation reactions were altered by antioxidants and metal catalysts [4]. Gum formation affects the fuel system as it will deposit along the vehicle fuel system, from the tank to the combustion chamber. Overtime deposition causes problems such as emission of gases (CO and NO), reduced acceleration, power loss, increased fuel consumption and choking [5].

1.2. Oil refinery operations

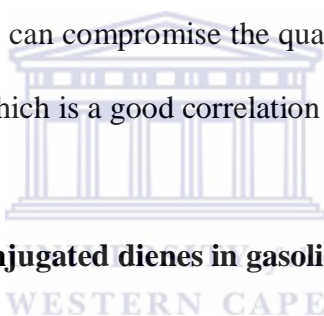


Scheme 1 Fractional distillation of crude oil and end products (<http://svr225.stepx.com:3388/oil-refinery>{published on Saturday, May 10th 2008: Edited by Kid Pighadshy, Perth, Australia}).

Raw or unprocessed crude oil is not useful in the form it comes in out of the ground or in its original form. Low viscosity, low sulfur oil has been used directly as a burner fuel for steam vessel propulsion, the lighter elements form explosive vapours in the fuel tank and it is quite dangerous. This leads to crude oil been separated in fractions as illusted in the scheme 1. The fractions that are found at the top of the column have a lower boiling points than the fractions found at the bottom part of the column. The heavy bottom fractions are often cracked into lighter, more useful products. All of the fractions are processed further in other refining units.

1.3. Mechanism of gum formation in cracked gasoline

The reaction that takes place when cracked gasoline is stored is of a complex nature when in contact with air. Several studies have been done and the first evidence of any change that have been detected is the formation of peroxidic products. Concerning this issue at hand the commercial standpoint, at least the final step in deterioration is the formation of gum. Beside these two products, aldehydic and acidic products have been reported. No one has conclusively shown what relationship exists between the peroxides, aldehydes and acids formed and what part they play in the gum forming process [6]. During catalytic cracking or heavy petroleum fractions olefins and diolefins can be formed. The conjugated dienes content are very important factor towards the quality of petroleum product formed in the oil industry. The presence of these compounds can compromise the quality of the product formed because of their tendency to polymerise which is a good correlation with gum formation [7].

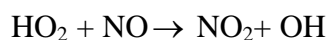
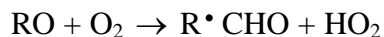
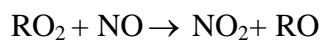
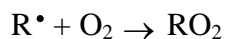


1.4. Risks associated with conjugated dienes in gasoline

Nitrogen dioxide has a great impact on human health at increased level of concentrations and it is one of the most significant urban air pollutants. The main effect is respiratory problems, inflames the lining of the lungs, and it can reduce immunity to lung infections. This can cause problems such as wheezing, coughing, colds, flu and bronchitis. The main source for the emission of NO_x in urban areas is vehicles in which the proportion of NO_2 is normally less than 10% [8].

Atkinson and co-workers [9] reported that NO_2 is reactive towards conjugated dienes and OH radicals are formed upon addition of NO to the reacting NO_2 alkene air system.





The hydroxyl radical which has been generated can later react with other reactive hydrocarbons to result in further production of peroxy radical which oxidise further NO to NO₂. This reaction provides a pathway to enhance free radical-mediated oxidation of NO to NO₂ in the atmosphere in the absence of sunlight driven initiation reaction. A rapid addition reaction of NO₂ with several conjugated dienes has been observed in the laboratory studies. Oxidation of NO to NO₂ in highly polluted urban air was investigated if whether the dienes-promoted reactions are able to explain the rate enhancement observed in the atmosphere. RO₂ + NO → NO₂ + RO are the main pathway for alkylperoxy radicals reacting with NO, although organic nitrate formation is an alternative route like RO₂ + NO → RO NO₂. Gasoline contains a large number of chemicals, some of them are carcinogenic. Among the chemicals found in gasoline to which human are exposed is 1,3-butadiene, 2-methyl-2-butadiene (conjugated dienes) benzene (aromatics) etc [10].

1.5. Rational and motivation

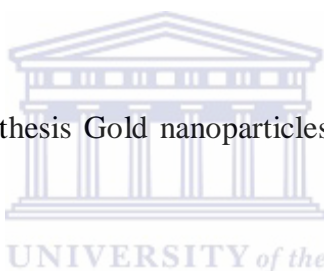
In consideration of the risks associated with the presence of conjugated dienes in gasoline as stated above it leaves no doubt that the levels of conjugated dienes are very important to monitor. Apart from the oil industry being in benefit with the findings it is also essential that the consumers who use the product on daily basis be informed how much levels of conjugated dienes are present in gasoline. Several analytical tools have been reported in the analysis of level of conjugated dienes. These analytical tools include UOP-326 method (maleic anhydride method), voltammetric method, gas chromatography method, high performance liquid chromatography method, supercritical fluid chromatography method, nuclear magnetic resonance method, spectrophotometric methods and ultraviolet and near infrared spectroscopy. UOP-326 method, voltammetric and GC/MS methods presented recovery values in the range of 60-90 %, 83-109 % and 90-104 % respectively. The UOP-326 method presented low recovery values which indicated that the method may present incomplete reactions with some specific conjugated dienes. Another limitation of the UOP-326 is the great analysis time (6-8 h), voltammetric (45-60 min), CG/MS (3 h) , SFC-UV (10 min), HPLC (10 min), spectrophotometric(2-4 h) and NIR method. This long analysis time of UOP-326 method implies a high man/hour ratio with consequently high costs. Considering sample aspect, less sample volume and manipulation are necessary in the voltammetric, CG/MS, SFC-UV, HPLC, spectrometric, NMR and NIR methods [11]. Voltammetric methods presented fewer limitations and some important advantage that makes it suitable to be used in the determination of conjugated dienes in Brazilian commercial gasoline sample. In this study electrochemical method in a form of a nano sensor will be developed for quantitative evaluation of conjugated dienes in gasoline. An existing knowledge of several methods being used including voltammetric methods for the study of conjugated dienes in gasoline provide and understanding behind the principle of electrochemical method, this will

be very useful on how to improve the voltammetric methods used by modification and consideration of different suitable electrodes [12].

1.6. Objectives

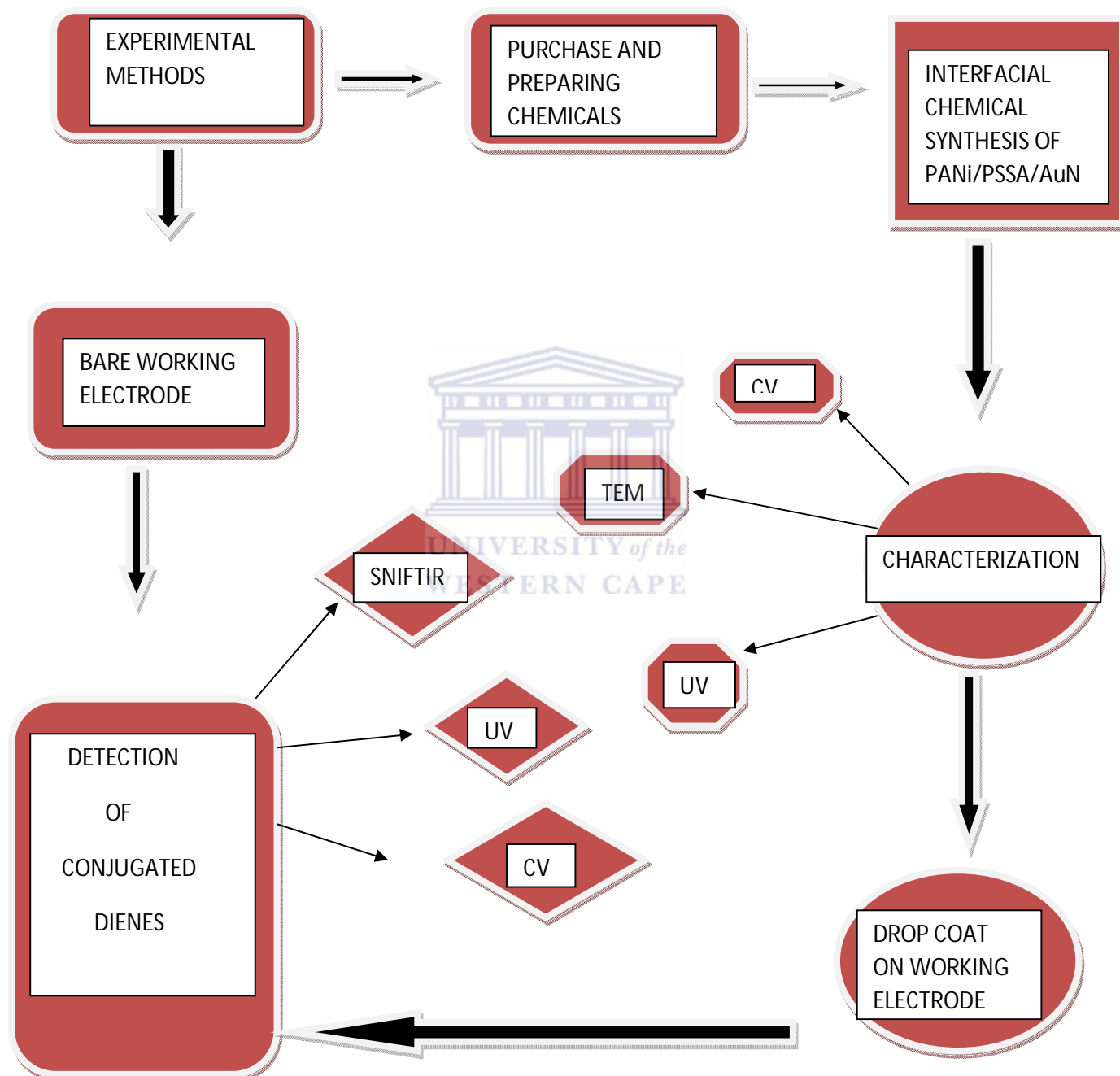
The main hypothesis of the study is to develop a sensor for the detection of conjugated dienes in gasoline. The project will investigate electrochemical interactions of 1,3-pentadiene, 2-methyl-1,3-butadiene, 1,3-cyclohexadiene and cyclooctadiene in an organic medium which will be mediated by a Pt electrode.

- To chemically synthesis Polyaniline (PANi) and characterise by TEM and UV spectroscopy.
- To chemically synthesis Gold nanoparticles (AuNP) and characterise by UV and TEM.
- To chemically synthesis two composites polyaniline and poly-styrene sulfonic acid (PANi/PSSA) composite and PANi/PSSA/AuNP composite.
- To demonstrate electrochemical response of conjugated dienes on a bare Pt electrode
- Study the kinetics of the electrode in an organic medium.
- To immobilize PANi and its two composites on a Pt electrode for the electrochemical detection of conjugated dienes in an organic medium
- To model the amperometric and kinetic response of the sensor.



1.7. Research frame work

In connection to the objectives, the framework of the study is as follows:



Scheme 2: Research frame work.

1.8. References

- [1] Oliveira FO, Teixeira LSG, Araujo MCU, Korn M. Screening analysis to detect adulterations in Brazilian gasoline samples using distillation curves. *Fuel*. 2004, 83(7-8): 917–923.
- [2] Gao J, Jiang D, Huang Z. Spray properties of alternative fuel: A comparative analysis of ethanol-gasoline blends and gasoline. *Fuel*. 2007, 86(10-11): 1645-1650.
- [3] Nagpal JM, Joshi GC, Singh J, Kumar K. Studies on the nature of gum formed in cracked naphthas. *Oxidation Communications*. 1998, 21(4): 468–477.
- [4] Walters EL, Minor HB, Yabroff DL. Chemistry of gum formation in cracked gasoline. Shell Development Company. 1949, 41(2): 1723-1728.
- [5] Nagpal JM, Joshi GC, Singh J. Gum forming olefinic precursors in motor gasoline. A model compound study. *Fuel Science and Technology International*. 1994, 12(6): 873–894.
- [6] Dryer CG, Lowry CD, JR, Morrell JC, Gustav E. Mechanism of gum formation in cracked gasoline formation of peroxide, aldehyde and acid in storage. Universal Oil Company, Chicago. 1934, 26(8): 885-888.
- [7] Velasco-Arjona A, de Castro MDL. Fully robotic method for the determination of diene value in several types of fuels. *Analyst*. 1998, 123(9): 1867-1869.
- [8] Harrison RM, Shi JP. Source of nitrogen dioxide in winter smog episodes. The 5th international symposium: highway and urban pollution. *Science and Total Environment*. 1996, 189(190): 391-399.
- [9] Atkinson R, Aschmann SM, Winer AM, Pitts JN Jr. Gas phase reaction of NO₂ with alkenes and dialkenes. *International Journal of Chemical Kinetics*. 1984, 16(6): 697-706.

[10] Mehlman AM. Dangerous and cancer-causing properties of products and chemicals in the oil refining and petrochemical industry. Health effects of motor fuel: carcinogenicity of gasoline –scientific update. *Environmental Research*. 1992, 59(1): 238-249.

[11] Andrade DF, Fernandes DR, Miranda JL. Methods for the determination of conjugated dienes in petroleum products: A review. *Fuel*. 2010, 89(8): 1798-1805.

[12] Andrade DF, Figueiredo E, D'Aguiar P, Troise MHF, Tristao ML, D'Elia E, Proposal of voltammetric methods for the determination of conjugated dienes in Brazilian naphtha. *Fuel*. 2006, 85(17-18): 2578-2585.



CHAPTER TWO

LITERATURE REVIEW



UNIVERSITY *of the*
WESTERN CAPE

2 Literature review

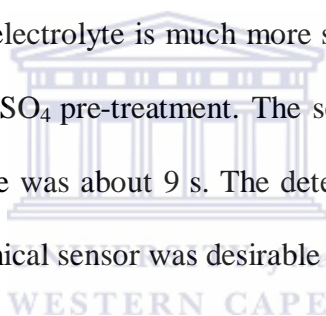
2.1 Introduction to sensors

Sensors are separated into chemical and physical sensors and there are those that cannot be easily classified like relative humidity sensors. Sensors are deliberated along the topic of actuators. Chemical sensors have a chemical or molecular target to be measured. Chemical sensors have been widely researched and used in applications such as critical care, safety, industrial hygiene, process controls, product quality control, human comfort control, emissions monitoring, automotive, clinical diagnostic, home safety alarms and more recently homeland security. Chemical sensor are known to be both economic and social beneficial, biosensors are defined as sensors that use biomolecule or structures to measure an element of biological implication or bioactivity. Biosensors target the biomolecule of interest for measurement or detection. The biosensors can be considered as a subset of chemical sensor because the transduction method or sensor platforms are the same as that of the chemical sensor. The signal from a sensor is an electronic like current, voltage or impedance/conductance change caused by changing analyte composition. Chemical sensors contain a physical transducer and a chemical sensitive layer [1].

2.1.1 Electrochemical sensor (liquid electrolyte)

There are two major classes that use liquid electrolyte, amperometric and potentiometric sensors. The earliest example of an amperometric gas sensor which is 40 years old is the Clark oxygen sensor used for the analysis of oxygen in the blood. The amperometric sensor produces current signal which is related to the concentration of the analyte by Faraday's law and the law of mass transport. The amperometric gas sensor with liquid electrolyte operates in a region where the mass transport is limiting and therefore has a linear response with concentration. This sensor has now been developed in many different geometries and for a

broad range of analytes such as CO, nitrogen oxide H₂S, O₂, glucose, unique gases like hydrazine and many more vapours [2]. The amperometric gas sensor has an advantage over many other kinds of sensor because it combines small size, low power, high sensitivity as well as relatively low price, making it ideal for portable toxic and explosive gas instrument. Wang and co-workers developed an electrochemical sensor which was composed of two gold plated iron electrodes, was developed to distinguish two stroke engine oil from four stroke engine oils. The sensor demonstrated its capabilities in detecting metallo-organic detergents and the sensor also had the potential to distinguish between the two strokes with different composition of detergents [3]. Chunbo Yu and co-workers reported for the first time that the performance of the electrochemical H₂S sensor with the nafion membrane pre-treated with concentrated H₂SO₄ as the solid electrolyte is much more stable than that for the sensor with the nafion membrane without H₂SO₄ pre-treatment. The sensitivity of the sensor was about 2.92 μA/ ppm. The response time was about 9 s. The detection limit is was about 0.1 ppm. Therefore the kind of electrochemical sensor was desirable for the practical applications [4].



2.1.2 Ion-selective electrodes

Ion selective electrodes belong to potentiometric chemical sensor group and are mostly based on the measurement of the interfacial potential at an electrode surface caused by a selective ion exchange reaction. The well-known glass pH electrode is a typical ion exchange electrode; this type of sensor has a long history [5]. The design of an ion selective membrane is the key to the development of this type of sensor. A lot of literature is found on ionophore-based potentiometric sensors and a number of improvements to this kind of device [6]. As opposed to the amperometric sensor, potentiometric sensors use the voltage at zero current that is typical representative of an equilibrium electrochemical process. These voltages arise

because an electrochemical reaction can occur at wires or at membrane in solid, liquid or condensed phases. Due to the signal representation is at equilibrium, the eventual signal is less influenced by mass transport characteristics or sensor dimension and provides a reading reflecting the local equilibrium conditions. The generated signal is known as an electromotive force that depends on the activity of the analyte which is described by Nernst's equation. The response time depends mostly on how fast the equilibrium can be established at the sensor interface.

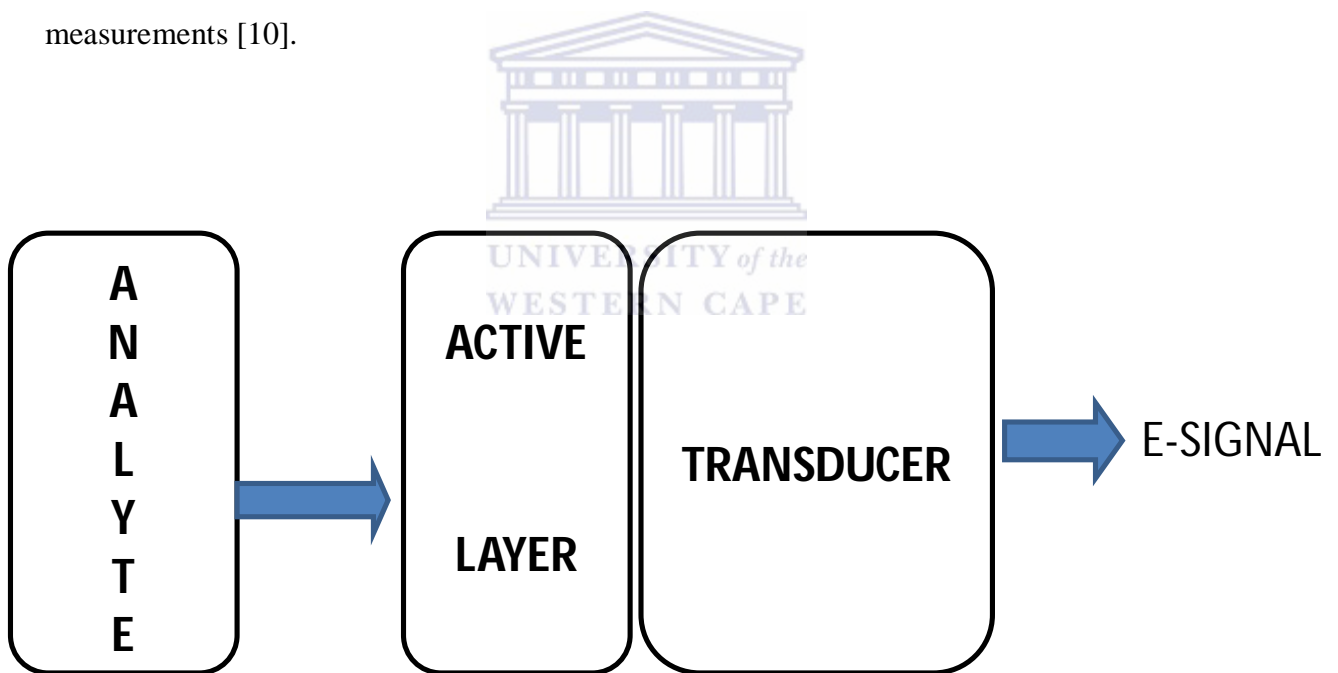
2.1.3 Solid electrode sensor

Where a solid electrode is used to replace a liquid electrode in an electrochemical sensor, a solid electrolyte sensor can be constructed. The design of solid electrolyte sensor is designed to operate at high temperature using either potentiometric or amperometric mode. Over the past 17 years two potentiometric designs evolved: surface modified gas sensor and mixed potential gas sensor [7, 8]. During mixed potential sensor design more than one electrochemical reaction takes place at the electrodes so that a mixed potential is established by competing reactions.

2.1.4 Piezoelectric sensors and optical sensors

The resonating frequency of the piezoelectric solid is used to measure the audio which is observing for a point of maximum admittance between two electrodes. The mass loading, temperature, density, viscosity and pressure are functions of resonant frequency. The main challenge is to measure only the mass that is proportional to the analyte concentration while other variables are kept constant. Audio gas sensor requires the crystal to be coated with an active layer, often a polymer or a non-volatile coating which performs a function similar to

the stationary phase in gas chromatograph [9]. Properties in coating causes changes in attenuation in the audio wave there are different types of examples on this particular sensor discussed. The sensor design frequently uses waveguide or optical fibre for convenient construction. The interaction of the analyte with the light is when the analyte is placed at the interface of the fibre and a coating. On situations where the conditions are accurate absorption or emission, the intensity and wavelength of the characteristic light provide the opportunity to obtain an analytical signal for quantitative or qualitative analysis. Optical techniques may often depend upon the coating therefore derive many analytical properties such as sensitivity, selectivity and stability from the choice of coating. The optical platforms are frequently choice for biosensors because of their sensitivity that accompany fluorescence measurements [10].



Scheme 3: General representation of a sensor.

2.1.5 Transducer

It is a device that converts one part of energy to another, the conversion can be electrical, electro mechanical, to other form of energy which will be found in the output. Most sensors use the transducer systems which are used to measure several features for instance the monitoring of the conductivity of conducting polymers or metal oxides, monitoring mass changes or optical absorption of polymer or monitoring current changes of electrochemical sensor. There are limitations in using one transducer principle obviously leads to limited resolution power of such sensor selection. Limited transducer principle translates into limited class of materials with their characteristic signal transfer mechanisms through only one transducer [11].

2.2. Conjugated dienes

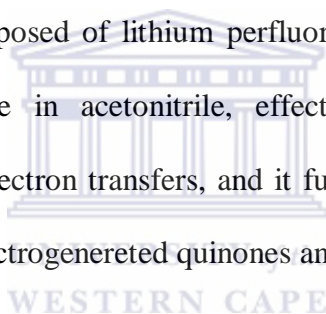
In organic chemistry a diene is known as a hydrocarbon that contains two carbon double bonds, where as a conjugated diene is a functional group with the following general formula C_nH_{2n-2} . Dienes are divided in to three different classes namely: cumulated diene, unconjugated diene and conjugated diene. Cumulated diene are those where a double bond shares a common atom, unconjugated dienes are those where a double bond is separated by two or single bond. Conjugated dienes contain two carbon-carbon double bond separated by one carbon-carbon single bond, where a set of adjacent sp^2 -hybridized carbon atoms which the interaction of p atomic orbitals causes the delocalization of pi (Π) electron system. The delocalized pi (Π) electron system lend them self to a unique stability and reactivity exhibited the molecule which process them. Zhang and co-workers where interested in the reactivity of more challenging dienes for the utilization of CO_2 and the product distribution law influenced by multiple substitution of diene structures. The communication was devoted to the electro analytical, synthetic and mechanical aspects of eletrocarboxylation of three conjugated dienes

(methyl sorbate, 3-methyl-1,3-pentadiene and 2,5-dimethyl-2,4-hexadiene) with CO₂ under mild conditions. The electrochemical behaviour of the conjugated dienes was monitored by cyclic voltammetry; the voltammetric and electrolytic study involved in the electro reductive carboxylation of multi-substituted aliphatic conjugated diene was successfully conducted. With methyl sorbate as the modal compound, acceptable yields of carboxylation and dimerization were achieved, which were influenced by various reaction conditions such as the supporting electrolyte, cathode nature, current density, charge passed and temperature. A correlation was first established between distinct electronic effects of the dienes and the electrochemical characteristics of their reduction and the distribution law of target products [12].

Cannes and co-workers reported on the electro analytical determination of the successive electron transfer/chemical steps involved in the nickel-catalysed electro synthesis of conjugated dienes from alkenyl halides in DMF. Two catalytic sequences were proposed, depending on the potential applied. The first mechanism was shown to proceed through oxidative addition of the vinyl halide to electro generated Ni⁰ and vinyl-Ni^I species. The diene was obtained by reductive elimination from a Ni^{III} species. An alternative coupling mechanism was proposed which involved both oxidative addition of RX on Ni⁰ to RNiX. The influence of various parameters on the rates was discussed, such as the nature of both the halide and the stereoisomer used, as well as the coordination environment of the nickel complex [13]. The cathodic reduction of the carbon-carbon double bond is a process of valuable theoretical and technological interest, which has been investigated extensively with several electrochemical techniques by a variety of researchers since the polarographic studies in the 1940s and 1950s by Wawzonek and Hoijtink [14, 15]. Farnia and co-workers reported on the electrochemical reduction of 1, 2, 3, 4-tetraphenyl-1,3-cyclopentadiene and 1, 2, 3, 4,

5-pentaphenyl-1.3-cyclopentadiene which was investigated in DMF. At low temperatures (≤ -30 °C) and under anhydrous conditions cyclic voltammetry experiments indicate that both substrates are reducible in two successive, chemically reversible, one-electron steps, affording the corresponding radical anions and dianions. More complex voltammetric behaviour was detected at higher temperatures, when the radical anions were protonated by the substrate itself, giving rise, via the so called 'father son' self-protonation process, to further reducible compounds generating additional basic intermediates. In exhaustive electrolyses, 1/3 of the starting substrate was converted into dihydroreduction products and 2/3 into its conjugated bases. The quantitative formation of the dihydroreduction products were observed when exhaustive electrolyses are carried out in the presence of phenol, which acts as the proton donor instead of the substrate. Under voltammetric conditions evidence of deprotonation of the substrate by the phenoxide anions thus generated was obtained, which indicated the occurrence of 'indirect father-son' self-protonation process, which took place since phenol was kinetically more acidic, but thermodynamically less acidic than the substrate itself. The mechanisms of decay of the radical anion were proposed on the basis of the comparison of the experimental and simulated voltammetric data; this approach allowed also the determination of the characteristic kinetic rate constant, some which are strongly dependent on the structure of the substrate and of the importance of the homoconjugated reactions involving phenol and phenoxide anions. The stereochemistry of the dihydroreduction process and the voltammetric behaviour of the corresponding products are considered also, even in relation to the voltammetric behaviour of the starting substrate [16]. Bergstad and co-workers reported on aerobic oxidation of conjugated dienes using a catalytic palladium (II)-quinone-heteropolyacid system for electron transfer from organic substrates to molecular oxygen. The heteropolyacid $H_5 PMo_{10}V_2O_{40} \cdot 3H_2O$ was found to be an efficient oxygen activating agent in palladium-catalyzed reactions. Aerobic 1.4-oxidation of

conjugated diene was carried out by employing a triple catalytic system consisting of palladium-quinone-heteropolyacid. With the system a mild electron transfer from the organic substrate to molecular oxygen occurs. 1,4-diacyloxylation and 1,4-dialkoxylation were studied in some detail. Some advantages of the heteropolyacid over previously employed metal macrocycles had high stability, easy access to an active catalyst and simpler workup procedure [17]. The potential of the electrochemical method has been highlighted by the general way in which electrochemistry can be used to generate reactive intermediates to construct a wide variety of products under mild conditions. Furthermore, the electro synthesis has been known as an eco-friendly, convenient way to oxidize/reduce organic compounds without using any oxidizing or reducing reagent. Chiba and co-workers reported on a micellar electrolytic reaction system composed of lithium perfluorooctanesulfonate (LiFOS), highly concentrated lithium perchlorate in acetonitrile, effectively dispersed slightly soluble compounds to promote anodic electron transfers, and it further accelerated the formation of desired cycloadducts between electrogenerated quinones and dienes [18].



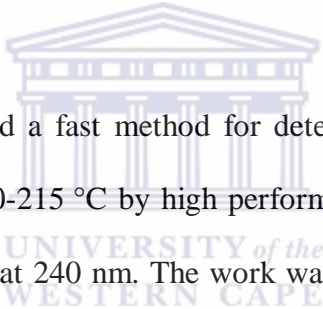
Stroebel and co-workers reported on the generation of the radical anion of 1,3-cyclohexadiene by sodium-ammonia reduction of the diene. There were different methods employed which are; by varying the composition of the medium and observation of the variation in product composition it was possible to determine. The various intermediates formed and assessed quantitatively, the partitioning of the overall reaction of anion among its several competitive modes. This included the protonation to 3-cyclohexenyl radical followed by its dimerization or further reduction, conjugated addition of the radical anion to substrate and coupling of 3-cyclohexenyl radical with the parent radical anion. This was made possible by the reduction of tricyclo-[6.4.0.0^{2,7}] dodeca-3,11: diene its ring-opened radical anion and observing the ratio of isomeric dihydro products so since they are common to the

reductive dimerization of 1,3-cyclohexadiene. A superficial examination of the reduction of 1,3-cyclooctadiene showed that its radical anion is significantly more basic than that of 1,3-cyclohexadiene and that the cyclooctadiene has a significantly smaller electron affinity than cyclohexadiene [19].

2.2.1. Determination of conjugated dienes in gasoline

The amount of conjugated dienes present in the pyrolysis gasoline and during distillation and hydrogenation of some petroleum fraction can affect the quality of product. As it has been highlighted in the introductions some of those problems caused by conjugated dienes, the gum formation is one of them which deposit in the fuel system of the vehicle. Several methods have been employed to address the problem. There are some advantages and also some major short coming of these methods employed. The methods of analysis include both chemical and instrumental techniques. The UOP-326 method (maleic anhydride method) the method was developed around 1965 by the universal oil product (UOP) and a lot of countries around the world still depend on the method for the determination of conjugated dienes in gasoline. The temperature at which conjugated dienes and mixtures of hydrocarbon are determined is $b.p \geq 204 \text{ }^{\circ}\text{C}$ using UOP-326. It is a quantitative method which uses maleic anhydride as a derivatization agent [20]. The way in which the diene content is measured is through the amount of maleic anhydride consumed in reacting with the dienes which is the diels-alder reaction in a complex mixture heated in a reflux in toluene for 3 hours [21]. The diels-alder reaction is an extremely useful reaction which results in the formation of carbocyclic or heterocyclic compounds of one or more rings. Over the years the reaction received considerable synthetic and theoretical attention as highlighted above. Under the conditions of this reaction a simple conjugated diene should give rise to 1:1 adduct and the

styrene-type compounds and its derives to a copolymer (1:1). The unreacted part of the maleic anhydride is hydrolysed at the end of the reaction (after several hours) and the amount of maleic acid formed is then determined by titration [22]. More over this method have some limitations i.e. the extremely long analysis time that implies a high man/hour ratio; the incomplete reaction with some conjugated some conjugated dienes, the large relative standard deviation and interference of some compounds such as ethanol, an important additive used in commercial gasoline particularly in Brazil [23]. The interference is caused by the esterification reaction between maleic anhydride and primary alcohol [24, 25]. Amongst the method used for analysis high performance liquid chromatography method has been widely used and tried for the estimation of saturates aromatics and olefins in petroleum samples [26, 27].



Ghazvini and co-workers reported a fast method for determination of conjugated diene in gasoline with boiling points of 30-215 °C by high performance liquid chromatography with ultraviolet detection (HPLC-UV) at 240 nm. The work was based on the standard IP 391/90 method that measures the diolefins and conjugated dienes via their light absorption at 240 nm. Their concentration is approximately quantified by the comparison of gasoline peak areas with chromatograms of the quantification and possible limitation of 1,3-cycloheptadiene as calibration compounds. The HPLC-UV results were compared with GC analyses. For more concentrated samples the results were greater for HPLC method than that of GC. What was more interesting a good correlation was possible to be done between HPLC method and the standard UOP-326 [28]. Although HPLC has the advantages of high degree of separation efficiency and short analysis time there are also some limitations, predominantly concerning the analysis of olefins from high boiling materials in the presence of other hydrocarbon compounds. The main problems are due to the detector response

limitations for different chemical classes resulting in to complex procedure for quantification. As an example unusual mobile phase (e.g. freon, perfluorocarbons), back-flush valves, multiple columns and columns switching, special columns (e.g. Ag⁺ treated) or unusual detectors (e.g. dielectric detectors) are necessary to be used. The choice of the method to be used for the determination of conjugated dienes depends on the purpose of the analysis, the accuracy needed and the nature of the sample as well as on the available laboratory equipment's and the most important the total cost of the analysis. In the case where equipment's are not available in the laboratory the only method that can be employed is the standard UOP-326 method. Even though they are some short coming, it should be emphasized it can be employed in samples without alcohol with the awareness of possible error.



2.2.2. Voltammetric analysis of conjugated dienes in gasoline

The voltammetric method is preferable for the analysis of conjugated dienes basically for two reasons: its lower analysis time and its precision. This determination is possible due to the electroactivity of the conjugated dienes in the -2.3 V_{SCE} to -2.9 V_{SCE} potential range (SCE= saturated calomel electrode) [29]. In this potential range the reduction reaction involving diaryl sulphides and polycyclic aromatics also occur, but they are not present not present in the studied samples due to their high ebullition points. During the electrode process, independently of the structure of the conjugated diene, one mol of double conjugated bonds always react with two moles of electrons in the voltammetric reduction [30]. Therefore it is possible to determine the number of moles of conjugated double bonds and the molar concentration of the conjugated diene by the analysis of the voltammetric wave height or of the voltammetric peak area. As neither the non-conjugated dienes nor the alcohols are

electroactive in the potential range considered the above. The proposed voltammetric analysis is a potential method for the determination of conjugated dienes in Brazilian commercial gasoline which could not be directly analysed by UOP-326 method. The comparisons with other techniques discussed above voltammetric methods presented fewer limitations and some important advantages that make it suitable to be used in the determination of conjugated dienes [31].

2.3. Ferrocene

Ferrocene namely bis-cyclopentadienyl iron (III) is a molecule with a sandwich-type structure in which the iron atom is sandwiched between two five membered carbon rings. It has been proposed that the oxidation of Ferrocene $\text{Fe}(\text{C}_2\text{H}_5)_2$ to ferrocenium cation $\text{Fe}(\text{C}_2\text{H}_5)_2^+$ is a standard one electron transfer reversible process because the rate of electron transfer is incredibly fast [32]. Consequently the redox system $\text{Fe}(\text{C}_2\text{H}_5)_2^+/\text{Fe}(\text{C}_2\text{H}_5)_2$ has received considerable attention in electrochemistry because it can be used for instrumental and reference potential calibrations in organic media [33]. During the last 30 years numerous electrochemical studies have been employed for the evaluation of both kinetic and thermodynamic parameters of the $\text{Fe}(\text{C}_2\text{H}_5)_2^+/\text{Fe}(\text{C}_2\text{H}_5)_2$ couple in organic solvents [34]. Crooks and Bard reported in acetonitrile at the temperature range from 298.15 to 573.15 K, in all the other cases the investigation has been done at the room temperature as a result studies of Ferrocene at a large temperature are very scarce [35]. Nikos reported ferrocene studied in non-aqueous solvents over a certain temperature range using the technique cyclic voltammetry. The anodic (E_{pa}) and the cathodic (E_{pc}) peak potential as well as the corresponding anodic (I_{pa}) and cathodic (I_{pc}) peak currents were obtained at different scan rates. The half-wave potential ($E_{1/2}$) of ferrocene and ferrocenium in the investigated medium

was evaluated. The diffusion coefficient was calculated using the Randle-Sevčik equation. The effects of changing the scan rate, the temperature and properties of the solvent medium such as viscosity and donor number on the electrochemical behaviour of ferrocene have been studied [36].

2.3.1. Ferrocene as an internal reference

In many instances electrochemical measurements in water are impossible due to the insolubility or instability of the compound. Unfortunately no universal reference electrode exists for non-aqueous solvents [37]. Since a number of reference electrodes have been used, in literature there is a number of reduction potentials which could not be related to each other and which are irregularly difficult to reproduce. There are two common methods reported to be used to report non-aqueous potentials, the SCE which inevitably includes unknown liquid junction potential and pseudo reference electrode such as a silver wire [38]. Studies have been of copper macrocyclic ligand complexes the most practical approach used to address the problem was to use the potential of the oxidation of ferrocene as an internal standard. After the electrochemistry was attributed to the compound of interest has been identified, ferrocene was added to the working compartment of the cell. The electrochemical experiment was repeated and the position of the wave was directly compared to the potential of the ferrocenium/ferrocene (Fe^+/Fe) couple [39]. The traditional reference electrode used for electrochemical measurements such as the calomel and silver/ silver chloride electrode have a limited range of application. The liquid junction is problematic with these electrodes. Pt wire can be a reference electrode, when Pt wire is immersed in molten NaCl/KCl can maintain a steady electrode potential for more than 12 hours and shows electrochemical irreversibility. It can therefore be used as a pseudo-reference electrode for the study of electrode reaction

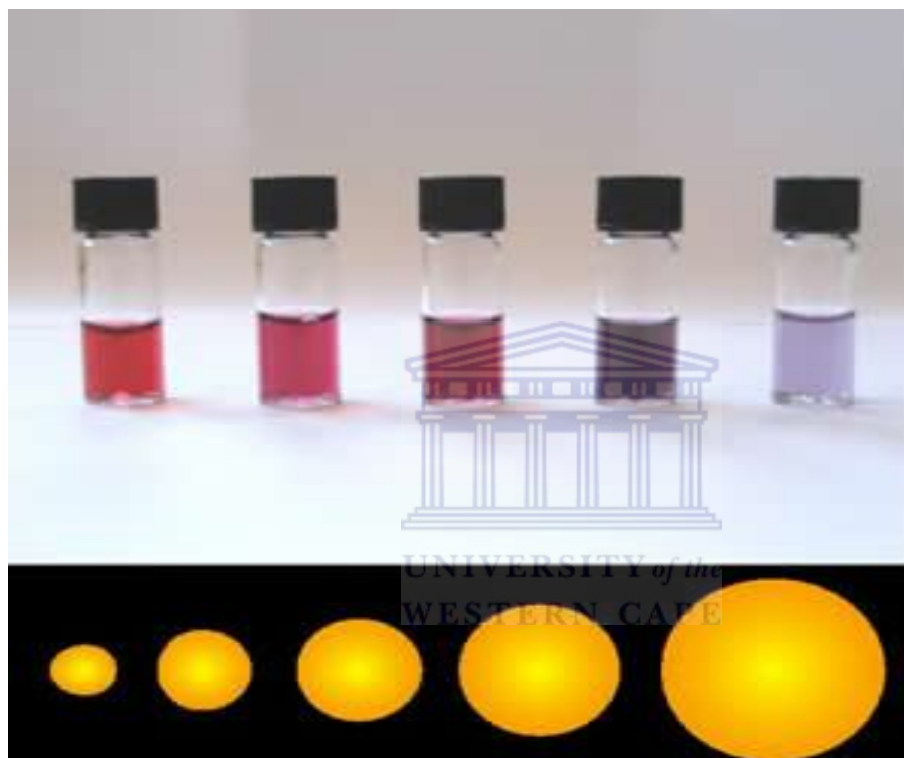
kinetics with the advantages of simplicity, convenience and ease to operate. Most electrochemical devices include an operational amplifier of high input impedance for the reference electrode to eliminate the possibility of any current passing through the reference electrode. Since no faradic process takes place at the reference electrode its area relative to that of working electrode has no effect on the electrochemical results [40]. Pournaghi-Azar reported on the oxidation process for ferrocene studied by cyclic voltammetry rotating disk voltammetry and chronoamperometry in chloroform. Different working electrodes were used with different supporting electrolyte like TBAP and Bu_4NClO_4 . The rotating disk voltammetry was used with IR compensation the charge transfer rate constant (k^0) and the charge transfer coefficient (α) was determined. The diffusion coefficient for ferrocene was determined by chronoamperometry was $1.87 \times 10^{-5} \text{ cm}^2 \text{ s}^{-1}$ in 0.5 chloroform solution of TBAP. The data that was obtained was in accordance with the approximate reversibility ferrocene/ferrocenium redox couple and that suggested that ferrocene can be used as a voltammetric standard in chloroform [41]. Pseudo-reference electrodes are simply metal wires immersed in the sample solution, although such electrodes do provide a constant potential. The reference potential is unknown and is dependent on the composition of the sample solution. Consequently redox potentials measured using a pseudo-reference electrode should be quoted relative to redox potential of the internal reference compound being ferrocene as indicated in the discussion above the advantages of using this compound. It has been indicated above the main advantage of using the pseudo reference is their low impedance.

2.4. Gold nanoparticles

Colloidal gold is a suspension of sub-micrometre sized particle of gold in a form of fluid usually water. The liquid is found in an intense red colour for particles less than 100 nm or dirty yellowish colour for larger particles. The interesting colour observation in gold solutions has led to extensive study of their optical spectroscopic properties in an effort to correlate their behaviour under different micro environmental conditions. Furthermore, gold is one of the few metals noble enough to survive as a nanoparticle undergoes atmospheric conditions. A large number of researches have been seen over the years for the synthesis and characterization of metal nanoparticles which is due to the interesting application in a broad spectrum for instance in physics, chemistry, biology, material science and their different interdisciplinary fields [42]. The evolution of dispersed small metallic particles with tight sized distribution is important; assembly of individual nanoparticles into well-defined aggregates has recently become the widely pursued objective. The pursued for aggregates is mainly for two reasons; rich optical and electrical characteristics that are distinctly different from a simple collection of individual particles or the extended solid [43].

In relation to the developing electronic technologies more sophisticated nanostructures are in demand for example nanowires, nanotubes, and their two dimensional and three dimensional nanoparticles accumulations. The optical properties contributed by the gold nanoparticles nano-clusters have been very fascinating to scientists since recent years because of their application as functional materials in optical devices, optical energy transport, near field scanning optical microscopy, surface enhanced Raman scattering spectroscopy and chemical and biological sensors [44]. Basu and co-workers reported on the biomolecule induced nanoparticles aggregation and the effect of size where a gold nanoparticle was prepared by reducing HAuCl_4 with trisodium citrate by frens method. It was found that gold particles produced well-ordered aggregated upon the interaction with the biomolecules, glutathione in

variable acidic pH which caused changes in their optical properties which arise due to electromagnetic interaction in the closed packed assembly. This study is among other studies to investigate the effect of size of gold nanoparticles, the smaller and aggregated the nanoparticles the better the expected results [45].



Scheme 4: Colour and size representation of gold nanoparticles.

http://www.bluesci.org/?option=com_content&task=view&id=588&Itemid=504&paged

[=22](#) Published on October 30 2009, Edited by Kathrin Holtzmann.

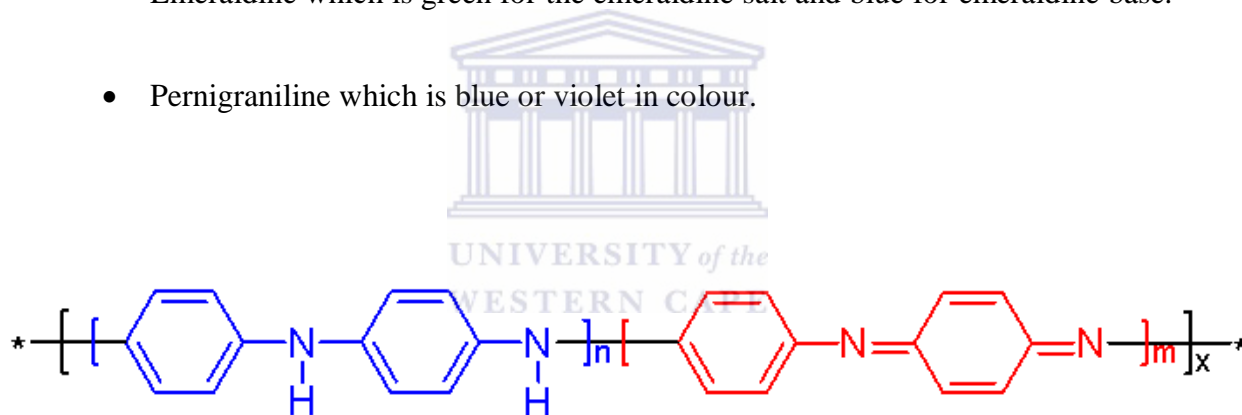
http://www.bluesci.org/?option=com_content&task=view&id=588&Itemid=504&paged

[=22](#)

2.5. Polyaniline

Polyaniline (PANi) has received much attention because of the properties that it possesses like electronic, thermoelectric and optical properties as well as its good environmental stability. Polyaniline is conventionally synthesised chemically or electrochemically, in the past years the results on the dopants and oxidants on the crystallinity of the polyaniline sample have been published [46]. Polyaniline is polymerized from the aniline monomer which is the building block. Polyaniline can be found in one of the three idealized oxidation states:

- Leucoemeraldine which is white/clear or colourless.
- Emeraldine which is green for the emeraldine salt and blue for emeraldine base.
- Pernigraniline which is blue or violet in colour.



Scheme 5: Polyaniline Structure.

In scheme 5, x represents the degree of polymerization. Leucoemeraldine has $n = 1$ and $m = 0$ in a fully reduced state. Pernigraniline in its full oxidized state $n = 0$ and $m = 1$ with imine links instead of amine. Emeraldine with $n = m = 0.5$ which is a form of polyaniline known as emeraldine base is neutral, if there is a dopant is called the emeraldine salts with the imine nitrogen protonated by an acid. Emeraldine base is the most useful form of polyaniline at room temperature and the salt is useful for electric conductivity mentioned above. The

problem associated with leucoemeraldine and pernigraniline is poor conductivity even in the presence of a dopant [47]. Liu and co-workers reported on polyaniline synthesized by an ultrasonic irradiation method and by magnetic stirring process. The structure of polyaniline was interrogated by using spectroscopic methods; the results showed the crystallinity of the polyaniline synthesized by the above mentioned method was higher than the stirring synthesis method under similar conditions. The conductivity and thermo power of polyaniline synthesized by the ultrasonic method was lower than the same properties exhibited by samples synthesized by the conventional method. The results indicated that polyaniline with higher crystallinity does not possess higher conductivity [48]. Polyaniline has a wide application; among those application is in biosensors with different types of dopants. Gopalan and co-workers reported on a glucose sensor which was fabricated by glucose oxidase into a new organic-inorganic hybrid nanocomposite. The preparation involved the formation of silica network into a nafion and subsequently loading polyaniline grafted multiwalled carbon nanotubes onto the nafion-silica nanocomposite. Microscopic and electrochemical methods where used to evaluate the performance of the sensor towards glucose, it was shown that the incorporation of the above mentioned material enhanced the performance of the biosensor towards electrochemical detection of glucose [49].

Crespilho and co-workers reported on a simple strategy how to obtain an efficient enzymatic bio electrochemical device in which urease was immobilized on electroactive membrane made with polyaniline and silver nanoparticles stabilized in polyvinyl alcohol. The fabrication method included chemical deposition of polyaniline followed by the drop coating of the composite mentioned above. Electrochemical methods where employed for the analysis of the enzyme immobilized by polyaniline and its nanocomposite. It was found that the electrode architecture employed was advantageous for the fabrication of enzymatic device

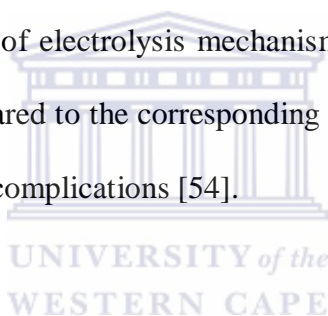
with improved bio catalytic properties [50]. Gu and co-workers reported polyaniline was doped with gold nanoparticles and polystyrene for the immobilization of HL-60 leukaemia cells to fabricate a cell electrochemical sensor. The immobilized cells exhibited irreversible voltammetry response and increased the electron transfer resistance with a good correlation to the logarithmic value of concentration and with a limited detection. The sensor was simple, low cost and disposable this implied that the polyaniline composite can be regarded for potential application for clinical application [51]. Polyaniline is also used for gas sensing which is critical to environmental monitoring, control of chemical processes, space mission and agricultural and medical application. Xu and co-workers reported on the cyclic voltammetry behaviour of polyaniline observed in acetonitrile. The peculiar cyclic voltammetry of polyaniline was observed only when PANi Film was deeply reduced by potential cycling in the potential window with a low potential limit being more negative. The electrical properties of PANi changed due to the treatment, therefore the fabrication of a concept ammonia sensor by using PANi pre-treated by the deep reduction significantly increased sensitivity [52].

Can and co-workers reported on the effect of thiophene on the electro preparation and properties of polyaniline. The presence of thiophene in solutions of aniline in acetonitrile accelerates the formation and causes improvement in the conductivity of polyaniline films. A catalytic mechanism related to the role of thiophene cation radicals which involved chemical and electrochemical oxidation step was proposed. In acidic solutions containing higher thiophene to aniline concentration ratio the thiophene entered into the structure of the polymer forming a copolymer. The structure and properties of the novel conducting polymer were clarified using cyclic voltammetry, GCMS, elemental analysis and DSC methods [53]. A number of researches have revolved around polyaniline based on the properties the

polymer possesses. The method of preparation can determine the chemical and physical properties as explained above with different applications. In relation to polyaniline being used for sensing conjugated dienes in gasoline or organic medium little or no literature has been reported for such a sensor. Polyaniline has been applied for different sensors in organic medium and the information gathered can be useful for the construction of the sensor of interest.

2.6. Kinetics of electrode

A stationary electrode voltammetry with linearly varying potential has a wide application in analysis and in the investigation of electrolysis mechanism. To present a logical discussion the kinetic cases should be compared to the corresponding reversible or irreversible reactions which take place without kinetic complications [54].



2.6.1. Reversible charge transfer

Reversible reduction of an oxidized species O to reduced species $RO + ne \leftrightarrow R$ which takes place at the surface electrode. The boundary value problem for stationary electrode

voltammetry is $\frac{C_o}{C_R} = \exp\left[\left(\frac{nF}{RT}\right)(E - E^0)\right]$ where C_0 and C_R are the concentration, n number

of electrons, E is the potential of the electrode, E^0 is the formal potential, and R, T and F have their usual significance [55].

2.6.2. Irreversible charge transfer

The irreversible reduction also takes place at the surface of the electrode, $O + ne \xrightarrow{k} R$ the boundary value problem for the electrode is much more similar to the reversible case where

$t > 0, x = 0; D_0 \frac{\sigma C_0}{\sigma x} = k C_0$ where $k = \exp\left[\left(\frac{\alpha n_\alpha F}{RT}\right)(E_i - E^0)\right]$ k is the rate constant at a

particular potential and the other parameters are the same as the reversible case [56]. An approach to obtain kinetic information from a stationary electrode voltammetry was describe more in detail by Reinmuth who reported that for an irreversible reaction , the current flowing at the foot of the wave is independent of the rate of voltage scan. The equation for simple way to obtain kinetic data follows;

$$i = nFAC_0^* k x \exp\left[\left(\frac{-\alpha n_\alpha F}{RT}\right)(E - E_i)\right]$$

The above equation was supported by combination of different equations in the past. The diffusion coefficient (D) is the amount of a particular substance that diffuses across a unit area in 1 s under the influence of a gradient of one unit. It is usually expressed in the units $\text{cm}^2 \text{s}^{-1}$ [57].

2.6.3. Analytical techniques

2.6.4. Cyclic voltammetry

Is the most widely used technique for obtaining qualitative information about electrochemical reactions. The working electrode potential is ramped linear versus the linear sweep voltammetry. Cyclic voltammetry takes the experiment a step further than linear sweep voltammetry which ends when it reaches a set potential. When cyclic voltammetry reaches a set potential the working potential ramp is inverted. The inversion can happen multiple times during an experiment. The current is plotted against the applied potential to give a cyclic voltammogram; cyclic voltammetry is used to study the electrochemical behaviour of an analyte in solution. There are numerous forms of voltammetry;

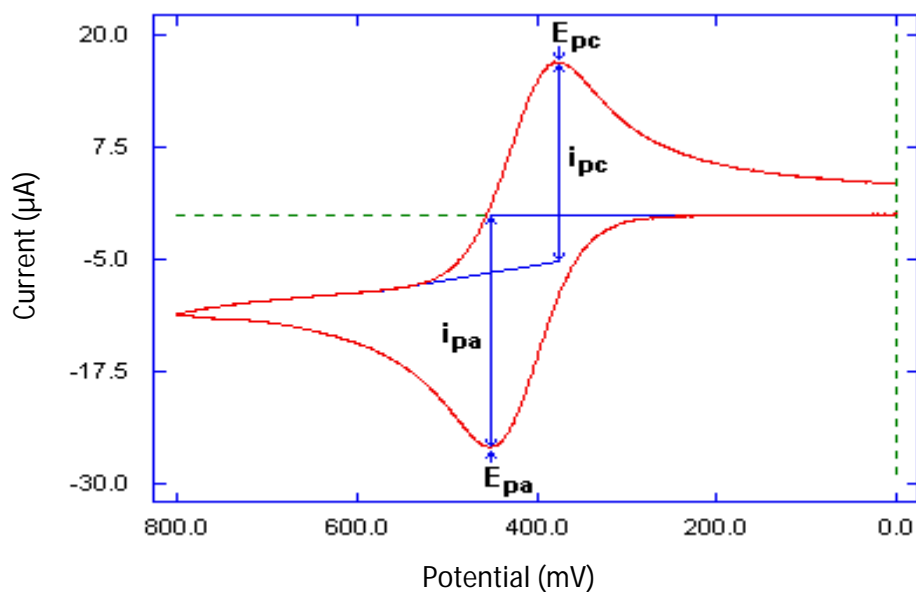
- Potential step- measures the applied voltage is instantaneously jumped from one value V_1 to another V_2 the resulting current is measured as a function of time. If we consider the reaction; $\text{Fe}^{3+}(\text{s}) + \text{e}^- \rightarrow \text{Fe}^{2+}(\text{s})$

Usually the range is set such that V_1 the reduction of (Fe^{3+}) is thermodynamically unfavourable. The second value of voltage V_2 is selected so that any Fe^{3+} close to the electrode surface is converted to product Fe^{2+} . The current rises instantaneously after the change in voltage and then begins to drop as a function of time.

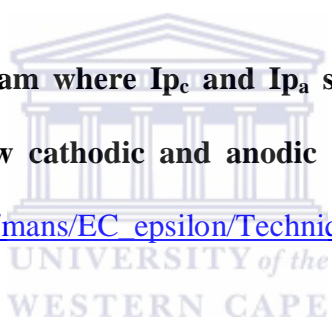
- Linear sweep- a fixed potential range is employed much like potential step measurements. However the linear sweep voltammetry the voltage is scanned from lower limit. The characteristics of the linear sweep voltammogram depends on a number of factors including;
 - The rate of electron transfer reaction
 - The chemical reactivity of the electroactive species

- The voltage scan rate

In linear sweep voltammetry measurements of the current response are plotted as a function of voltage rather than time unlike potential step measurements. The scan begins from the left hand side to the current /voltage plot where no current flows [58]. Cyclic voltammetry is very similar to linear sweep voltammetry; in this case the voltage is swept between two values at the fixed rate. When the voltage reaches V_2 the scan is reversed and the voltage is swept back to V_1 . Cyclic voltammetry is highly dependent on the analyte being studied; the analyte has to be redox active within the experimental potential window. It is highly desirable for analyte to show reversible wave, reversible couple contain polarization over potential display hysteresis between absolute potential between the reduction (E_{p_c}) and oxidation peak (E_{p_a}). This over potential arises from a combination of analyte diffusion rate intrinsic activation barrier of transferring electrons from an electrode to analyte. A theoretical description of polarization over potential is in part described by the Butler-volmer equation and Cottrell equation. Conveniently in an ideal system the relationship reduces to, $|E_{p_c} - E_{p_a}| = 59 \text{ mV}/n$, for an n electron process. Reversible couples will display a ratio of the peak currents passed at reduction (i_{p_c}) and oxidation (i_{p_a}) that is near unity $1 = \frac{i_{p_a}}{i_{p_c}}$. This ratio can be perturbed for reversible couples in the presence of a following chemical reaction, stripping wave, or nucleation event. When such reversible peaks are observed thermodynamic information in the form of half-cell potential $E^0_{1/2}$ can be determined [59].



Scheme 6: Cyclic Voltammogram where I_{p_c} and I_{p_a} show cathodic and anodic peak current and E_{p_a} and E_{p_c} show cathodic and anodic peak potential for a reversible reaction. http://www.basinc.com/mans/EC_epsilon/Techniques/CycVolt/cv.html



The electronegativity is the affinity for electrons; the atoms of the various elements differ in their affinity for electrons which contributes greatly in the electric charges and conductivity of the solvents. The key to drive an electrode reaction is by the application of voltage if the

units of volts are considered to be;
$$V = \frac{\text{Joule}}{\text{Coulomb}}$$

This simply means volts are required energy to move charge. When voltage is applied to an electrode it supplies electrical energy. There are three forms of mass transport that can influence an electrolysis reaction;

- Diffusion- which occur in solution and arises from local uneven concentration of reagents. Entropic forces act to smooth out the uneven distribution of concentration and are therefore the main driving forces for this process. Diffusion is particularly significant in an electrolysis experiment since the conversion reaction only occurs at the surface of the electrode. The rate of movement of material by diffusion can be predicted mathematically;

$$J_0 = \frac{-D_0 \sigma C_0}{\sigma x}$$

- Convection- results from action of a force on the solution. There are two forms of convections;

- Natural convection- generated by thermal or density differences and act to mix the solution in a random and unpredictable manner.
- Forced convection- several orders of magnitude greater than any natural convection effects and therefore effectively removes the random aspects from the experimental measurements.

- Migration- the final form of mass transport we need to consider is migration. This is essentially an electrostatic effect which arises due the application of a voltage on the electrodes. This effectively creates a charged interface (the electrodes). Any charged species near that interface will either be attracted or repelled from it by electrostatic forces [60].

In the Randles-Sevcik equation the magnitude of the peak ip in cyclic voltammogram is a function of the temperature, bulk concentration c_{analyte} , electrode area A, the number of

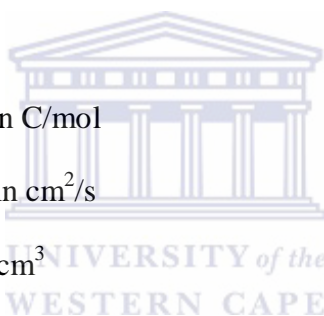
electrons transferred n , the diffusion coefficient D and the speed at which the potential is scanned ν . the Randles-Sevcik equation is as follows;

$$i_p = 0.4463nFAC \left(\frac{nF\nu D}{RT} \right)^{1/2}$$

Or if the solution is at room temperature:

$$i_p = (269.000)n^{3/2}AD^{1/2}C\nu^{1/2}$$

- i_p = Current maximum in amps
- n = Number of electrons transferred in the redox event (usually 1)
- A = Electrode area in cm^2
- F = The faraday constant in C/mol
- D = Diffusion coefficient in cm^2/s
- C = Concentration in mol/cm^3
- ν = Scan rate in V/s .



2.6.5. Subtractive normalized interfacial fourier transform infra-red spectroscopy

It is when a spectroscopic investigation is performed at the same time as the electrochemical changes occur then the measurement is said to be an in situ measurement. Where the term in situ in latin terms means for 'same place'. The working electrode used for spectroelectrochemistry is an 8 mm platinum disk. A saturated calomel electrode (SCE) in a lugging capillary is used as a reference electrode and platinum wire placed symmetrically around the working electrode to serve as an auxiliary electrode. All potentials are reported vs SCE. For measurements done in a bulk solution the platinum electrode should be pulled 1 cm

back from the CaF₂ window in the bulk solution. SNIFTIF is the incorporation of Fourier transformation and the Michelson interferometer into modern IR spectrometers, provided several breakthroughs for optical spectroscopy, including higher optical throughput and diminished sampling times due to the multiplex advantage. Concurrently, spectroelectrochemical techniques employing FT-IR spectrometers were developed. The potential is repeatedly switched between E₁ and E₂, at each potential a spectra is collected. This process is repeated several times in order to avoid or minimize contribution to the IR spectra from mechanical and electronic drift in the instrument [61].

2.6.6. Ultra-violet visible spectroscopy

Refers to the reflectance of spectroscopy in these defined ranges of radiation by the following;

Ultraviolet (UV) 200-350 nm

Visible (Vis) 350-700 nm

Near-infrared (NIR) 700-1000 nm

This means it uses light in the visible and adjacent near-UV and NIR ranges. The reflectance in the visible range directly affects the perceived colour of the chemicals involved. In the region of electromagnetic spectrum molecules undergo electronic transitions which are very complementary to fluorescence spectroscopy which deals with transitions from excited state to the ground state, while the absorption measures transition from the ground state to the excited state [62]. The optical absorbance, Abs, is defined by the following equation:

$$Abs = \log_{10} \left(\frac{T_{Reference}}{T_{Sample}} \right)$$

Where T is the transmittance of the light beam following its passage through the cell. The method that is used more often to quantitatively determine the concentration of the absorbing species in solution is known as Beer-Lambert law;

$$A = \log_{10} \left(\frac{I_0}{I} \right) = \epsilon c L,$$

Where A is the absorbance, I_0 is the intensity of the incident light at a given wavelength, I is the Transmitted intensity, L is the path length through the sample and c is the concentration of the absorbing species. For each species and wavelength ϵ is a constant known as the molar absorptivity or extinction coefficient [63].

2.6.7. Transmission electron microscopy

Is a microscopy technique whereby a beam of electrons is transmitted through an ultra thin specimen, interacting with the specimen as it passes through. An image is formed from the interaction of the electrons transmitted through the specimen; the image is magnified and focused onto an imaging device, such as a fluorescent screen, on a layer of photographic film, or to be detected by a sensor such as a CCD camera. It is capable of imaging at a significantly higher resolution than light microscopes, owing to the small de Broglie wavelength of electrons. This enables the instrument's user to examine fine detail even as small as a single column of atoms, which is tens of thousands times smaller than the smallest resolvable object in a light microscope. TEM forms a major analysis method in a range of scientific fields, in both physical and biological sciences. At smaller magnifications TEM image contrast is due to absorption of electrons in the material, due to the thickness and composition of the material. At higher magnifications complex wave interactions modulate the intensity of the

image, requiring expert analysis of observed images. Alternate modes of use allow for the TEM to observe modulations in chemical identity, crystal orientation, electronic structure and sample induced electron phase shift as well as the regular absorption based imaging [64].



8. References

- [1] Stetter JR, Penrose WR, Yao S. Sensors, chemical sensors, electrochemical sensors and ECS. *Journal of the Electrochemical Society*. 2003, 150(2): 11-16.
- [2] Cao Z, Buttner WJ, Stetter JR. The properties and applications of amperometric. Gas sensors. *Electroanalysis*. 1992, 4(3): 253-266.
- [3] Wang SS, Lee H. An electrochemical sensor for distinguishing two stroke engine oils. *Sensor and Actuators B: Chemical*. 1997, 40(2-3): 199-203.
- [4] Yu C, Wang Y, Hua K, Xing W, Lu T. Electrochemical H₂S sensor with H₂SO₄ pre-treated Nafion membrane as solid polymer electrolyte. *Sensor and Actuators B: Chemical*. 2002, 86(2-3): 259-265.
- [5] Galster H. pH measurements-fundamentals, Methods, Applications, Instruments, VCH publishers, New York.1991. *Journal of Chemical Education*. 2006, 83(5): 752-757.
- [6] Yao S, Wang M, Madou M. A pH electrode based on melt-oxidized iridium oxide. *Journal of the Electrochemical Society*. 2001, 148(4): 29-36.
- [7] Miura N, Lu G, Yamazoe N. A solid electrolyte and a mixture of Au and various metal oxides as a sensing electrode Semiconductors of *n*-type metal oxides such as WO₃ , MoO₃ and V₂O₃. *Solid State Ionics*. 2000, 533(3): 136-137.
- [8] Mukundan R, Brosa EL, Brown DR, Garzon FH. Electrochemical potentiometric NOx sensors based on yttria-stabilized zirconia with zeolite modified electrode. *Electrochemical Solid-State Letters*. 1999, 2(1): 412-414.
- [9] Grate JW. Acoustic Wave Microsensor Arrays for Vapor Sensing. *Chemical Review*. 2000, 100(3): 2627-2648.

- [10] Stetter J, Penrose WR. Artificial chemical sensing: Olfaction and the electronic nose. Eds Electrochemical Society: Pennington, NJ. 2001:8-14.
- [11] Ulmer H, Mitrovics J, Weimer U, Gopel W. Sensor arrays with only one or several transducer principle. *Sensor and Actuators B: Chemical*. 2000, 65(1-3): 79-81.
- [12] Zhang K, Xiao Y, Lan Y, Zhu M, Wang H, Lu J. Electrochemical reduction of aliphatic conjugated dienes in the presence of carbon dioxide. *Electrochemistry Communications*. 2010, 12(12): 1698-1702.
- [13] Cannes C, Labbe E, Durandetti M, Devaud M, Nedelec JY. Nickel- catalyzed electrochemical homocoupling of alkenyl halide: rates and mechanisms. *Journal of Electroanalytical Chemistry*. 1996, 412(1-2): 85-93.
- [14] Wawzonek S, Laitinen HA. Polarographic studies in acetonitrile and dimethylformamide. *Journal of Electrochemical Society*. 1960, 107(6): 537-540.
- [15] Hoijtink GJ, De Boer E, Van der Meij PH. Reduction potential of various aromatic hydrocarbons and their univalent anions. *Recueil de Travaux*. 1956, 75(5): 487-503.
- [16] Farnia G, Marcuzzi F, Sandona G. Electrochemical reduction of phenyl-substituted cyclopentadiene: a case of an 'indirect father-son' self -protonation process. *Journal of Electroanalytical Chemistry*. 1999, 460(1-2): 160-175.
- [17] Bergstad K, Grennberg H, Backvall JE. Aerobic oxidation of conjugated dienes using a catalytic palladium (II)-quinone-heteropolyacid system for electron transfer from organic substrate to molecular oxygen. *Organometallics*. 1998, 17(2): 45-50.
- [18] Chiba K, Kono Y, Kitayama M, Uchiyama R, Kim S, Kitano Y, Tada M. A perfluorinated micellar reaction system in lithium perchlorate/Acetonitrile; enhanced

efficiency in anodic electron-transfer and intermolecular cycloaddition. *Electrochemistry Communications*. 2001, 3(2): 63-66.

[19] Stroebel GG, Myers DY, Grabbe RR, Gardner PD. Competitive Reaction Modes of the 1, 3-Cyclohexadiene Radical Anion. American chemical society. *Journal of Physical Chemistry*. 1978, 82(10): 1121-1125.

[20] Diene value by maleic acid anhydride addition reaction (UOP-326), des plaines, IL. test method for diene value (MAV). Diene value by maleic anhydride addition reaction, UOP method no. Universal Oil Product Company. West Conshohocken. PA: ASTM International. 1965, 326-382.

[21] Badoni RP, Bhagat SD, Joshi GC. Analysis of olefinic hydrocarbons in cracked petroleum stock: a review. *Fuel*. 1992, 71(5): 483-491.

[22] Rogers FE, Quan SW. Thermo chemistry of the Diels-Alder reaction. III. Heat of addition of cyclopentadiene to maleic anhydride. *Journal of Physical Chemistry*. 1973, 77(6): 828-831.

[23] Oguntoye E, Szunerits S, Utley JHP, Wyatt PB. Electro-organic reactions. Part 46, diels-alder trapping of o-quinodimethane generated by redox-mediated cathodic reduction of α, α' -dibromo-o-xylene in the presence of hindered dienophile. *Tetrahedron*. 1996, 52(22): 7771-7778.

[24] Roger FE. Thermochemistry of the diels-alder reaction II. Heat of addition of several dienes to the tetracyanoethylene. *Journal of Physical Chemistry*. 1972, 76(1): 106-109.

- [25] Maltadeven V. Report of the literature review committee annual review of the literature on fats, oils and detergents part 1. *Journal of American Oil Chemist's Society*. 1965, 42(7): 364-381.
- [26] O'Brien AP, Ray JE. Studies of methods for hydrocarbon type analysis of gasoline. *Analyst*. 1985, 10(6): 592-593.
- [27] Matsushita S, Tada Y, Ikushige T. Rapid hydrocarbon group analysis of gasoline by high-performance liquid chromatography. *Journal of Chromatography A*. 1981, 208(2): 429-432.
- [28] Ghazvini M, Hanry R, Jackle HW, Steinhauer E. Determination of conjugated diolefins in gasoline by high performance liquid chromatography. *Analytical*. 1996, 112(3): 210-212.
- [29] Nijhuis TA, Dautzenberg FM, Moulijn JA. Chemical modelling of monolithic and tricked-bed reactors for the hydrogenation of styrene. *Engineering Science*. 2003, 58(7): 1113-1124.
- [30] Lipari F, Swarin SJ. Determination of formaldehyde and other aldehydes in automobile exhaust with an improved 2,4-dinitrophenylhydrazine method. *Journal of Chromatography*. 1982, 247(2): 297-306.
- [31] Polak J, Janacek L, Volke J. Polarographic determination of conjugated dienes in hydrogenation products of pyrolysed gasoline. *Analyst*. 1986, 111(10): 1207-1210.
- [32] Kealy TJ, Paulson PL. A new type of organo-iron compound nature. *Applied Materials and Interfaces*. 1951, 168(19): 1039-1040.
- [33] Wilkinson G, Rosenblum M, Whiting MC, Woodward RB. The structure of iron bis-cyclopentadienyl. *Journal of American Chemical Society*. 1952, 74(3): 2125-2126.

- [34] Nielson RM, Lyon LA, Hupp JT. Primitive molecular recognition effects in electron transfer processes: modulation of (trimethylammonia) methyl ferrocenium/ferrocene self-exchange kinetics via hydrophobic encapsulation. *Inorganic Chemistry*. 1996, 35(4): 970-973.
- [35] Crooks RM, Bard AJ. Electrochemistry in near critical and supercritical fluids. The electrochemistry of Ferrocene and phenazine in acetonitrile between 25 and 300⁰C. *Journal of Electroanalytical Chemistry*. 1988, 243(1): 117-131.
- [36] Nikos GT. Cyclic voltammetry studies of Ferrocene in non-aqueous solvents in the temperature range from 248.15 to 298.15. *Journal of Solid State Chemistry*. 2007, 36(3): 289-302.
- [37] Mann CK, Barnes KK. *Electrochemical reaction in non-aqueous systems*. Marcel Dekker, New York: 1970, 283.
- [38] Merz A, Bard AJ. A stable surface modified platinum electrode prepared by coating with electroactive polymer. *Journal of American Chemical Society*. 1978, 100(10): 3222-3223.
- [39] Gagne RR, Koval CA, Lisensky GC. Ferrocene as an internal standard for electrochemical measurements. *Inorganic Chemistry*. 1980, 19(9): 2854-2855.
- [40] Huber B, Roling B. Development of a Ag/Ag⁺ micro-reference electrode for electrochemical measurements in ionic liquids. *Electrochimica Acta*. 2011, 56(19): 6569-6572.
- [41] Pournaghi-Azar MH, Ojani R. Electrode kinetic parameters of the ferrocene oxidation at platinum, gold and glassy carbon electrode in chloroform. *Electrochimica Acta*. 1994, 39(7): 953-955.

- [42] Gaponik NP, Talapin DV, Rogach AL. Thiol-capping of CdTe nanocrystals: An alternative to organometallic synthetic routes. *Journal of Physical Chemistry*. 2002, 106(29): 7177-7185.
- [43] Chen J, Jiang J, Gao X, Gong J, Shen G, Yu R. Gold aggregated, dye embedded, polymer-protected nanoparticles (GDDNs): A new type of tags for detection with SERS. *Colloids and surfaces A: Physicochemical and Engineering Aspects*. 2007, 294(1-3): 80-85.
- [44] Qian X, Park HS. The influence of mechanical strain on the optical properties of spherical gold nanoparticles. *Journal of the Mechanics and Physics of Solid*. 2010, 58(3): 330-345.
- [45] Basu S, Ghosh KS, Kundu S, Panigrahi S, Praharaj S, Pande S, Jana S, Pal T. Biomolecule induced nanoparticle aggregation: Effect of particle size on interparticle coupling. *Journal of Colloid and Interface Science*. 2007, 313(2): 724-734.
- [46] Feast WJ, Tsibouklis J, Pouwer KL, Goenendaal L, Meijer EW. Synthesis, processing and material properties of conjugated polymers. *Polymer*. 1996, 37(22): 5017-5047.
- [47] Jamadade VS, Dhawale DS, Lokhande CD. Studies of electropolymerised Leucoemeraldine, emeraldine and Pernigraniline forms of polyaniline films and their supercapacity behaviour. *Synthetic Metals*. 2010, 160(9-10): 955-960.
- [48] Liu H, Hu XB, Wang JY, Boughton RI. Structure, conductivity and thermopower of crystalline polyaniline synthesis by the ultrasonic irradiation polymerization method. *Talanta*. 2002, 35(3): 9414-9419.

- [49] Gopalan AI, Lee KP, Ragupathy D, Lee SH, Lee WJ. An electrochemical glucose biosensor exploiting a polyaniline grafted multiwalled carbon nanotube/perfluorosulfonate ionomer-silica nanocomposite. *Biomaterials*. 2009, 30(30): 5999-6005.
- [50] Crespilho FN, Lost RM, Travain SA, Oliveira ON, Zucolotto V. Enzyme immobilization on Ag nanoparticles/polyaniline nanocomposites. *Biosensor and Bioelectronics*. 2009, 24(10): 3073-3077.
- [51] Gu M, Zhang J, Li Y, Jiang L, Zhu J. Fabrication of a novel impedance cell sensor based on the polystyrene/polyaniline/Au nanocomposite. *Talanta*. 2009, 80(1): 246-249.
- [52] Xu K, Zhu L, Zhang A, Jiang G, Tang H. A peculiar cyclic voltammetry behaviour of polyaniline in acetonitrile and its application in ammonia vapour sensor. *Journal of Electroanalytical Chemistry*. 2007, 608(2): 141-147.
- [53] Can M, Pekmez K, Pekmez N, Yildiz A. Electropolymerization of acetonitrile solution containing aniline and thiophene. *Synthetic Metals*. 1999, 104(1): 9-17.
- [54] Reinmuth WH. Irreversible electron transfer process in solution phase. *Analytical Chemistry*. 1960, 32(4): 1891-1892.
- [55] Garrido JA, Rodriguez RM, Bastida RM, Brillas E. Study by cyclic voltammetry of a reversible surface charge transfer reaction when the reactant diffuses to the electrode. *Journal of Electroanalytical Chemistry*. 1992, 324(1-2): 19-32.
- [56] Nicholson RS, Shain I. Theory of stationary electrode polarography. Single scan and cyclic method. Applied to reversible, irreversible and kinetic system. *Analytical Chemistry*. 1964, 36(4): 706-723.

[57] Mizoguchi T, Adam RN. Anodic oxidation studies of N,N-dimethylaniline voltammetric and spectroscopic investigations at platinum electrodes. *Journal of American Chemistry Society*. 1962, 84(11): 2058-2061.

[58] Bard AJ, Larry RF. *Electrochemistry methods: fundamentals and application*. 2nd edition. 2000:12-18.

[59] Nicholson RS, Irving S. Theory of stationary electrode polarography single scan and cyclic methods applied to reversible, irreversible and kinetic system. *Analytical Chemistry*. 1964, 36(4): 706-723.

[60] Heinze J. *Cyclic voltammetry- electrochemical spectroscopy. New analytical methods, angewandte chemistry. International Edition*. 1984, 25(5): 831-847.

[61] Korzeniewski C, Pons S. In situ infrared spectroelectrochemistry. *Journal of Vacuum Science and Technology*. 1985, 5(1): 1421-1424.

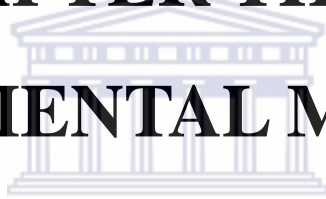
[62] Skoog, E A. *Principles of instrumental analysis*; 6th edition. Thomson Brooks/Cole. 2007: 169-173.

[63] Monk PMS. *Fundamentals of electro-analytical chemistry*. New York, USA. John Willy & Son. 2001: 239-245.

[64] Ernst F, M Ruhle. Present developments microscopy in high-resolution transmission electron. *Current Opinion in Solid State and Materials Science*. 1997, 2(3): 469-476.

CHAPTER THREE

EXPERIMENTAL METHODS



UNIVERSITY *of the*
WESTERN CAPE

3. Experimental

3.1. Instrumentation

All electrochemical were carried using a BAS100W integrated and automated electrochemical work station from bio analytical systems (BAS, West Lafayette, IN) operated in the cyclic voltammetry and potential amperometry. A 10 mL electrochemical cell was used in a three electrode configuration consisting of a 0.0201 cm² Pt and 0.071 cm² GCE working electrode (BAS, West Lafayette, IN), Pt wire auxiliary electrode and pseudo Pt wire reference electrode. The experiments were carried out at a control room temperature of 25 °C. The ultraviolet-visible spectrum was recorded at a range of 190-1000 nm using 3 cm³ quartz cuvettes with a GBS UV/VIS 920. Transmission electron microscopy (TEM) images were acquired using a Tecnai G² F20 X-Twin MAT. TEM experimentation were performed by placing a drop of the solution on a carbon coated copper grid and dried under electric bulb for 20 min. Subtractive normalized interfacial fourier transform infra-red spectroscopy (SNIFTIR) spectra were obtained using vertex 80 V and BASi Epsilon.EC. A 50 mL electrochemical cell was used in a three electrode configuration consisting of 8 mm Pt working electrode, Pt wire auxiliary electrode and Pseudo Pt wire reference electrode.

3.2. Reagents

Reagents that were used in this study included; aniline (99 %) which was distilled via fractional distillation under nitrogen gas. Chloroform (99 %), Ammonium persulfate (99.9 %), Hydrochloric acid (37 %), Poly(4-Styrenesulfonic Acid) (30 wt % in H₂O), Tri-sodium Citrate (1 %), H₂AuCl₄ (99.9 %), Tetrabutylammoniumperchlorate (99.9 %), Acetonitrile (99.99 %), Ferrocene (99 %), 1.3-Cyclooctadiene (99 %), 1.3-Cyclohexadiene (97 %), Trans-Piperylene (96 %), 2-Methyl-1.3-butadiene (99 %) were obtained from Sigma Aldrich. 1.0 M of 1.3-cyclooctadiene, 1.3-cyclohexadiene, trans-piperylene and 2-methyl-1.3-butadiene 1 M

stock solutions were prepared and kept in the refrigerator under 18 °C when not used. Deionised water (18.2 MΩ) purified by a milli-QTM system (Millipore) was used for aqueous solution preparations and interference studies.

3.3. Preliminary preparation of gold nanoparticles

25 mL of 0.165 M HAuCl_4 was introduced into a conical flask on a stirring hot plate, the magnetic stirrer was added and the solution was brought to boiling point. To the boiling solution added 7.5 mL of 1 % sodium citrate ($\text{Na}_2\text{C}_6\text{H}_5\text{O}_7 \cdot 2\text{H}_2\text{O}$) solution. The stirring continued on the gold solution till it was reduced to a reddish colour. When a deep red colour appeared the heating was stopped, the solution was allowed to cool down. It was characterized by ultraviolet visible spectroscopy.



3.4. First attempt synthesis of PANi, PANi/PSSA and PANi/PSSA/AuNP composites.

3.4.1. Interfacial chemical synthesis of PANi and its two composites

Typically the interfacial reactions were performed in a 250 mL volumetric flask. The details are described as follows: A solution of 0.016 M aniline was prepared in chloroform (100 mL) (designed as A solution). A solution of 0.004 M ammonium peroxodisulfide (APS) was prepared in 100 mL of 0.4 M HCl (designed as B solution). A solution of 0.004 M APS and 0.4 M PSSA was prepared in 100 mL of 0.4 M HCl (designed as C solution). A solution of 0.002 M AuNP and 0.4 M PSSA were prepared in 100 mL 0.4 M HCl (designed as D solution). The aniline/chloroform solution (A solution) was transferred into 250 mL volumetric flask, Followed by B(C, D) solutions. The A solution formed a lower organic layer and B(C, D) solution formed the upper aqueous layer and the resulting two phase system was covered with polyethylene film to minimize solvent evaporation and was be left

undisturbed. A few minutes later it was expected that a thin green layer appeared at the interface, then slowly migrate in the aqueous layer then later the entire aqueous layer was filled with a dark green product. After 24 hours the reaction mixture was suction filtered and a dark precipitate was washed with distilled water. Mixture of solution A+B PANi will be obtained, solution A+C PANI/PSSA will be obtained and solution A+D obtained PANi/PSSA/AuNP composite.

3.4.2. Voltammetric analysis

Before the experiment started the GCE was polished thoroughly with 1, 0.3 and 0.05 μm slurries alumina and respectively rinsed with deionised water after each polishing step. This was followed with ultra sonication of GCE in deionised water for 5 min. 10 mL of acetonitrile and 0.1 M tetrabutylammoniumperchlorate solution was measured into an electrochemical cell and purged with argon for 300 s. 4 μL of PANi, PANi/PSSA and PANi/PSSA/AuNP was drop coated on the GCE and air dried. The following potential range was used the initial potential E_i of -1.6 V to a switch potential E_λ of +2.1 V scan rate of 100 mV/s for 10 cycle. Further voltammetric cyclic were performed to assess the reproducibility and stability of the PANi and its two composites in an organic medium. Uv-visible spectrum and TEM was used for characterization of PANi and its two composites.

3.5. Second attempt electrosynthesis of PANi

3.5.1. Voltammetric analysis

A three electrode arrangement was set up, GCE as a working electrode, Pt wire as a counter electrode and Ag/AgCl as a reference electrode. 0.05 M aniline was dissolved 0.1 M H_2SO_4 on a previously cleaned GCE following the exact procedure of cleaning as explained above in

3.4.2. The aniline/ H₂SO₄ was first degassed by passing argon through the solution for 10 min and kept the argon gas as a blanket through the electrosynthesis. During the potentiodynamics electrosynthesis, the potential was cycled from initial potential E_i of -0.4 V to a switch potential E_λ of +1 V at 100 mV/s scan rate the deposition process was stopped after 10 cycles. The PANi modified electrode was rinsed with deionised water and used as working electrode in subsequent studies.

3.6. Preparation of ferrocene.

3.6.1. Voltammetric analysis

Ferrocene was used as an internal reference in organic medium for the determination of conjugated dienes. The Pt and GCE were polished with 1; 0.3 and 0.05 μm slurries alumina and were rinsed with deionised water. Followed by ultra sonication first in ethanol for 5 min and then in deionised water for the next 5 min. electrolyte was acetonitrile with 0.1 M tetrabutylammoniumperchlorate being a supporting electrolyte. 10 mL of the electrolyte was transferred in an electrochemical cell and there was no purging. A three electrode set up was used where the working electrode was Pt electrode interchanged with GCE, the counter electrode was Pt wire and the reference electrode was a pseudo Pt wire. Added 0.001 M ferrocene and 0.002 M of one of the conjugated diene (1.3-cyclohexadiene, 1.3-cyclooctadiene, trans-1.3-pentadiene and 2-methyl-1.3-butadiene) at a time. The scan rate was varied from 1000, 750, 500, 400, 300, 200, 150, 100, 75, 50, 25, 10 and 5 mV/s. The cyclic voltammetry of each scan rate was repeated three times to ensure reproducibility.

3.7. Preparation of COD, CHD, PD and MBD

3.7.1 Voltammetric analysis

Three electrode cell set up was used, Pt and GCE as working electrode, Pt wire as counter electrode and Pseudo Pt wire was reference electrode. For experiments all the experiments there was no purging. The working electrode was polished by 1; 0.3 and 0.05 μm slurries alumina and was rinsed with deionised water. The working electrode was ultra sonicated in ethanol for 5 min followed by 5 min ultra sonication in deionised water. Acetonitrile containing 0.1 M TBAP was added in 10 mL electrochemical cell without any purging.

3.7.1.1 Concentration variation

The background CV was recorded three times to ensure reproducibility. The conjugated dienes (CHD, COD, PD and MBD) was analysed one at a time and the electrolyte was changed every time another conjugated diene was analysed and also the cleaning procedure was performed as explained above. 1 M solution of each diene was prepared and stored in the refrigerator at 8 °C. Into a 10 mL acetonitrile containing 0.1 M TBAP supporting electrolyte 0.5, 1, 2, 4, 5 and 0.01 M of conjugated diene was varied and repeated three times at each concentration to ensure reproducibility. The initial potential E_i for all dienes was 0 V and switch potential E_λ for CHD and COD was +1.9 V, for PD was +2 V and for MBD was +2.2 V.

3.7.1.2 Scan rate variation

The background CV was recorded three times at each scan rate at zero concentration of conjugated diene. 0.0025 M of conjugated diene (CHD, COD, PD and MBD) was added to 10 mL acetonitrile containing 0.1 M TBAP one diene at a time and used a fresh electrolyte

and polished electrode with the above mentioned procedure. The potential range for CHD and COD were initial potential E_i of 0 V and switch potential E_λ of +1.9 V, the initial potential for PD was 0 V with switch potential of +2 V and initial potential of 0 V and switch potential of +2.2 V for MBD. The scan rate was from 1000, 750, 500, 400, 300, 200, 150, 100, 75, 50, 25 and 20 mV/s. The CV was repeated three times for each scan rate for reproducibility.

3.7.2 SNIFTIR

A three electrode set up was used, (8 mm) Pt electrode as a working electrode, Pt wire was reference electrode and pseudo Pt wire as reference electrode. The working electrode was cleaned with 1; 0.3 and 0.05 μm slurries alumina and successively rinsed with deionised water. The working electrode was ultra sonicated in deionised water for 10 min. The experiment was done without any purging at room temperature. 50 mL acetonitrile and 0.1 M TBAP was added in round bottom flask which had three necks. Added 0.0025 M CHD in the solution. A background SNIFTIR and experimental SNIFTIR at different potential, the potentials were as follows; $E_{\text{ref}1} = 0 \text{ mV}$, $E_1 = 0$; $E_{\text{ref}2} = 0 \text{ mV}$, $E_2 = 770 \text{ mV}$; $E_{\text{ref}3} = 0 \text{ mV}$, $E_3 = 1120 \text{ mV}$; $E_{\text{ref}4} = 0 \text{ mV}$, $E_4 = 1300 \text{ mV}$; $E_{\text{ref}5} = 0 \text{ mV}$, $E_5 = 1425 \text{ mV}$; $E_{\text{ref}6} = 0 \text{ mV}$, $E_6 = 1532 \text{ mV}$; $E_{\text{ref}7} = 0 \text{ mV}$, and $E_7 = 1638 \text{ mV}$.

3.7.3. Ultra-violet visible spectroscopy

0.0005 M of conjugated dienes (CHD, COD, PD and MBD) was added in a 3 cm^3 cuvette one at a time and every time another conjugated diene was analysed the cuvette was cleaned in 0.1 M Nitric Acid and rinsed with deionised water and dried by nitrogen gas. The analysis was done between 200 and 1000 nm wavelength. The UV was done on 1 M (CHD, COD, PD

and MBD) which was prepared and different times and stored at 8 °C refrigerator. The solutions were from October 2010, March 2011 and June 2011.

3.8. Interference studies

Several substances suspected to interfere with the detection of conjugated dienes by the developed biosensor were investigated. They included ethanol, water or moisture, storage time. Special attention was paid to water because it is commonly present and can be dissolved in acetonitrile. Water can be deposited in the electrochemical cell through moisture and needed to study the effect in order to be able to cancel the effect. A three electrode set up was used. The potential range for CHD and COD was initial potential E_i of 0 V and switch potential E_λ of +1.9 V; the potential range for PD was initial potential E_i of 0 V and switch potential E_λ of +2 V and the potential range of MBD with initial potential E_i of 0 V and switch potential E_λ of +2.2 V. Added the 0.0025 M conjugated diene (CHD, COD, PD and MBD) one at a time in acetonitrile containing 0.1 M TBAP without any purging. When using another conjugated diene the electrolyte was changed and electrodes cleaned as explained above. The concentration of the conjugated diene was kept constant and varied the addition of deionised water. The deionised water was added in the following increments; 10, 20 and 50 μ L with constant stirring for 1 min at 200 rpm. The CV was recorded three times for each addition of water to ensure reproducibility.

3.9. Steady state amperometry

0.1 M 1,3-cyclohexadiene was prepared for the organic sensor measurements. Cyclic voltammetry was performed in order to be able to characterize Pt electrode for application for steady state amperometry. As it was discovered that CHD was catalytically oxidized at -1404

mV, the amperometric measurements were done at this constant potential. 10 mL of acetonitrile containing 0.1 M TBAP was introduced to an electrochemical cell without any purging of argon the electrolyte was air saturated. Besides keeping the electrolyte in open air it was constantly stirred at 500 rpm .The current was allowed to retain a steady state, the first injection of CHD 5 μ L which is equal to 0.00005 M was introduced to the cell and a response was monitored over a period of time. Another addition of 0.00005 M followed by 40 μ L = 0.0004 M, 50 μ L = 0.0005 M then 100 μ L = 0.001 M in order to establish the lifetime of the organic sensor.



CHAPTER FOUR

RESULTS AND DISCUSSION



UNIVERSITY *of the*
WESTERN CAPE

4. Results and Discussion

4.1. Preliminary characterization of gold nanoparticles

4.1.1 Ultra-violet visible spectroscopy

The formation of gold nanoparticles by reduction of chlorauric acid by 1 % sodium citrate which resulted into a deep reddish colour was confirmed by ultra-violet visible spectroscopy.

In figure 1 an absorption band was observed at 585 nm which corresponds to a known surface plasmon absorption band of gold nanoparticles [1].

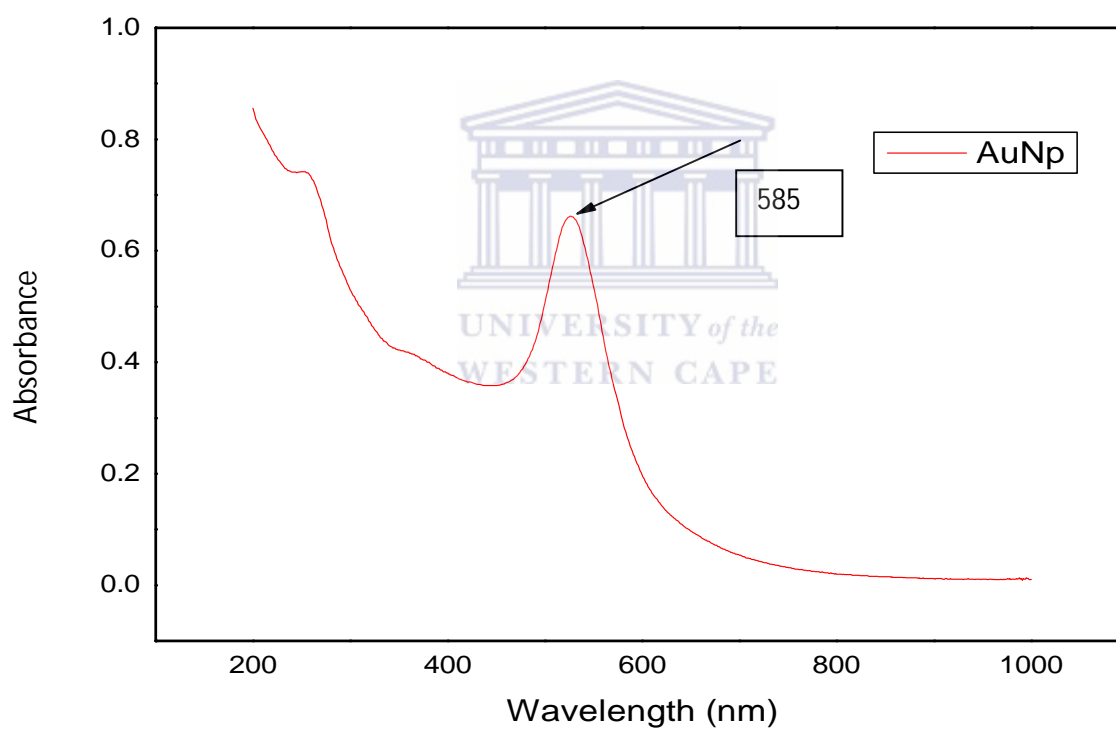


Figure 1: Ultra-violet visible spectroscopy of gold nanoparticles.

4.1.2 High resolution transmission electron spectroscopy

Further characterization of gold nanoparticles was done by TEM where a drop of the solution was coated on a carbon copper grid and dried under electric bulb for 20 min. in figure 2 spherical shaped gold nanoparticles was observed at 5 nm, to confirm the presence of gold nanoparticles an EDX spectrum was obtained of a single particle isolated on a copper grid in an HRTEM microscope. Peaks from each element are clearly represented in the particle as shown in figure 3 has confirmed that what was really observed was gold nanoparticles [2].

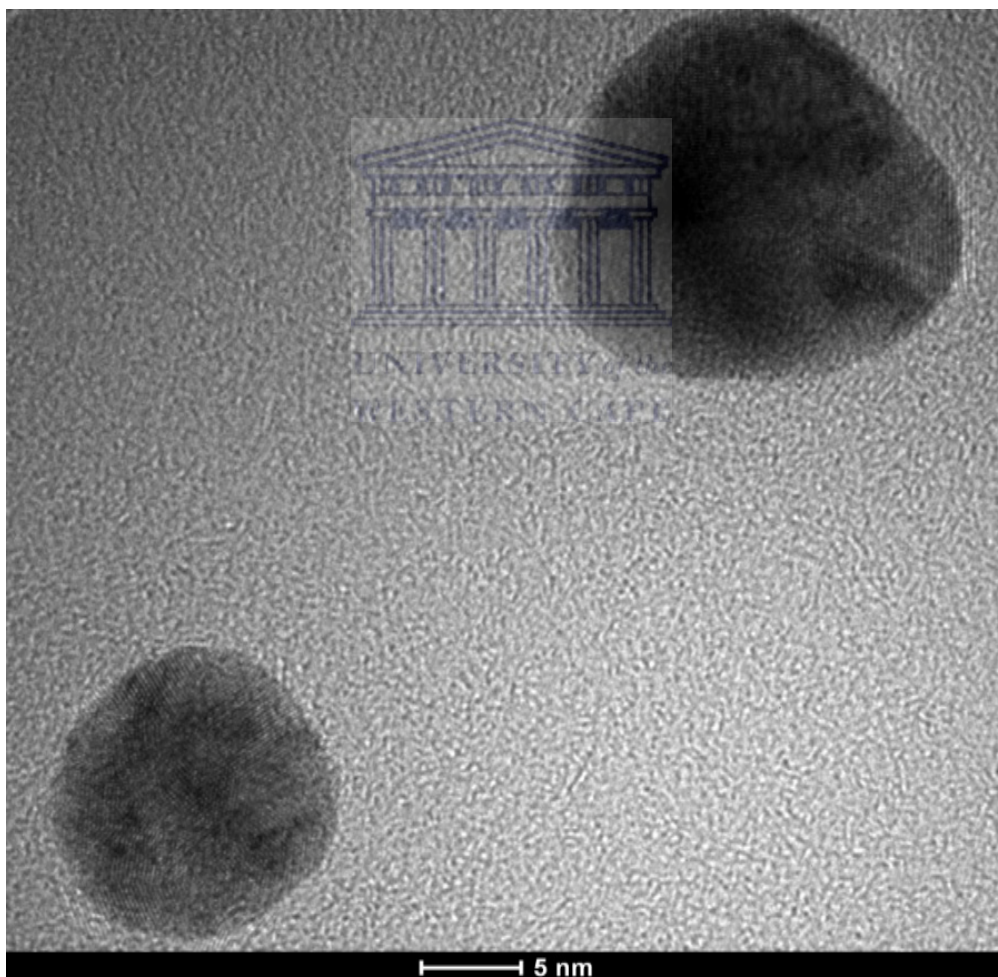


Figure 2: HRTEM for gold nanoparticles at 5 nm.

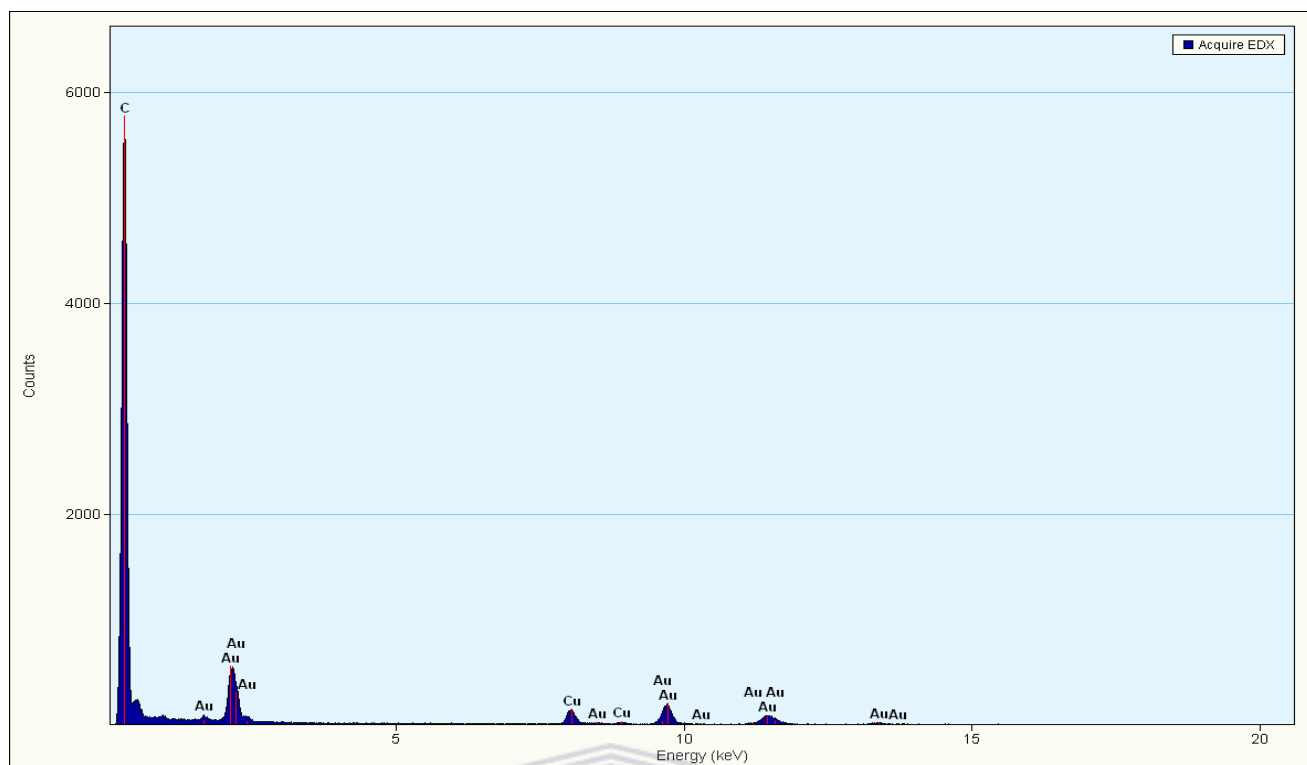


Figure 3: EDX for gold nanoparticles.

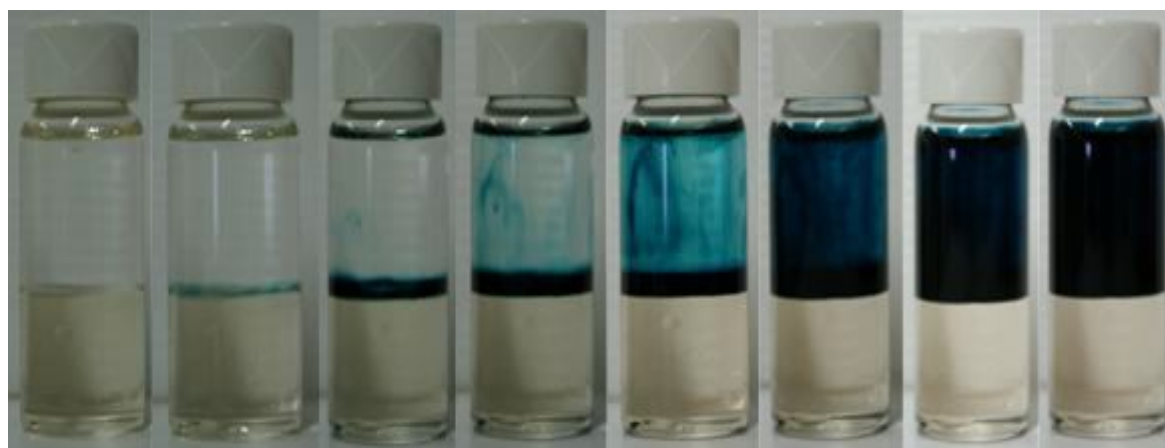


Figure 4: Interfacial polymerization of PANi, PANi/PSSA and PANi/PSSA/AuNP.

4.2. Preliminary characterization of interfacial chemical synthesis of PANi/PSSA/AuNP

4.2.1. Cyclic voltammetry

Having discussed the synthesis of the composites in the previous chapter and also illustrated in figure 4, now we turn to explore the electrochemical properties of these materials with different chemical properties. All the samples were dispersed in deionised water to form 1.0 mg/mL solution suspension and then 4 μL was drop coated on to a GCE.

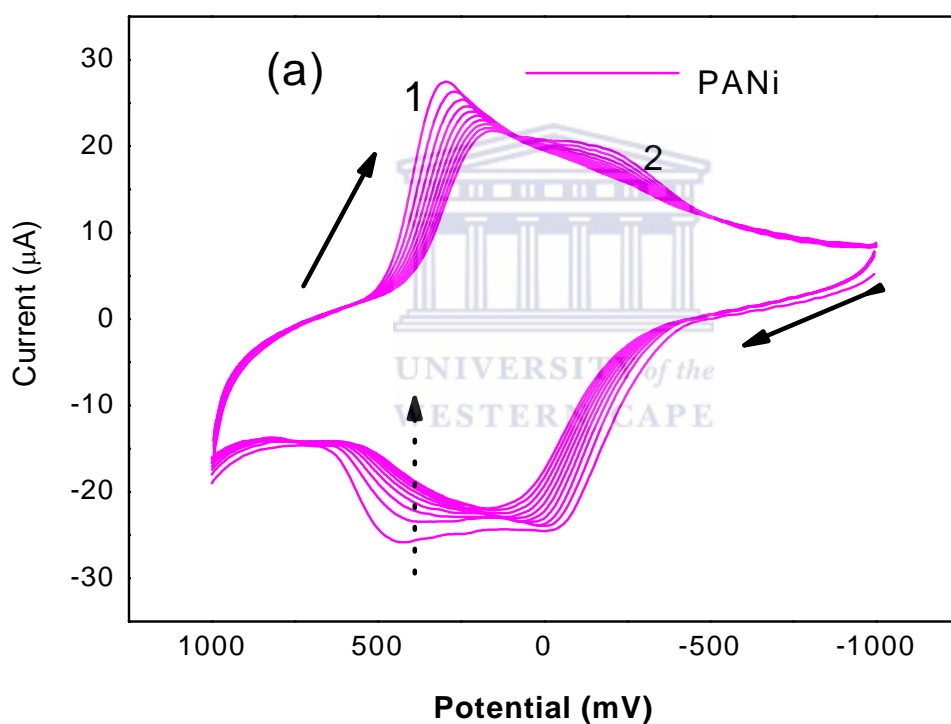


Figure 5: 10-cycle CV's of GCE modified with (a) PANi recorded in acetonitrile containing 0.1 M TBAP at 100 mV/s.

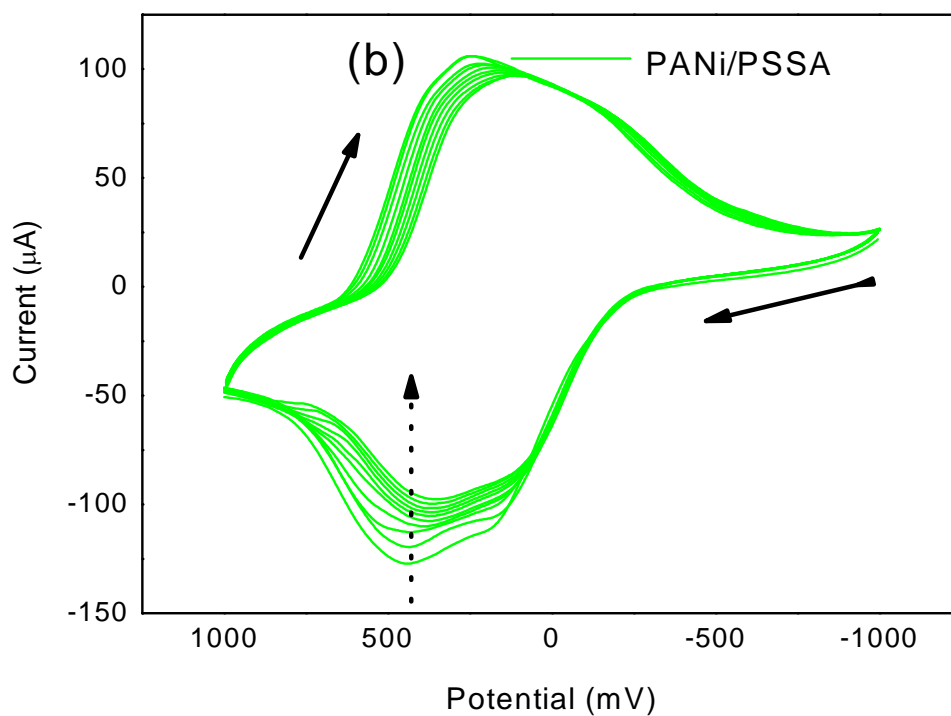


Figure 5: 10-cycle CV's of GCE modified with (b) PANi/PSSA recorded in acetonitrile containing 0.1 M TBAP at 100 mV/s.

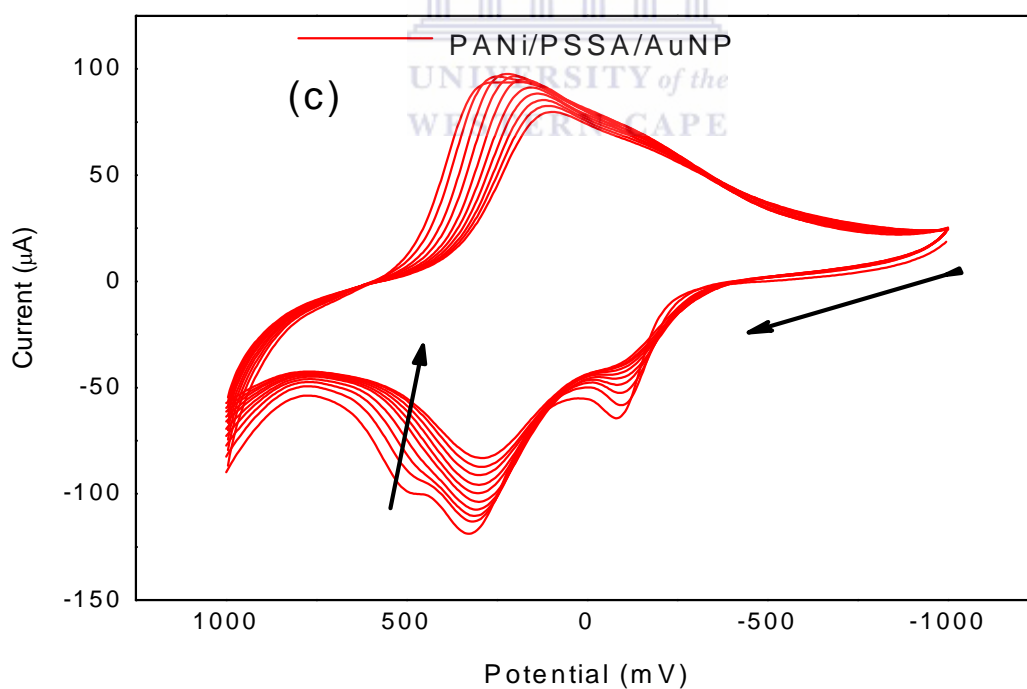


Figure 5: 10-cycle CV's of GCE modified with (c) PANi/PSSA/AuNP recorded in acetonitrile containing 0.1 M TBAP at 100 mV/s.

Figure 5(a) shows the cyclic voltammograms (CV's) obtained at the GCE/PANi, GCE/PANi/PSSA and GCE/PANi/PSSA/AuNP in 0.1 M acetonitrile+TBAP at a scan rate of 100 mV/s after 10 cycles. PANi and PANi/PSSA/AuNP are very similar in shape even though there is a much great difference in the current response. PSSA has more influence on the electrochemistry of PANi than AuNP [3]. There are three pairs of redox couple observed for polyaniline and polyaniline based composites in organic medium. The redox corresponded to the conversion of leucoemeraldine to emeraldine (peak 1) and the conversion of emeraldine to pernigraniline (peak 2). From figure 5 it can be observed that as the number of cycles increases the PANi and its two composites continues to decrease in current. There was stability issues associated with PANi and its two composites and the consideration of a suitable supporting electrolyte came into place. Perchloric acid (HClO_4) and lithium perchlorate (LiClO_4) were other supporting electrolyte used due to the different chemistry expected [4]. The experiment was done for each supporting electrolyte at 40 cycles for PANi at its two composites; it was observed that at 40 cycles LiClO_4 and HClO_4 were dying out giving a straight line at zero current and TBAP gave better results because after 40 cycles there was still PANi and its composites and it became zero after 80 cycles. Based on the state of the results a kind of sensor that will be developed it will be possible to use once and then discarded. The reason for decrease in current till zero is because of the impurities that were present in the solution during the storage of PANi and its two composites which caused degradation, PANi and its two composites were leaching out. PANi conducting polymers the same as other reactive and conducting organic materials suffer from their poor thermal stability in air because of the chemical reaction of oxygen with the highly conjugated system of PANi [5]. The same experiment was done in an acid medium 0.1 M H_2SO_4 for PANi and its two composites showed stability and the current was increasing. The focus of the study is not in inorganic medium it's in organic medium [6]. However, the dienes exhibited no redox

peaks between -1.0 V and +1.5 V, beyond which PANi would otherwise be overoxidized and lose its electroactivity. Furthermore, the drop-coated films did not give reproducible and steady background voltammogram as a result of which they could not be tested further for electrochemical sensing of the dienes.

Table 1: Theoretical yield characterization of PANi/PSSA/AuNP.

	Aniline	PSSA	Au
Amount in Reaction Mixture (μmol)	1600	40000	200
Mass in Reaction Mixture (mg)	149	8247	39.394
Mass/Mass/Mass Ratio in Reaction Mixture	3.78	209	1
Mol/Mol/Mol Ratio in Reaction Mixture	8	200	1

In table 1 it is clearly indicated the theoretical mole ratio of PANi/PSSA/AuNP which is important in order to be able to justify the nature of results observed. This proves that PSSA influenced the electroactivity of PANi due to its higher molar ratio reaction mixture observed in the above table.

4.2.2. High resolution transmission electron spectroscopy

The characterization of PANi by TEM nanofibers was observed at 100 nm in figure 6. In interfacial polymerization the interaction between initiator molecule and monomer are limited to essentially a two-dimensional spaces the aqueous/organic interface. Therefore only those

initiator molecules at the interface are capable of producing nucleation centres. Characterization of PANi/PSSA by TEM a spherical shape was observed due to agglomeration as illustrated in figure 7, this is caused by PSSA incorporating in the nanofibers filling the gaps and not uniformly distributed forming a spherically shaped structure. Characterization of PANi/PSSA/AuNP by TEM a dendritic structure with a dimension range of 100 nm is observed in figure 8, it is shown that PSSA slightly affect the shape of PANi because AuNP can still be observed in the structure. This proves AuNP is incorporated in PANi which is uniformly distributed [7].

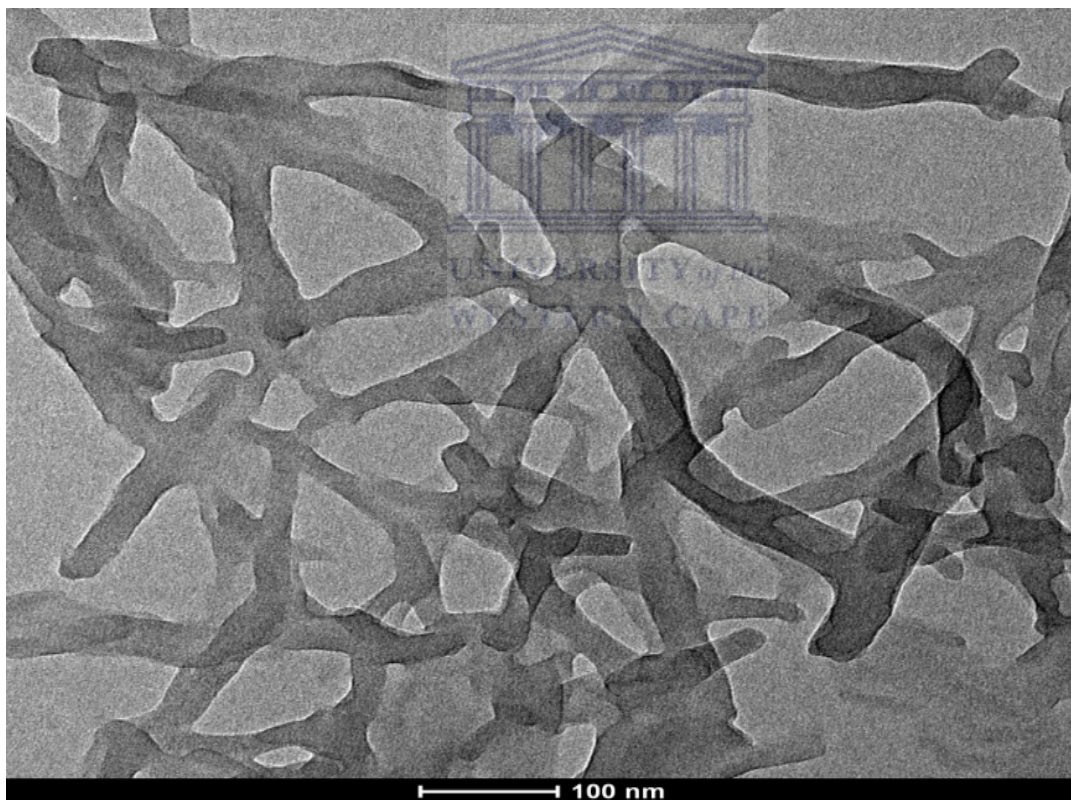


Figure 6: HRTEM for PANi nanofibers at 100 nm.

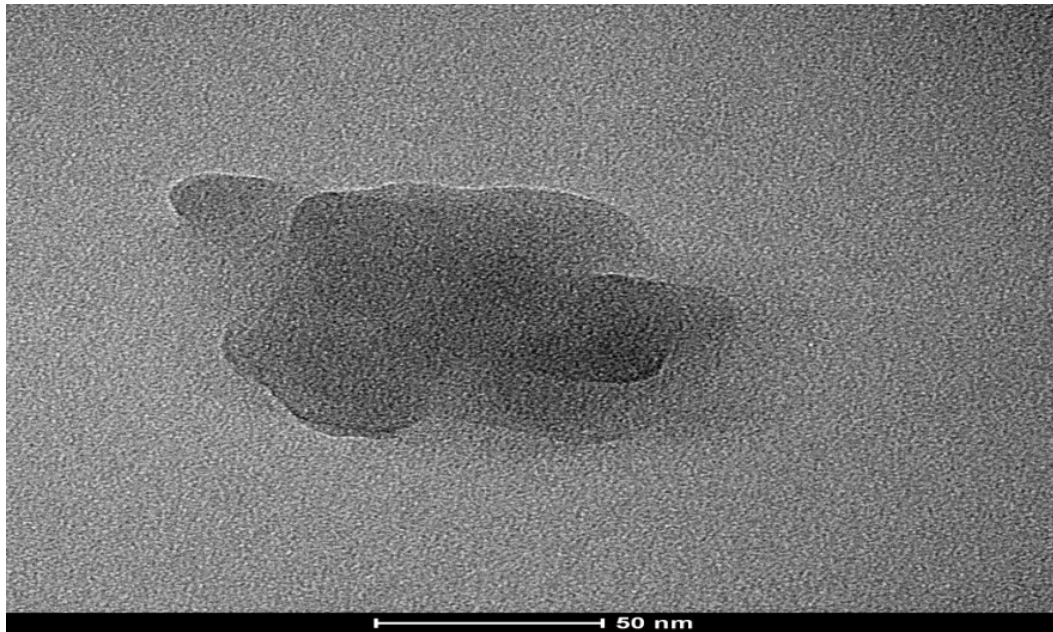


Figure 7: HRTEM of PANi/PSSA at 50 nm.

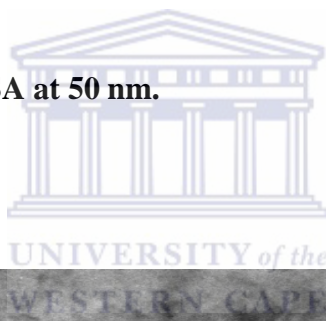


Figure 8: HRTEM for PANi/PSSA/AuNP at 100 nm.

4.2.3. Ultra-violet visible spectroscopy

The interfacial polymerization of PANi, PANi/PSSA and PANi/PSSA/AuNP was characterized by ultra visible spectroscopy. The UV-vis spectrum of PANi shows three bands at 320 nm, 430 nm and 710 nm in figure 9, characteristic of doped polyaniline in its emeraldine salt form, and the bands are attributed to $\pi-\pi^*$, polaron- π^* and π -polaron transition [8]. There are two adsorption bands in the uv-vis spectra of PANi/PSSA and PANi/PSSA/AuNP where two of them are characteristic bands of doped PANi and a new peak at 226 nm is attributed to $\pi-\pi^*$ transition of a benzene ring present in PSSA. The intensity of the polaron band at 700-1000 nm is significantly increased for PANi/PSSA when compared to PANi/PSSA/AuNP [9]. Increased peak intensity was attributed to the increase in proton doping. The polaron band in the case of PANi/PSSA (730 nm) is more blue shifted with more increasing peak intensity compared to that of PANi/PSSA/AuNP (770 nm). Since the absorption of the polaron band is strongly dependent on the molecular weight and proton action level of the PANi, this indicates a difference in molecular weight or protonation level of the polymer. AuNP appears at 585 nm is not observed it is well known that surface Plasmon resonance band of metal nanoparticles are sensitive to their surrounding environment and certain environment may result in the diminishing of the AuNP peak in its composite[10]

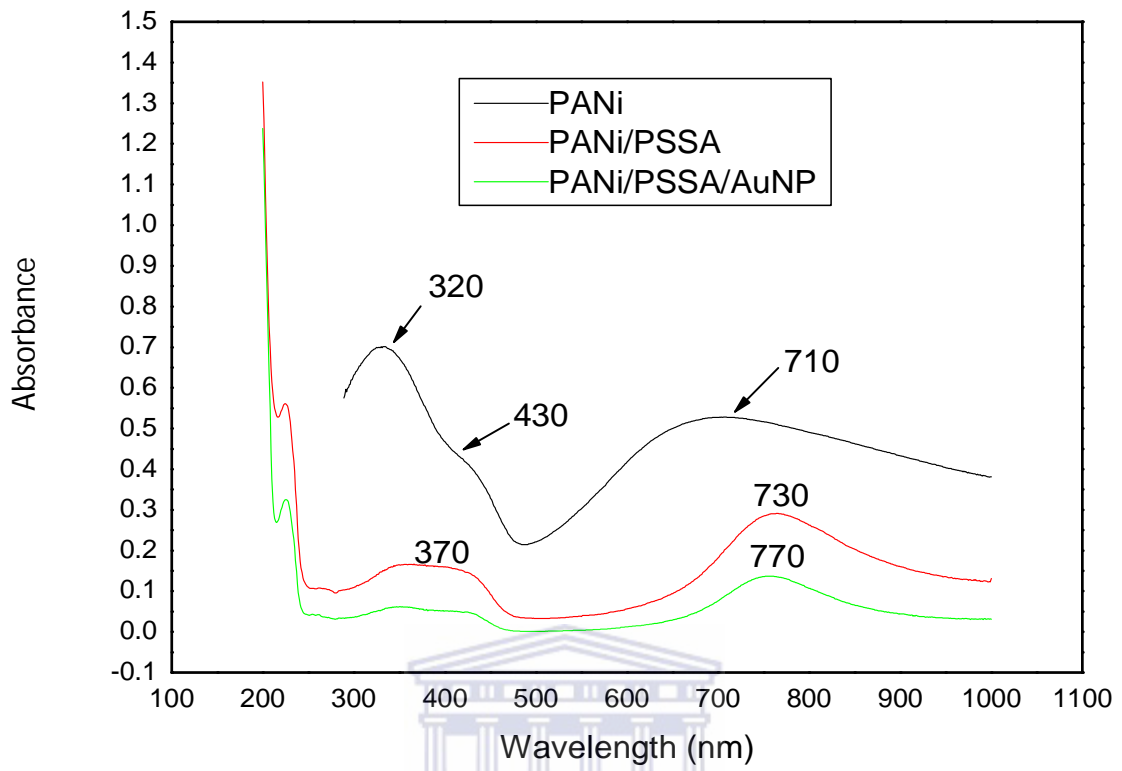


Figure 9: UV-vis absorption spectra of PANi, PANi/PSSA and PANi/PSSA/AuNP.

4.4. Preliminary electrosynthesised PANi

4.4.1. Cyclic voltammetry

Well pronounced redox couple conversion of leucoemeraldine to emeraldine in (peak 1) and to the conversion of emeraldine to pernigraniline is observed in (peak 3) of figure 10. There is also an intermediate redox pair to the degradation of the polymer in peak 2 in 0.1 M H_2SO_4 . In acetonitrile containing 0.1 M TBAP the leucoemeraldine to emeraldine and emeraldine to pernigraniline peak is not that well pronounced as compared to the peak in 0.1 M H_2SO_4 . The major highlight about electropolymerization of PANi in both electrolytes there is reproducibility due to the level of purity. Current does not decrease with number of cycles, PANi is very stable and pure [11]. Dienes exhibited no redox peaks between -1.0 V and +1.5 V, beyond which PANi would otherwise be overoxidized and loss its electroactivity. PANi is not useful for this study reproducibility is not an issue for constructing a sensor.

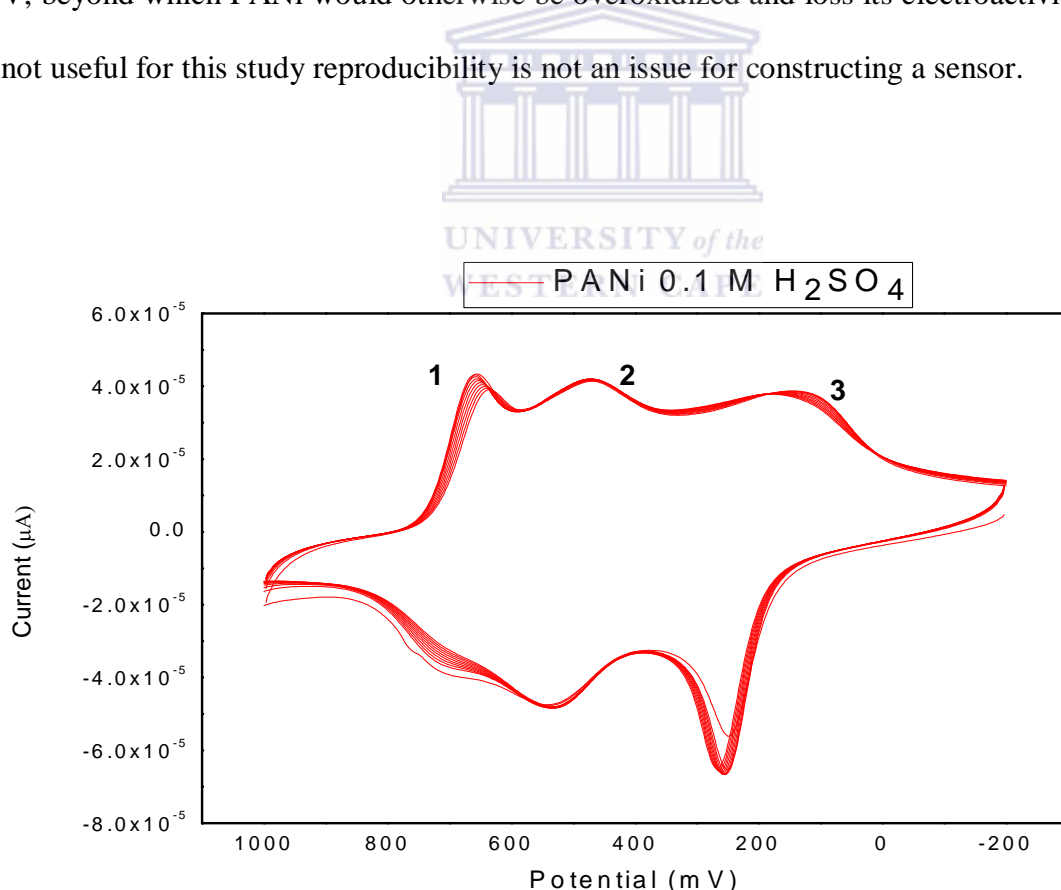


Figure 10: 10-cycle CV of electropolymerised PANi on GCE in 0.1 M H_2SO_4 at 100 mV/s.

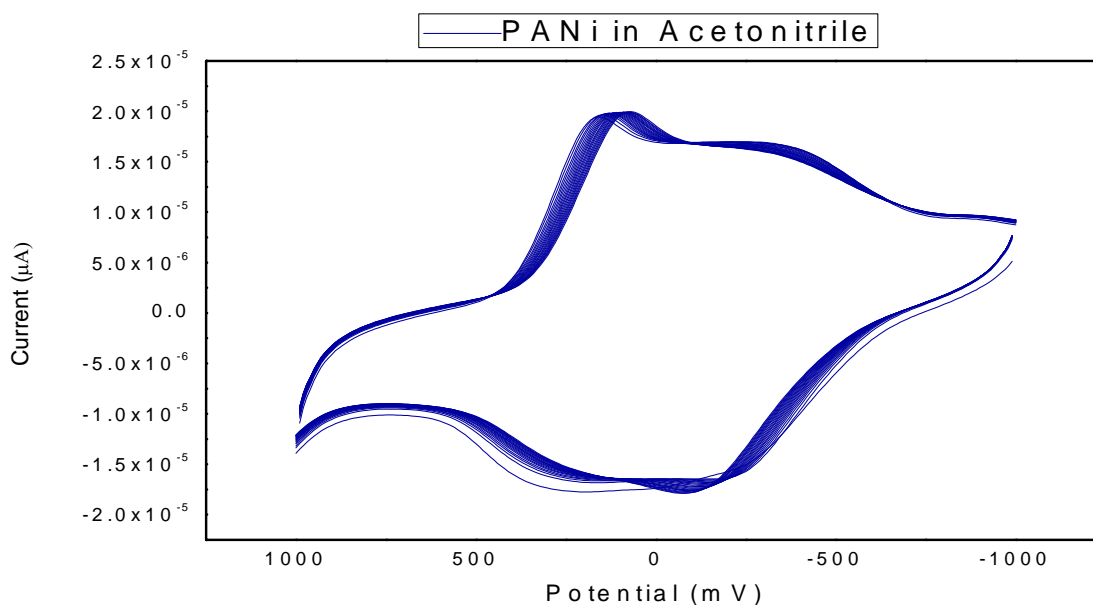


Figure 11: 10-cycle CV of electropolymerised PANi on GCE in acetonitrile containing 0.1 M TBAP at 100 mV/s.

4.5. Ferrocene

Pt wire has been used as a pseudo reference electrode for the study of electrode reaction kinetics and has an advantage of simplicity, convenience and easy to operate unlike Ag/AgCl electrode. The Ag/AgCl electrode has a limited range of application; the liquid junction is problematic with this electrode more especially in organic medium. The Pt wire can maintain a steady potential for more than 12 hours when immersed in molten NaCl/KCl. Since lots of voltammetric studies have been done on oxidation of ferrocene, it can be used as an internal reference [12]. Adding the analyte and ferrocene in solution then subtract the potential of the analyte from the potential of ferrocene can give the exact potential of the analyte. Some of the problems associated with the reference electrode can be solved outside the electrochemical cell. A reference electrode is defined as an ideal non-polarisable electrode thus its current does not vary with the current passing. In practical terms no reference electrode follows this ideal behaviour, consequently the interfacial potential of the counter

electrode in the two electrode system varies with the flow of current which can be overcome with a three electrode system. In reference to this experiment the electrochemical experiment was repeated and the position of the wave was directly compared to the potential of the ferrocenium/ferrocene couple [13].

4.5.1 Cyclic voltammetry

The cyclic voltammetry was performed where 0.001 M ferrocene was added together with 0.002 M conjugated diene in 10 mL acetonitrile containing 0.1 M TBAP. Where ferrocene was an internal reference as explained above.

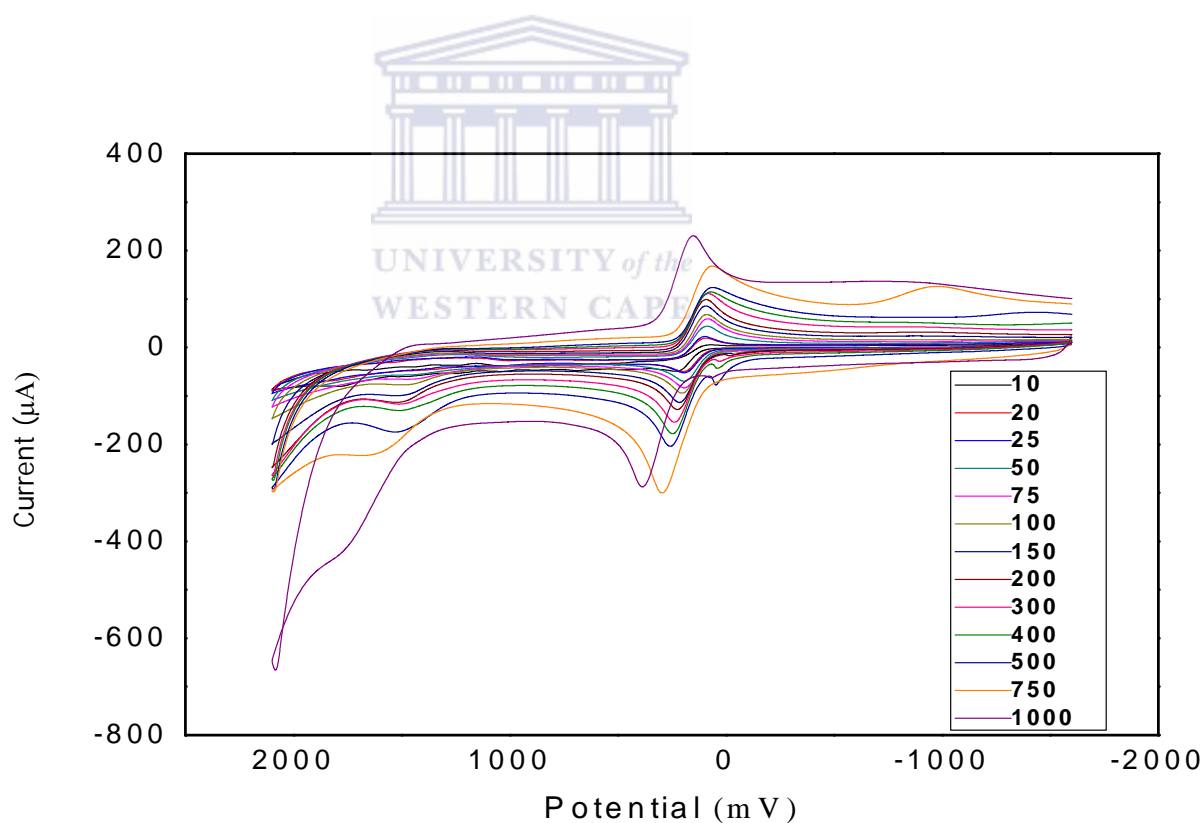


Figure 12: CV of 0.001 M ferrocene in acetonitrile containing 0.1 M TBAP on GCE.

The above cyclic voltammetric figure **12** can be observed ferrocene gave a redox couple, as expected as the scan rate decreases a decrease in current is observed. The ferrocene is not the major focus of the study even though is useful to report the exact position of the wave of the analyte of interest.

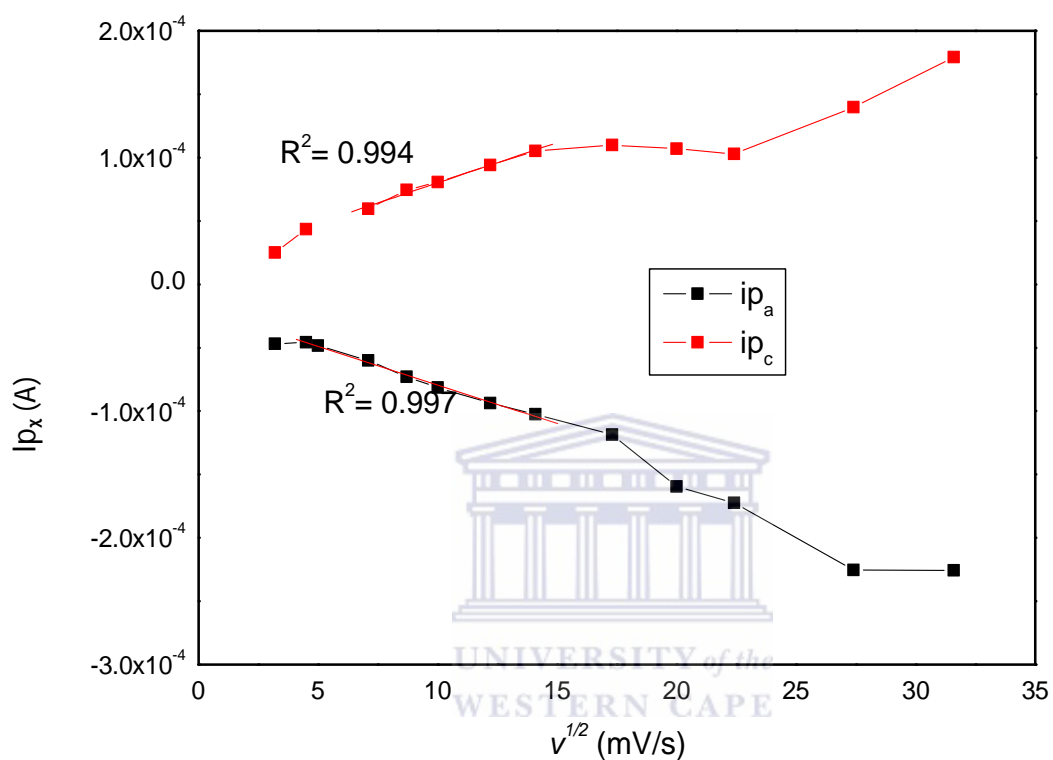


Figure 13: ip_a and ip_c versus $v^{1/2}$ of ferrocene.

In the above figure the peak current should be linear with the $v^{1/2}$, it shows characteristics of linearity

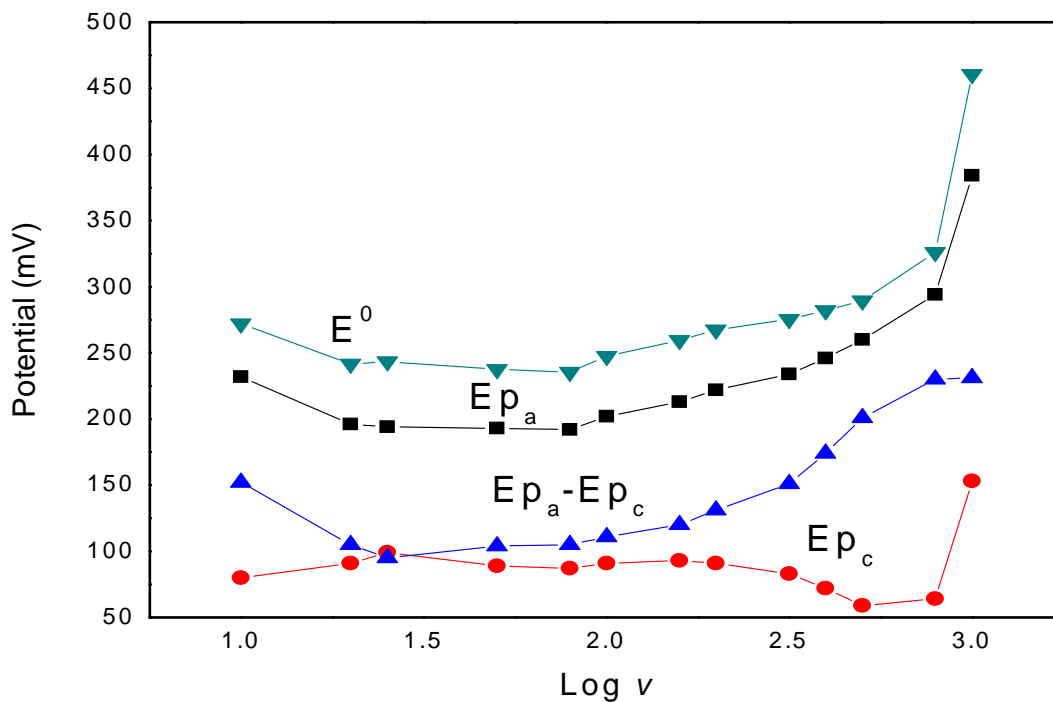
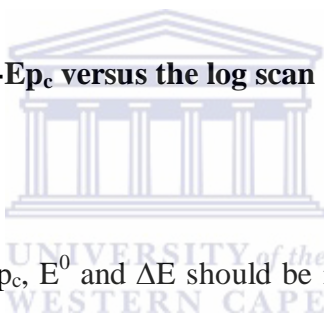


Figure 14: E_{p_a} , E_{p_c} , E^0 and $E_{p_a} - E_{p_c}$ versus the log scan rate of ferrocene.



The above figure 14 were E_{p_a} , E_{p_c} , E^0 and ΔE should be invariant with the log of scan rate and the slope = 0. The general tendency of invariance was observed during the experiment. There are several possible causes of deviation which in this experiment were experimental error and the uncompensated solution resistance. Ferrocene can be used to calculate the effective area of the electrode when the conjugated dienes are added in the electrolyte and be compared with the actual area to observe how much of the analyte was deposited on the electrode surface [14].

4.6. Electrochemical characterization of conjugated dienes

There has been much more focus on conjugated dienes due to their disadvantages caused. Much more focus has been on chromatographic, spectrometric methods and maleic anhydride reaction less attention has been given to voltammetric methods. There is little or no information on the kinetics of dienes and their electrochemistry. Most studies has been done on Brazilian gasoline where working electrode was hanging mercury drop electrode, the voltammogram was recorded in a potential range between -2.25 and -2.95 V. A platinum wire was a counter electrode and all potentials were quoted against a non-aqueous reference electrode filled with saturated LiCl in ethanol. The conjugated dienes are well known of two electron reduction at the mercury electrode in the presence of proton donors. Isolated double bonds and non-conjugated dienes were known of being inactive electrochemically. For practical proposes regardless of the structure of the diene, 1 mol of conjugated double bonds always consumes 2 mol of electrons in the voltammetric reduction. The voltammetric analysis of conjugated dienes in this study by GCE and Pt electrode has never been reported according to the authors. The kinetics investigation will be of great benefit for a development of a sensor for the detection of this conjugated dienes in gasoline.

4.6.1 Cyclic voltammetry

4.6.1.1 Concentration variation of conjugated dienes

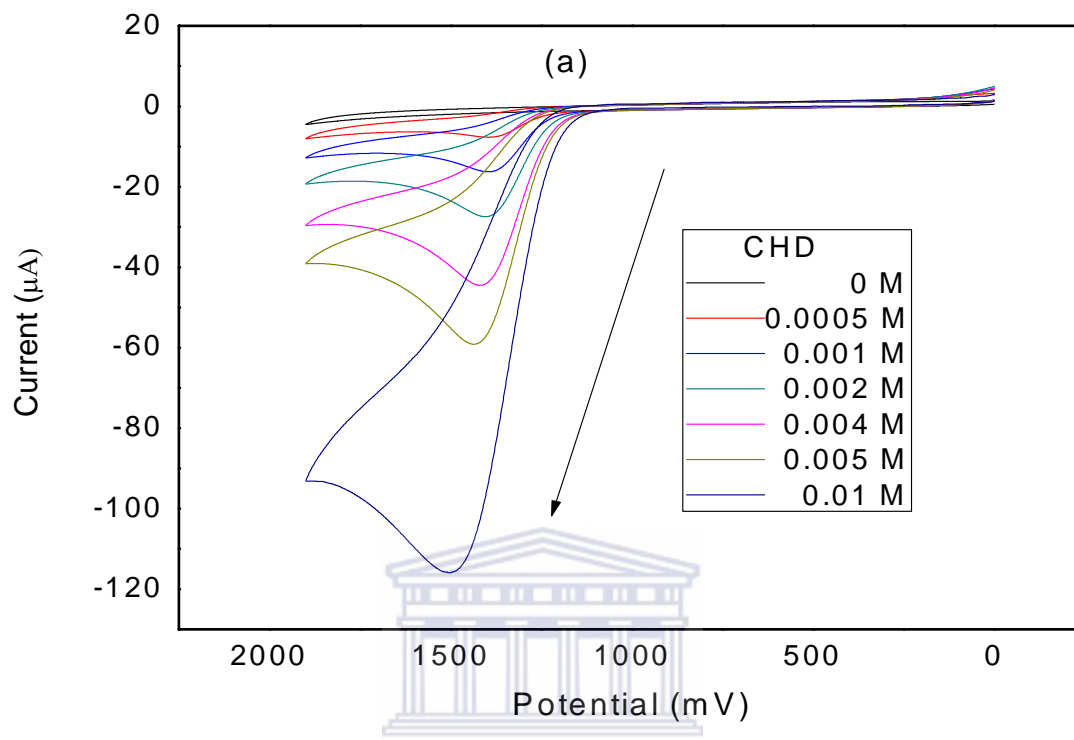


Figure 15: (a) Cyclic voltammogram of 1,3-cyclohexadiene in acetonitrile containing 0.1 M TBAP at 100 mV/s.

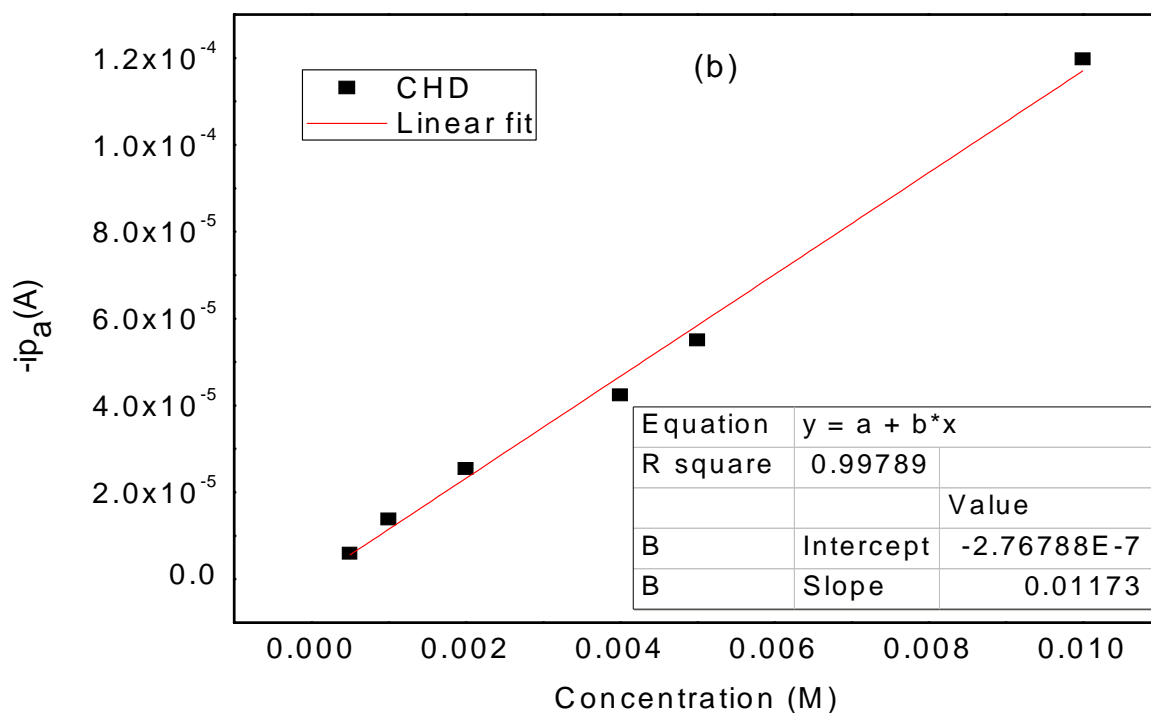
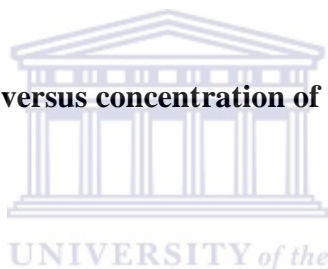


Figure 15: (b) A plot of current versus concentration of CHD.



In figure **15(a)** an oxidation peak of CHD is observed at a potential between 1544 mV at high concentration and 1238 mV at low concentration with the variation in concentration. A linear plot has been observed in figure **15(b)** with a $R^2 = 0.99789$ which is an indication that CHD can be applied for the development of an organic sensor. Previous studies has been done on CHD with a GCE where the $R^2 = 0.55804$ which was an indication that there was a process of fouling at the electrode surface. Pt electrode has minimised the effect of fouling. The detection limit for CHD from standard solution was calculated as the concentration to the signal three times the standard deviation of the blank measurement was 0.0106 M. The

following formula was used to obtain detection limit; $DL = \frac{3 \times SD}{Slope}$.

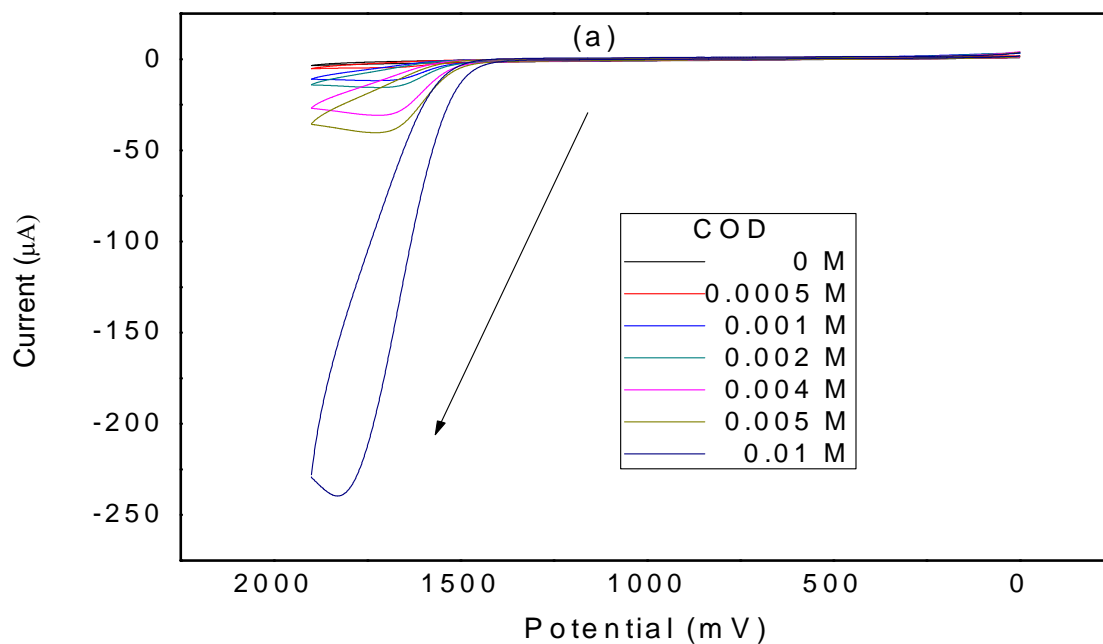


Figure 16: (a) Cyclic voltammogram of 1.3-cyclooctadiene in acetonitrile containing 0.1 M TBAP at 100 mV/s.

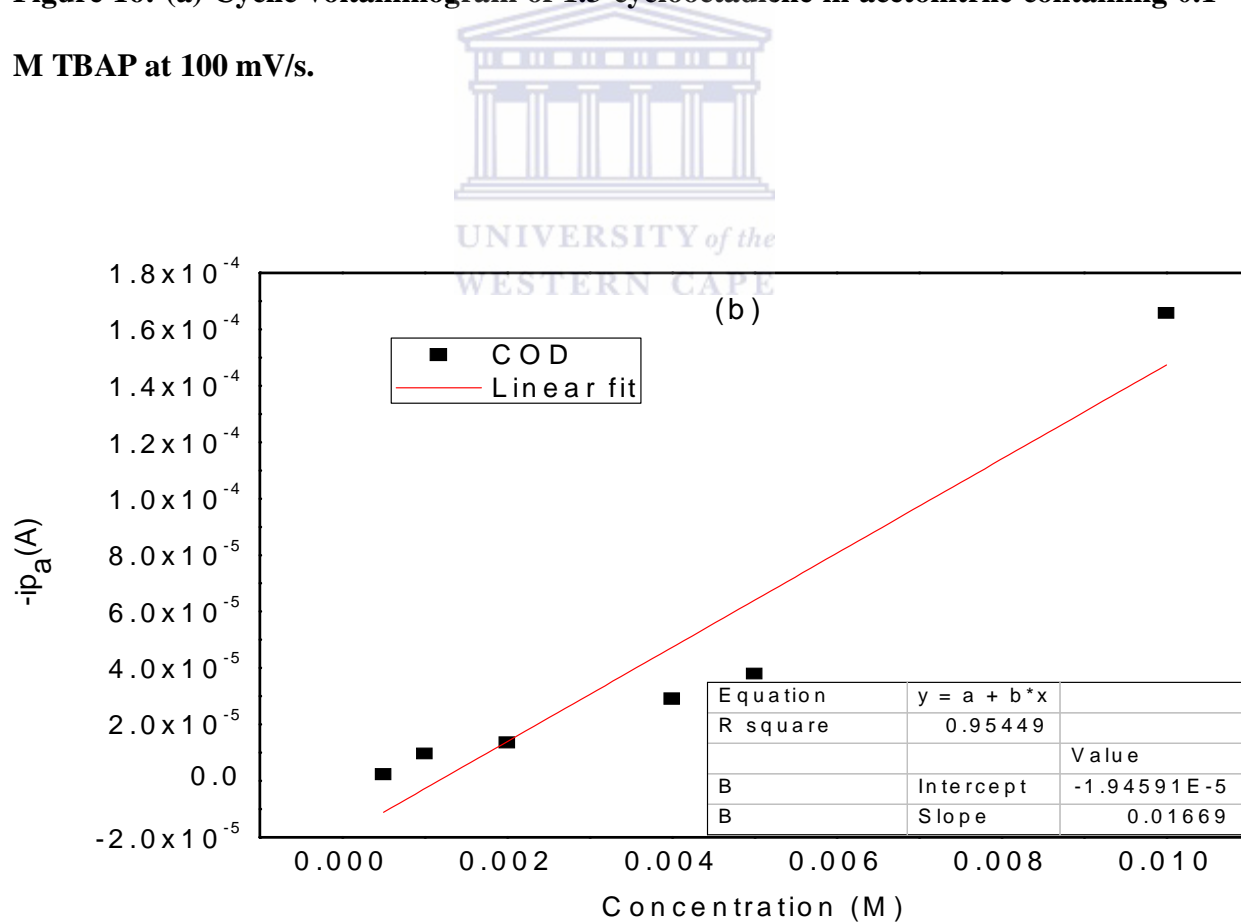


Figure 16: (b) A plot of current versus concentration of COD.

In figure **16(a)** an oxidation peak potential is observed between 1682 mV at high concentration and 1626 mV at low concentration with a variation in concentration. A linear plot of COD in figure **16(b)** has an $R^2 = 0.95449$ which is an indication that there might be a slight fouling which can be decrease by an immobilization of a conducting material on the electrode surface. When the R^2 value is asset one can confidently state the conjugated diene shows an indication that it can be used for the development of an organic sensor. When this same study was done on the GCE it was observes that the linear plot R^2 value was much better than that of Pt electrode which was 0.98913. The reason that Pt electrode is much better suited for the study is because in figure **15(b)** it gave a much better response as compared to GCE and for COD there is an alternative how to improve the results as suggested above. In the case of CHD on GCE there was no solution due to advanced fouling. The detection limit for COD from standard solution was calculated as the concentration to the signal three times the standard deviation of the blank measurement was 0.0111 M. The following formula was used to obtain detection limit; $DL = \frac{3 \times SD}{Slope}$.

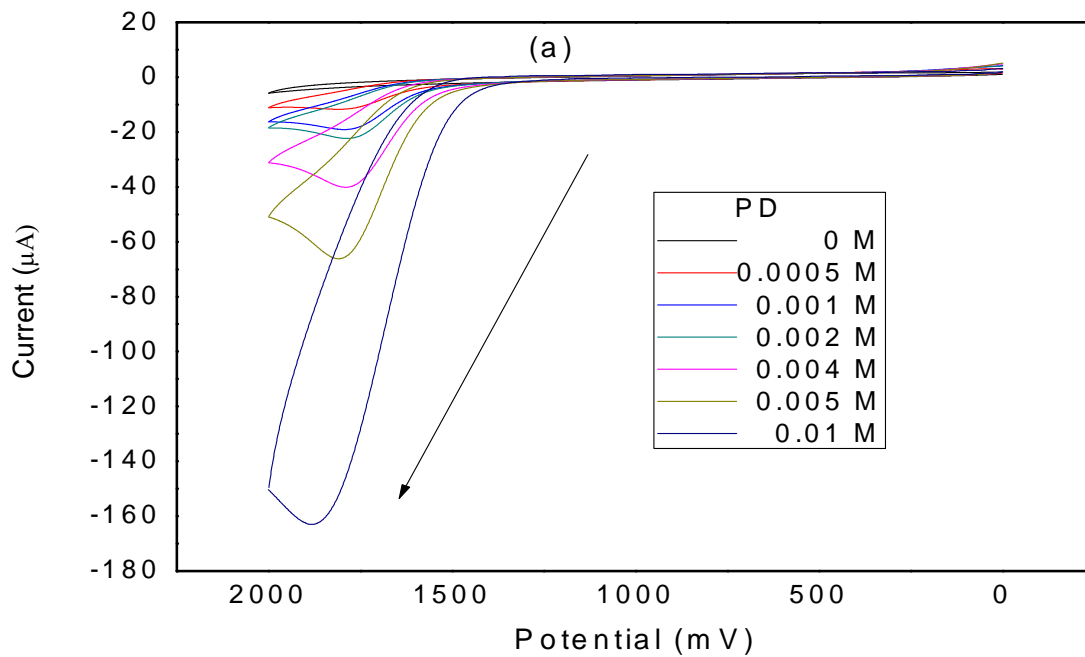


Figure 17: (a) Cyclic voltammogram of trans-1.3-pentadiene in acetonitrile containing 0.1 M TBAP at 100 mV/s.

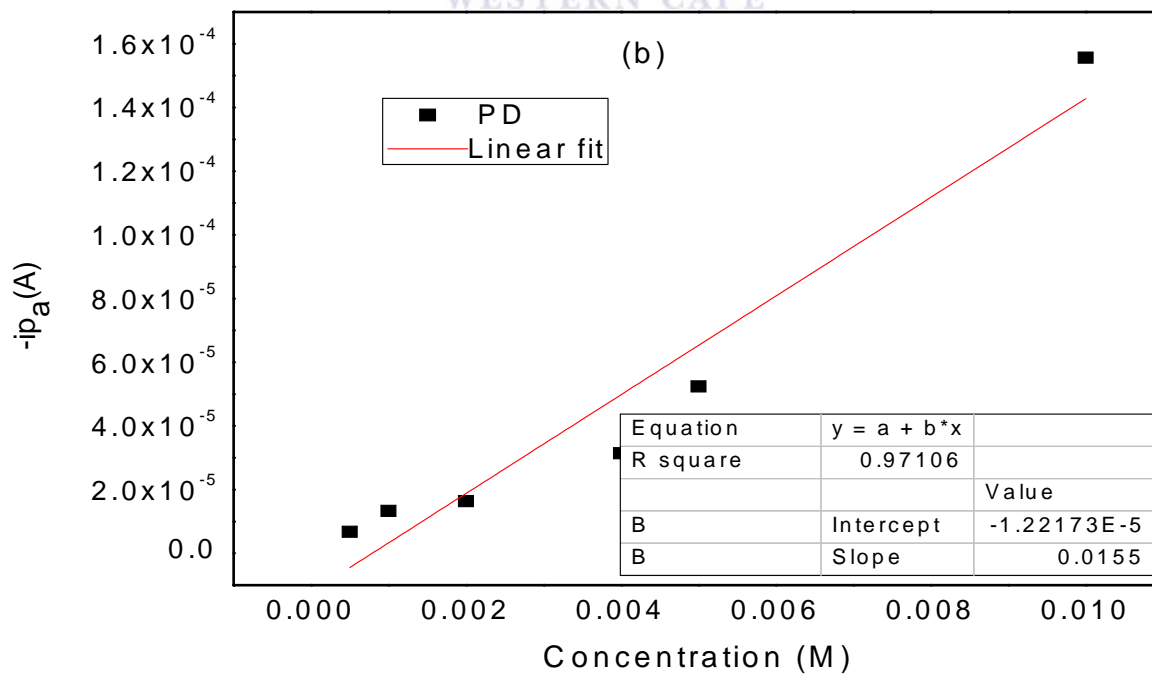


Figure 17: (b) A plot of current versus concentration of PD.

In figure 17(a) an oxidation peak is observed at a potential between 1972 mV at high concentration and a potential of 1662 mV at low concentration. In figure 17(b) a linear plot of PD has an $R^2 = 0.97106$ on a Pt electrode which indicate that PD can be used for the development of an organic sensor. On a GCE the $R^2 = 0.94801$ one can clearly state that Pt electrode shows better result. This is proving that the conjugated dienes has the tendency to produce products that adhere to the electrode surface and that effect is minimized by a Pt electrode. The detection limit for PD from standard solution was calculated as the concentration to the signal three times the standard deviation of the blank measurement was 0.0109 M. The following formula was used to obtain detection limit; $DL = \frac{3 \times SD}{Slope}$.

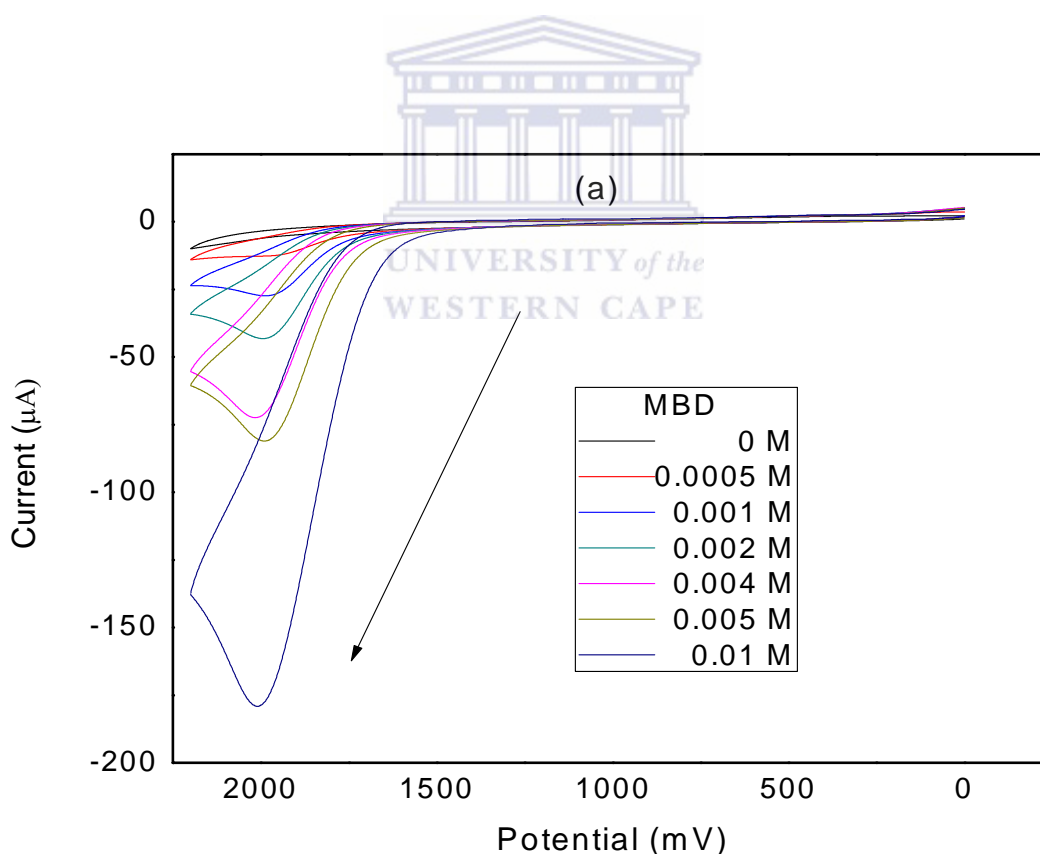


Figure 18: (a) Cyclic voltammogram of 2-methyl-1,3-butadiene in acetonitrile containing 0.1 M TBAP at 100 mV/s.

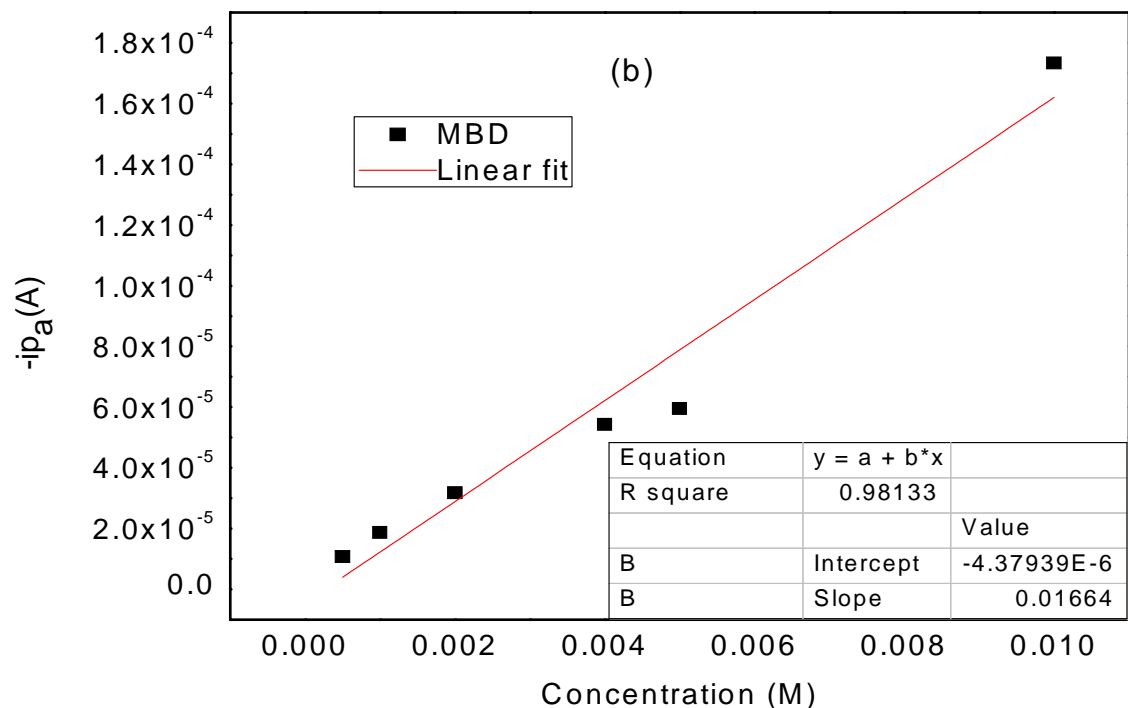


Figure 18: (b) A plot of current versus concentration of MBD.



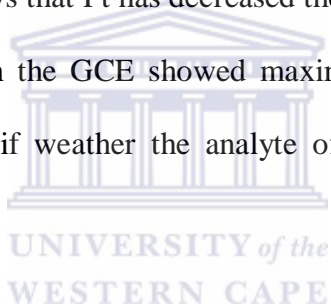
In figure **18(a)** an oxidation peak is observed between 1989 mV at higher concentration and 1932 at lower concentration. In figure **18(b)** a linear plot has an $R^2 = 0.98133$ which is also an indication that this conjugated diene can be applied for the development of an organic sensor. On a GCE the $R^2 = 0.90612$ which shows clearly Pt has decreased the effect of fouling. The detection limit for MBD from standard solution was calculated as the concentration to the signal three times the standard deviation of the blank measurement was 0.0107 M. The

following formula was used to obtain detection limit; $DL = \frac{3 \times SD}{Slope}$.

Table 2: Comparison of linear regression of GCE and Pt electrode of conjugated dienes

Conjugated Dienes	GCE Linear Regression	Pt Electrode Linear Regression
1.3-cyclohexadiene	0.55804	0.99789
1.3-Cyclooctadiene	0.98913	0.95449
Trans-1.3-Pentadiene	0.94801	0.97106
2-Methyl-Butadiene	0.90612	0.98133

On the table above it clearly shows that Pt has decreased the effect of fouling more especially for 1.3-cyclohexadiene which on the GCE showed maximum level of fouling. The linear regression is useful to indicate if weather the analyte of interest can be applied for the development of a sensor.



4.6.1.2 Scan rate variation of conjugated dienes.

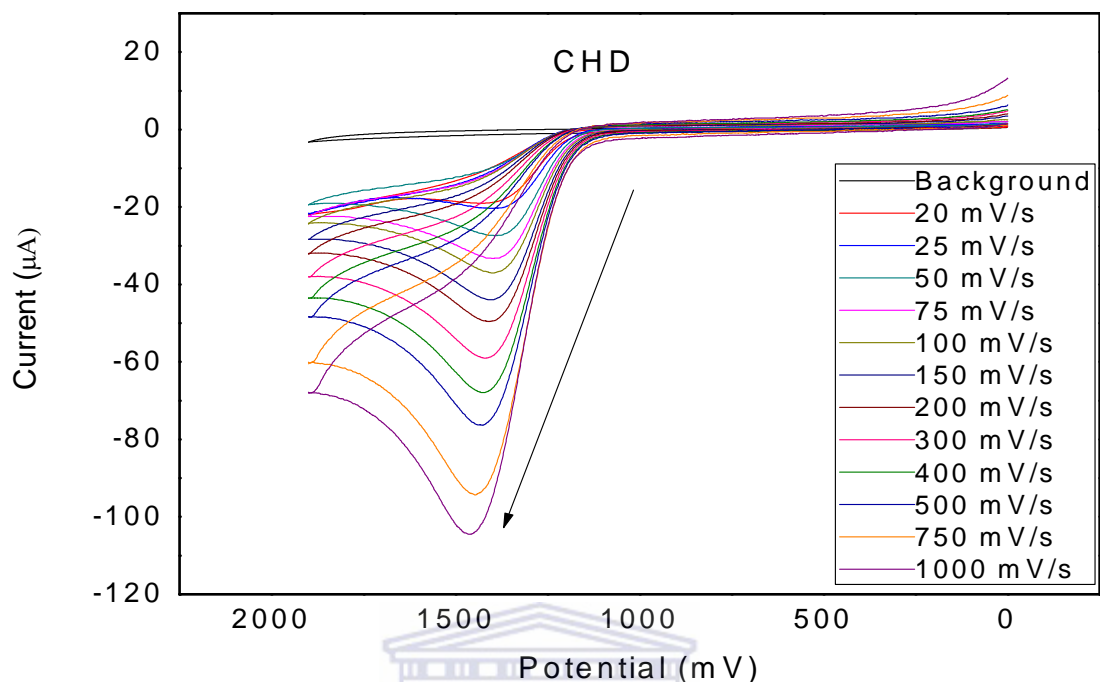


Figure 19: Cyclic voltammogram of 1.3-cyclohexadiene on Pt working electrode in acetonitrile containing 0.1 M TBAP with variation of scan rate from 1000, 750, 500, 400, 300, 200, 150, 100, 75, 50, 25 and 20 mV/s.

In figure **19** an oxidative peak is observed which the current decreases with the scan rate, the peak potential of 1.3-cyclohexadiene was not constant. There was a slight shift in the potential peak with the decrease in scan rate. Between 1000, 750, 500, 400, 300 and 200 mV/s the peak potential is more or less the same and the potential peak for 150, 100, 75, 50, 25 and 20 mV/s is more or less the same. The experiment was repeated three times at each scan rate, this was performed to observe if there was any form of deposition at the electrode surface and if weather the results are reproducible. It was found that the results were reproducible.

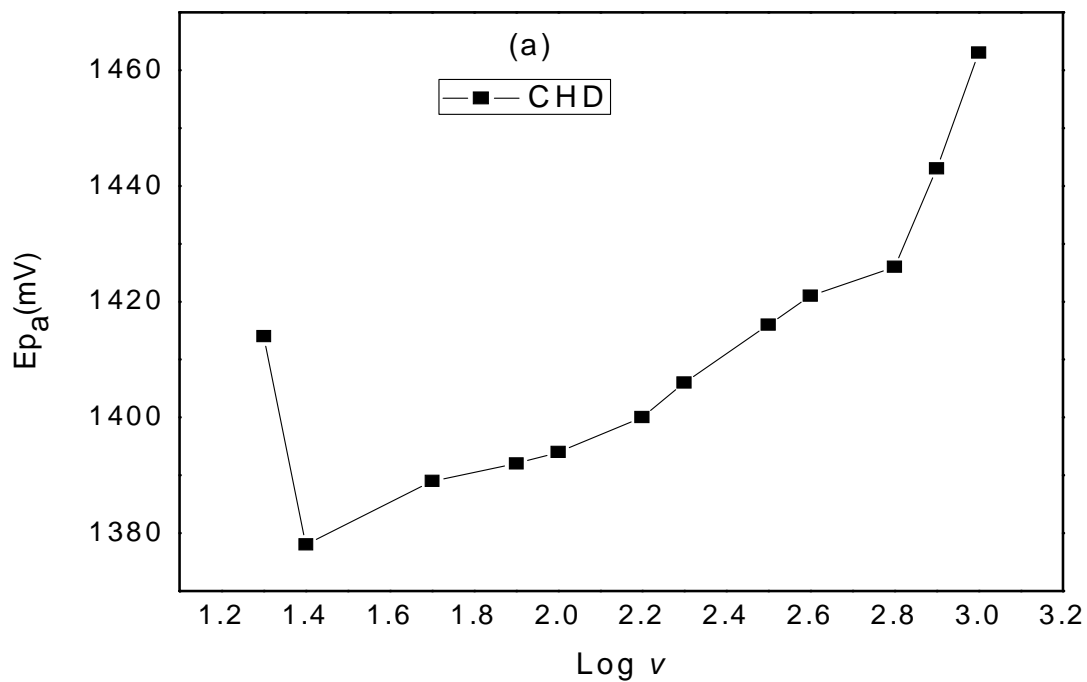


Figure 20: (a) A plot of anodic peak potential versus log of scan rate of CHD.

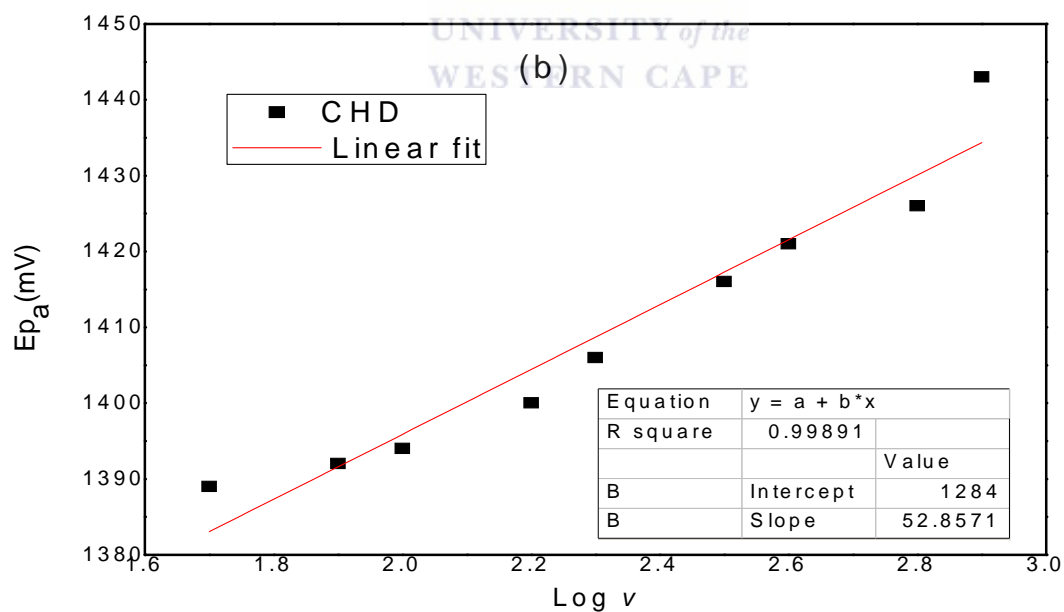


Figure 20: (b) A linear plot of anodic peak potential versus log scan rate for CHD.

In the above figure **20(a)** shows characteristics of irreversibility more especially at higher scan rate. The linear plot in figure **20(b)** is done at higher scan rate which shows good linear regression value of 0.99891. The slope of 53 was used to calculate the number of electrons

and α value with the following formula; $Slope = \frac{30}{\alpha n_{\alpha}}$

$n = 1.132 \approx 1$ and $\alpha = 0.49 \approx 0.5$

The suggested mechanism of the reaction at the electrode surface it involves a one electron transfer is as follows;



Where CHD is a neutral species and CHD^+ is a radical cationic which explains the oxidation peak observed in figure **19**.

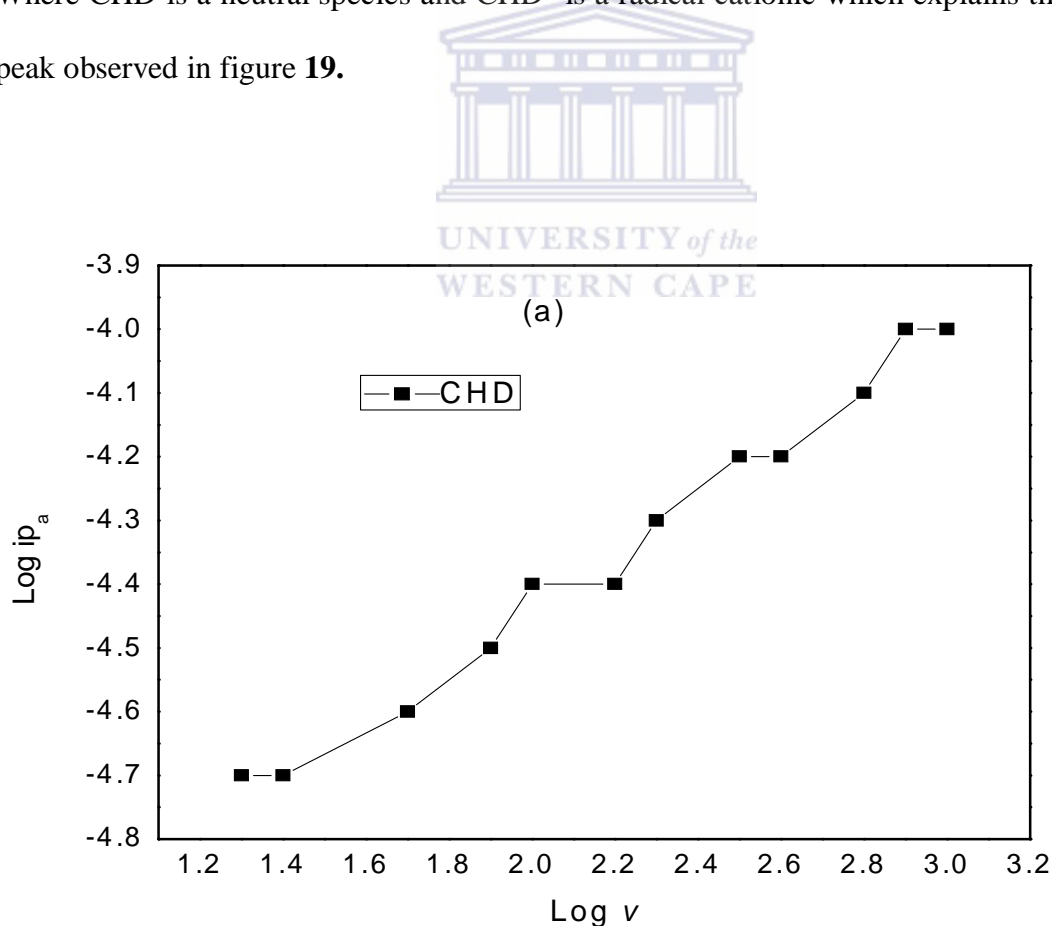


Figure 21: (a) A plot of log of anodic peak current versus log scan rate for CHD.

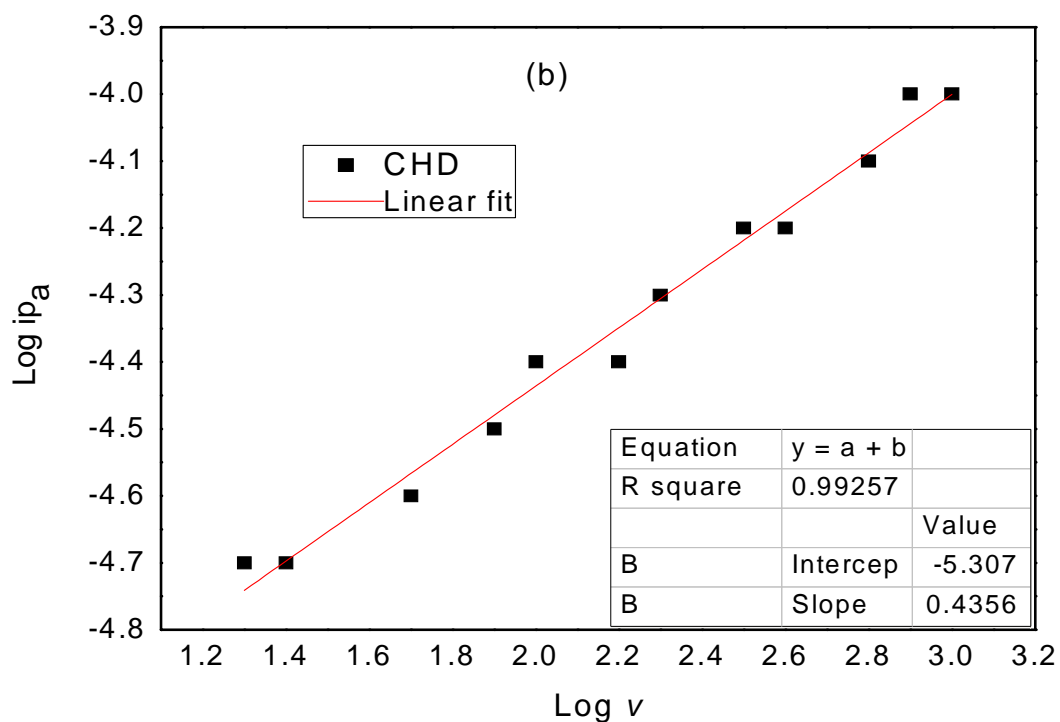


Figure 21: (b) A linear plot of log of anodic current versus log of scan rate for CHD.

In the above figure **21(a)** shows the logarithmic of peak current increases with logarithmic of scan rate which gives an ideal linear plot in figure **21(b)** with a linear regression of 0.99257. The slope = 0.436 which confirms that the reaction is diffusion controlled due to the unequal charge distribution (i.e. in such a zone the principle of electro-neutrality is not valid) due to the electron transfer processes occurring at the electrode surface.

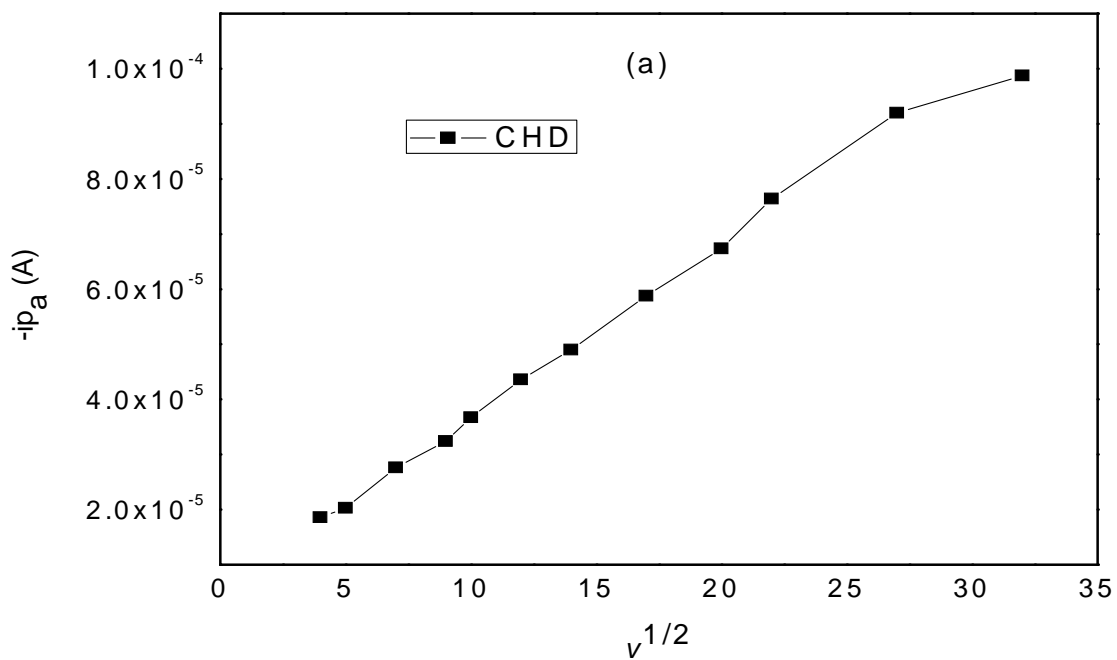


Figure 22: (a) A plot of anodic peak current versus square root of scan rate of CHD.

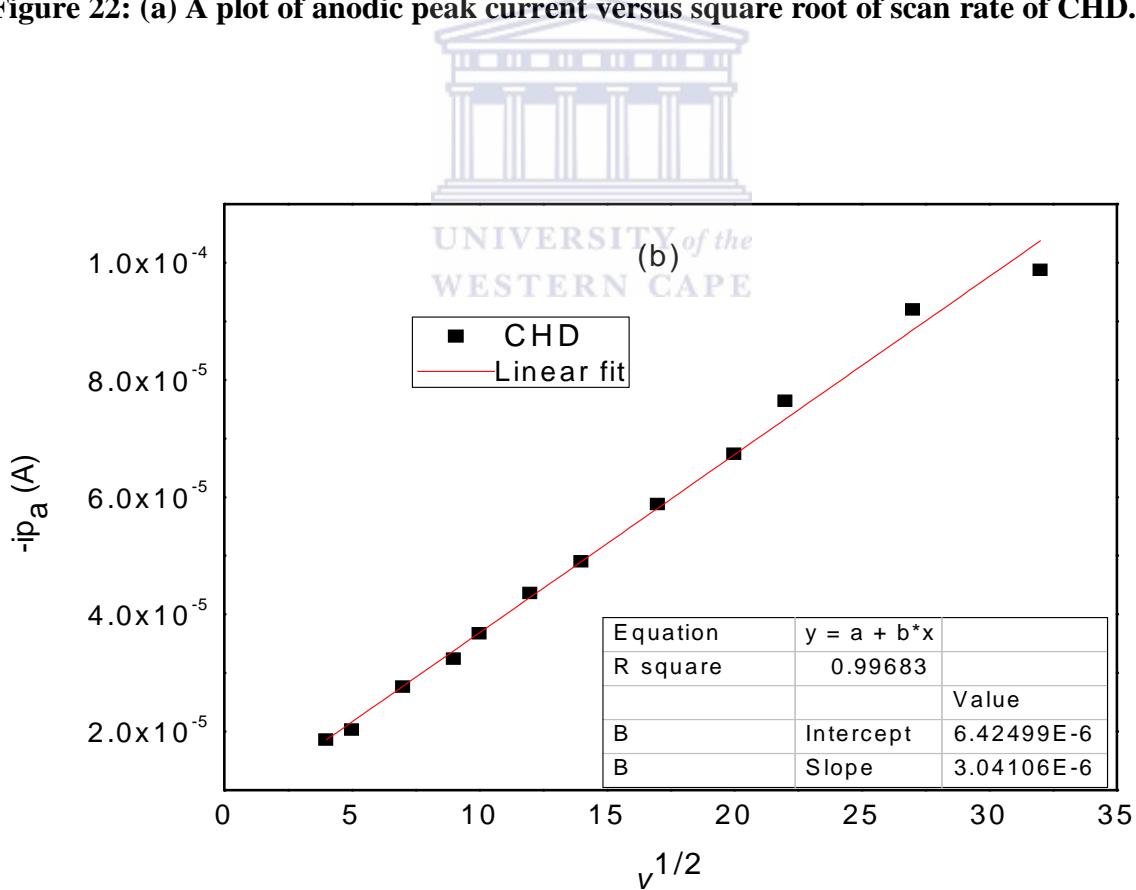


Figure 22: (b) A linear plot of anodic current versus square root of scan rate of CHD.

In the above figure **22(a)** the anodic peak current shows a good linear response with the square root of scan rate. This linearity observed in figure **22(b)** resulted in a good linear regression of 0.99683 observed in figure **22(b)**. The information obtained in Figure **22** was used to calculate the $D_{ox}^{1/2}$ (diffusion coefficient) with the following equation;

$$ip_a = 2.99 \times 10^5 n_a^{3/2} \alpha^{1/2} A D_{ox}^{1/2} C_{ox} v^{1/2}$$

$$\text{Area of Pt electrode} = 0.0201 \text{ cm}^2$$

$$\text{Constant} = 2.99 \times 10^5 \text{ C mol}^{-1} \text{V}^{1/2}$$

$$\text{Number of electrons} = 1$$

$$\text{Concentration} = 2 \times 10^{-10} \text{ mol/cm}^3$$

$$\text{Slope} = 3.041 \times 10^{-6} \text{ mV}^{-1/2} \text{s}^{1/2} = 9.62 \times 10^{-5} \text{ C/V}^{1/2} \text{s}^{1/2}$$

$$D_{ox}^{1/2} = \text{Slope} / 2.99 \times 10^5 n_a^{3/2} \alpha^{1/2} A C_{ox}$$

$$\text{With a } D_{ox} = 10.65 \text{ cm}^2/\text{s}.$$



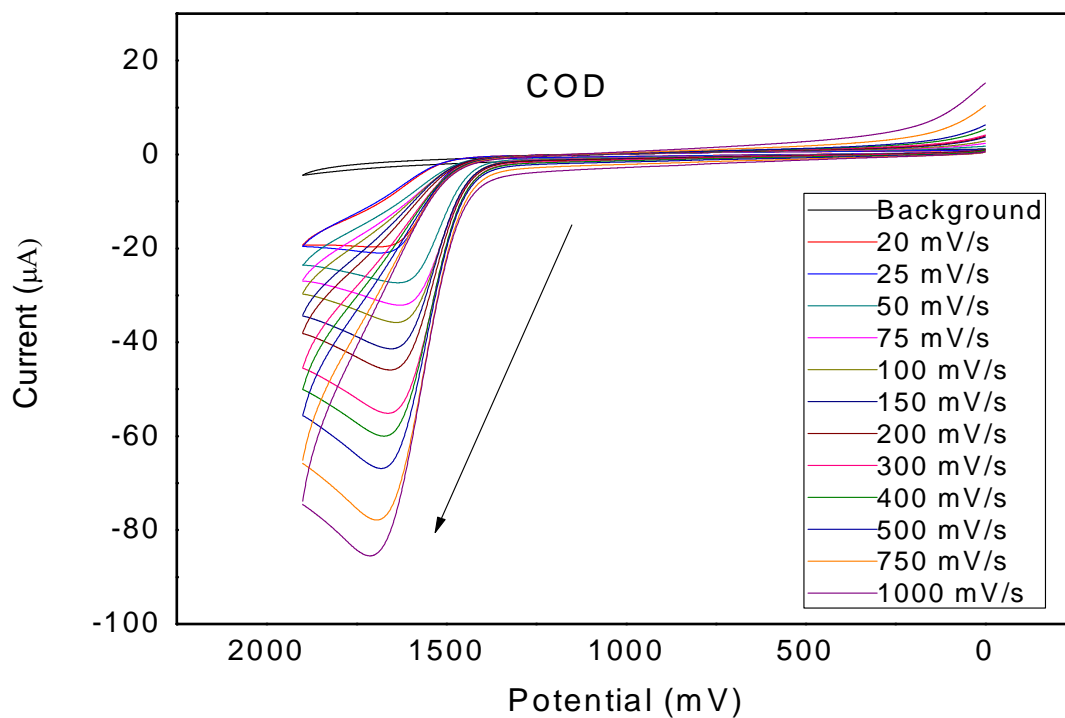
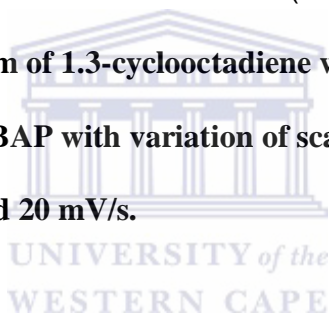


Figure 23: Cyclic voltammogram of 1.3-cyclooctadiene with Pt working electrode in acetonitrile containing 0.1 M TBAP with variation of scan rate from 1000, 750, 500, 400, 300, 200, 150, 100, 75, 50, 25 and 20 mV/s.



In the above figure 23 an oxidation peak of 1.3-cyclooctadiene is observed, the peak current decreases with the decrease in scan rate. The peak potential is not constant, there is a slight shift. The experiment for this analyte was repeated three times to ensure reproducibility and confirm if there is any electron fouling experienced at the electrode surface. The COD experiment was reproducible, which is a good indication for a development of a sensor.

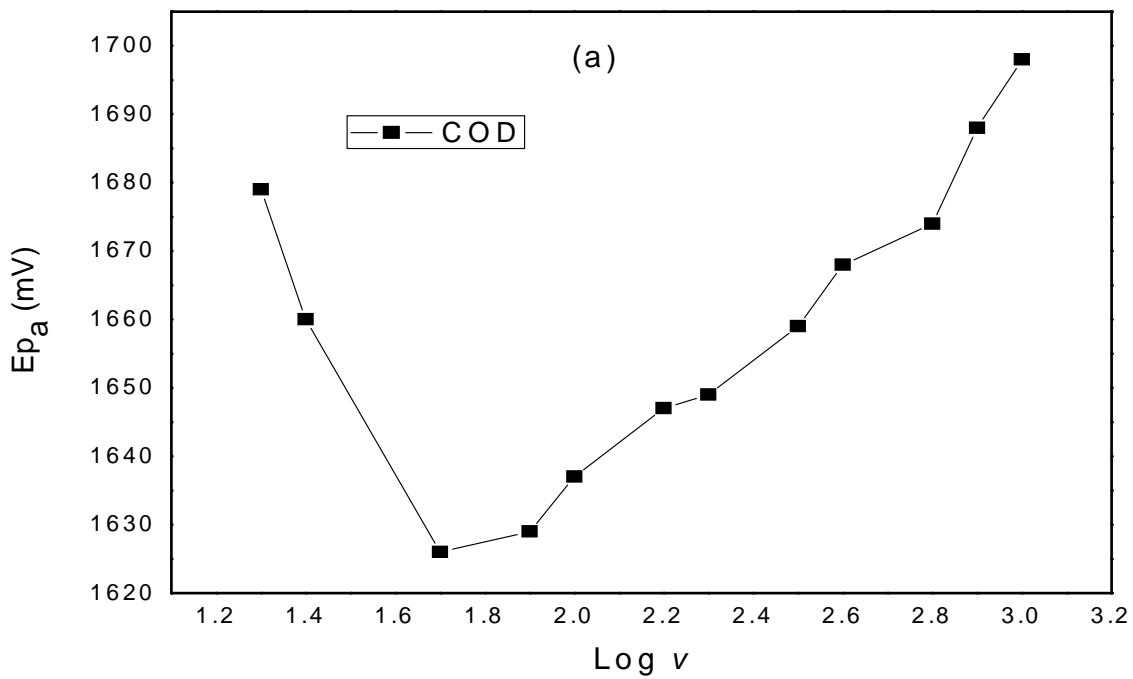


Figure 24: (a) A plot of anodic peak potential versus log of scan rate of COD.

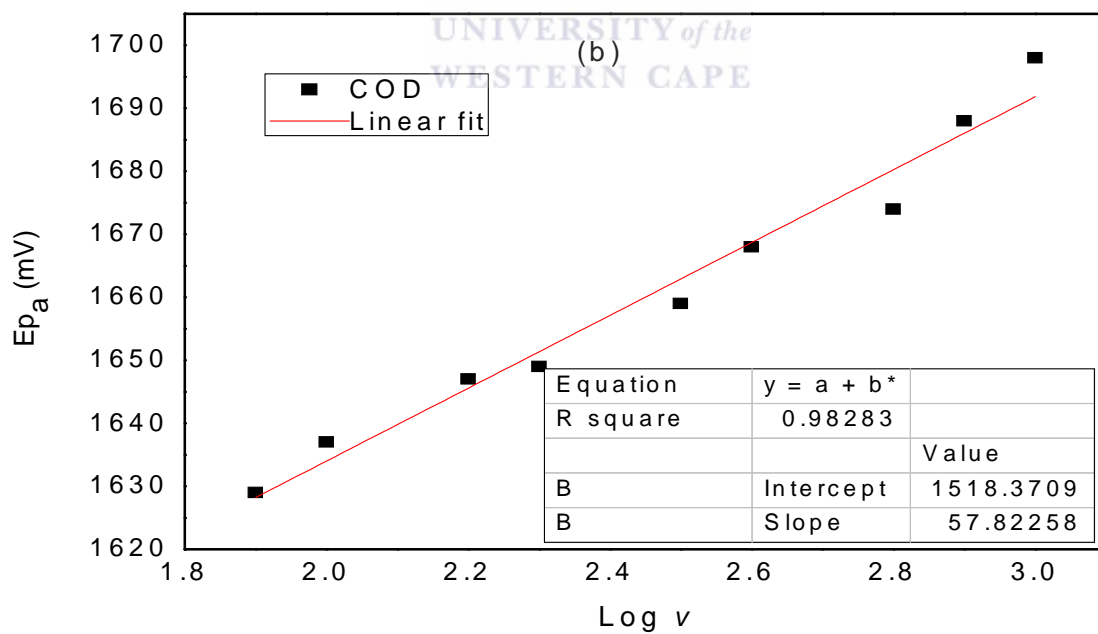


Figure 24: (b) A linear plot of anodic peak potential versus log of scan rate of COD.

The above figure **24(a)** shows a quasi-reversible process, at lower scan rate reversibility is observed and at higher scan rate irreversibility is observed. The linear plot for anodic peak potential in figure **24(b)** a linear regression of 0.98283 is observed. The linear plot was determined at higher scan rate which is a characteristic of irreversibility and the anodic peak potential illustrates more irreversibility than reversibility. There is invariance that can be observed in the above figure where at low scan rate the reversibility it is not clearly noted. The numbers of electrons were calculated from the above slope in figure **24(b)** which is equal

to 57.82, the following formula used; $Slope = \frac{30}{\alpha n_{\alpha}}$

$n = 1.037 \approx 1$ and $\alpha = 0.49 \approx 0.5$

The suggested mechanism at the electrode surface is $COD \rightarrow COD^+ + e^-$ which is a clear explanation of one oxidation peak observed when potential is applied.

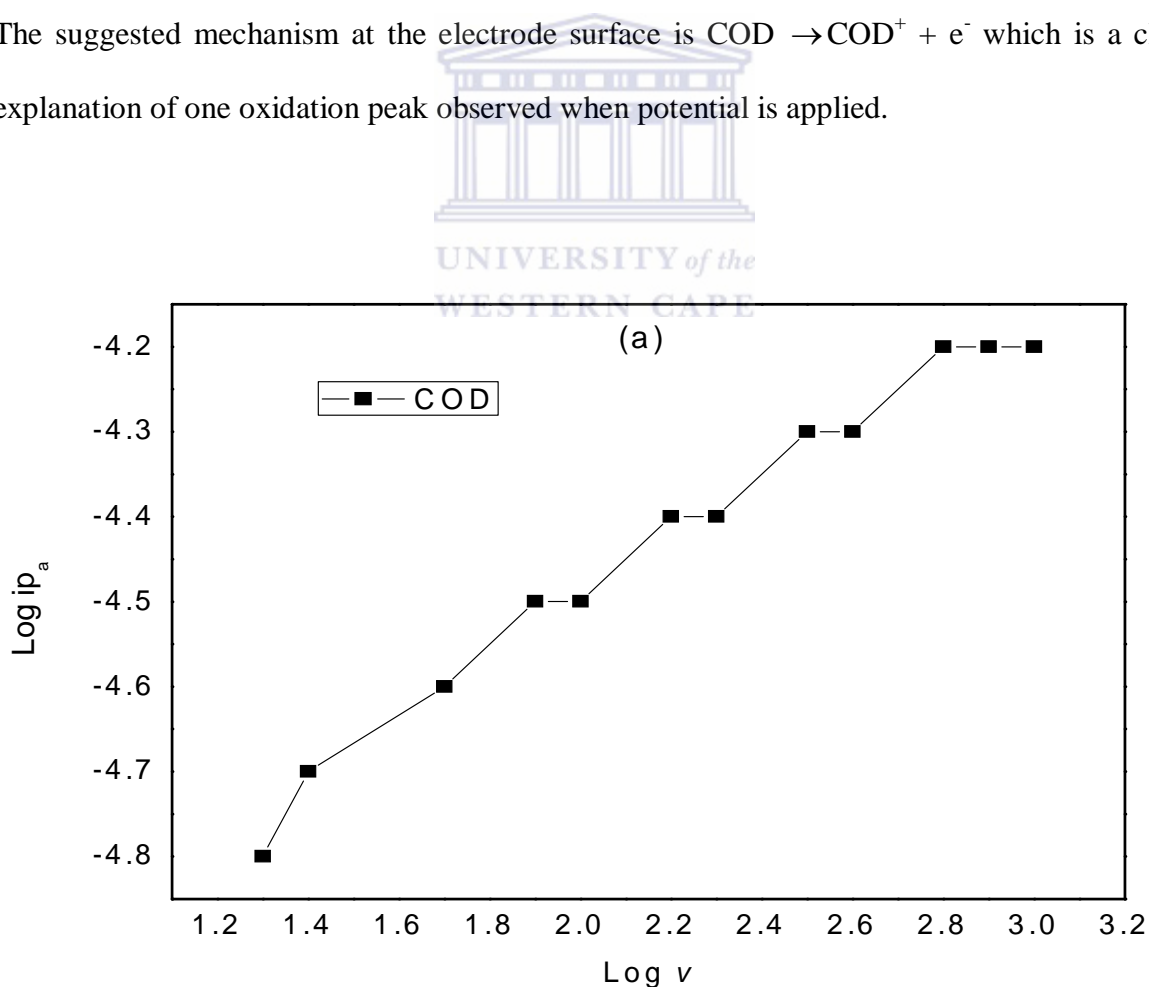


Figure 25: (a) A plot of log anodic peak current versus log of scan rate of COD.

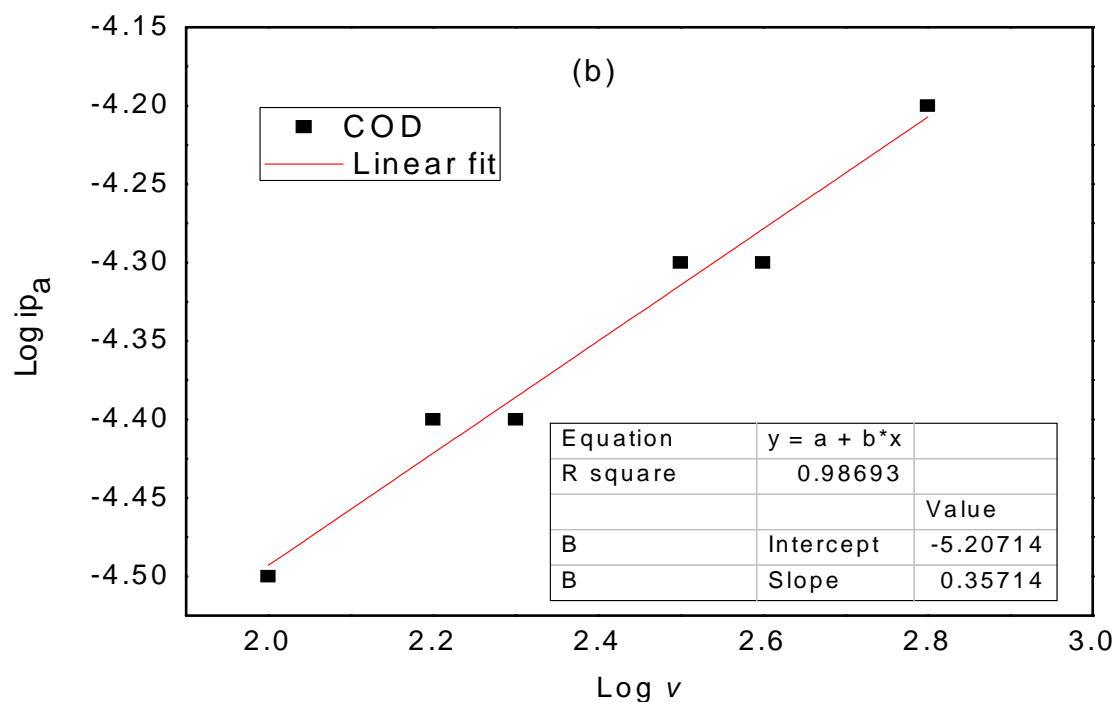


Figure 25: (b) A linear plot of log anodic peak current versus log of scan rate of COD.

In the above figure **25(a)** the logarithmic anodic peak current increases with logarithmic of scan rate at lower scan rate, as the scan rate increases it can be observed that current becomes constant with an increase in scan rate. It shows that there was a factor that was interfering with the experiment. In figure **25(b)** a linear regression of 0.98693 was reported at higher scan rate with a slope = 0.35714 which proves that the reaction is diffusion controlled.

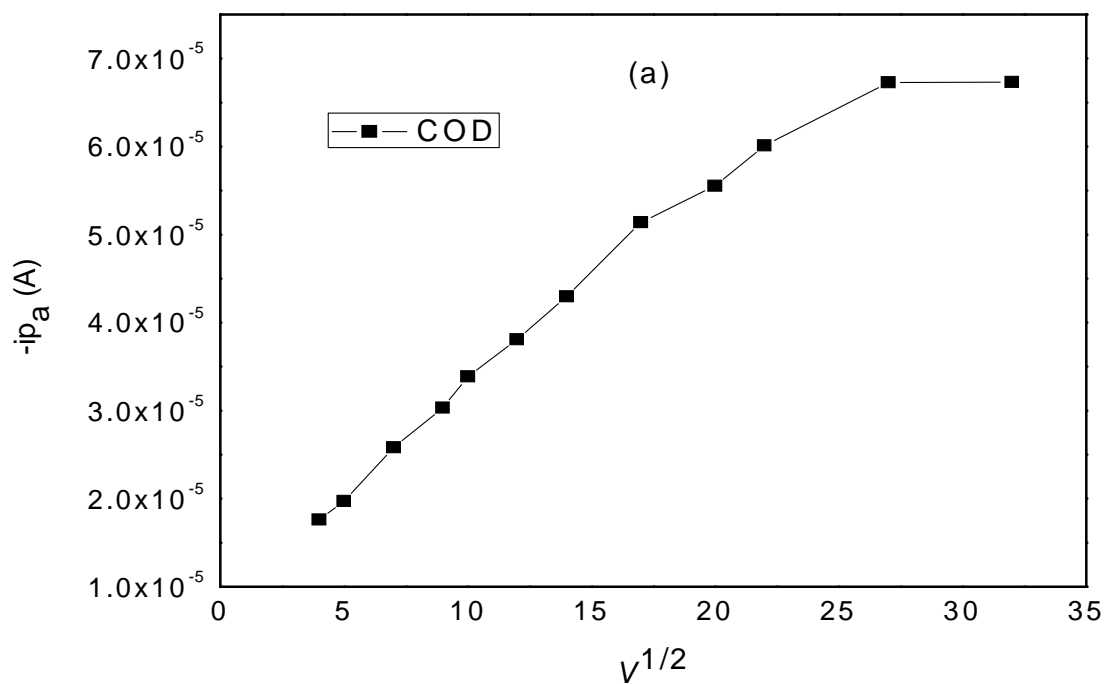


Figure 26: (a) A plot of anodic peak current versus square root of scan rate of COD.

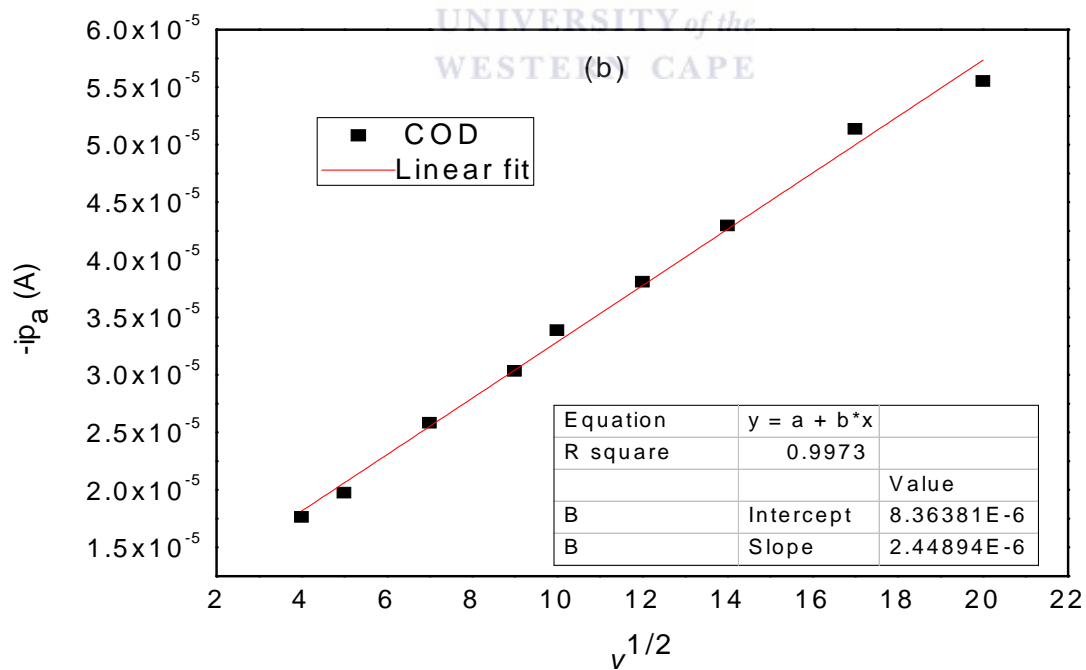


Figure 26: (b) A linear plot of anodic peak current versus square root of scan rate of COD.

In the above figure **26(a)** there is an increase in peak current with increase in square root of scan rate. a linear plot in figure **26(b)** a good linear regression of 0.9973 which is an indication of good linearity. The slope of 2.44E-6 will be used to calculate the diffusion coefficient D_{ox} of COD. The following equation will be used;

$$ip_a = 2.99 \times 10^5 n_a^{3/2} \alpha^{1/2} A D_{ox}^{1/2} C_{ox} v^{1/2}$$

$$\text{Area of Pt electrode} = 0.0201 \text{ cm}^2$$

$$\text{Constant} = 2.99 \times 10^5 \text{ C mol}^{-1} \text{ V}^{1/2}$$

$$\text{Number of electrons} = 1$$

$$\text{Concentration} = 2 \times 10^{-10} \text{ mol/cm}^3$$

$$\text{Slope} = 2.449 \text{E-}6 \text{ mV}^{-1/2} \text{ s}^{1/2} = 7.74 \times 10^{-5} \text{ C. V}^{-1/2} \text{ s}^{-1/2}$$

$$D_{ox}^{1/2} = \text{Slope} / 2.99 \times 10^5 n_a^{3/2} \alpha^{1/2} A C_{ox}$$

$$\text{With a } D_{ox} = 9.55 \text{ cm}^2/\text{s}$$



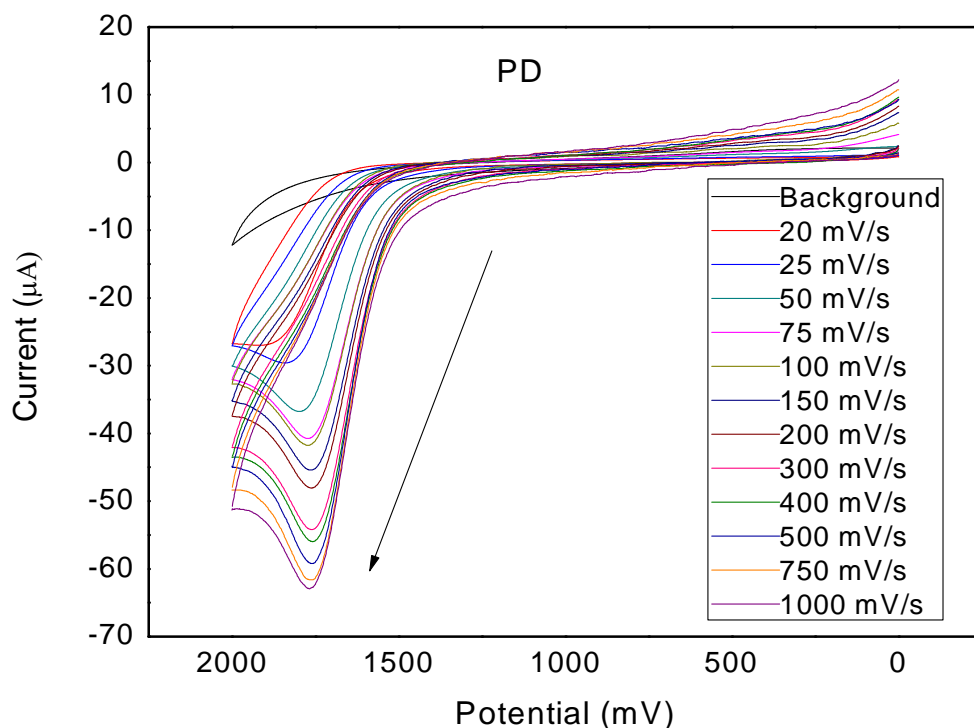
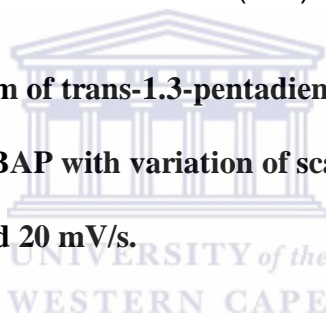


Figure 27: Cyclic voltammogram of trans-1,3-pentadiene with a Pt working electrode in acetonitrile containing 0.1 M TBAP with variation of scan rate from 1000, 750, 500, 400, 300, 200, 150, 100, 75, 50, 25 and 20 mV/s.



In the above figure **27** an oxidation peak can be observed which is much similar response to the other conjugated dienes above, the difference is in the peak potential and the potential window which the diene response to the potential applied. As the scan rate decreases there is also an decrease in peak current. This is a good a good response which shows this conjugated dienes can be applied for the development of a sensor. The experiment for this diene was repeated three times to ensure reproducibility and consistency with every scan rate performed above. It was found that the results obtained were reproducible and consistent with scan rate.

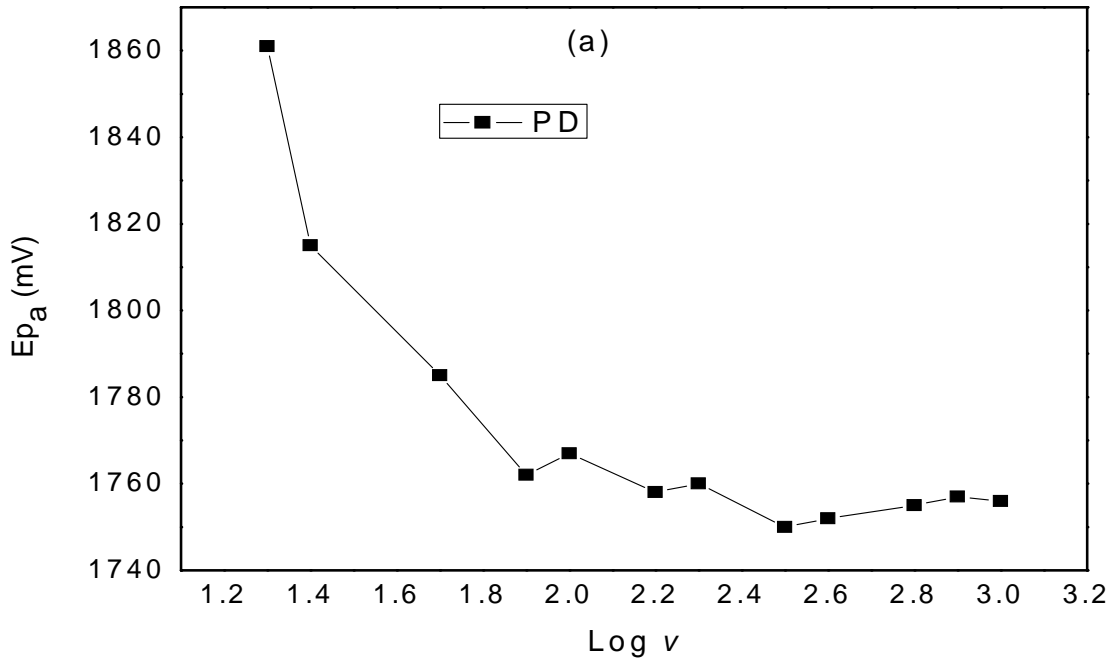


Figure 28: (a) A plot of anodic peak potential versus log of scan rate of PD.

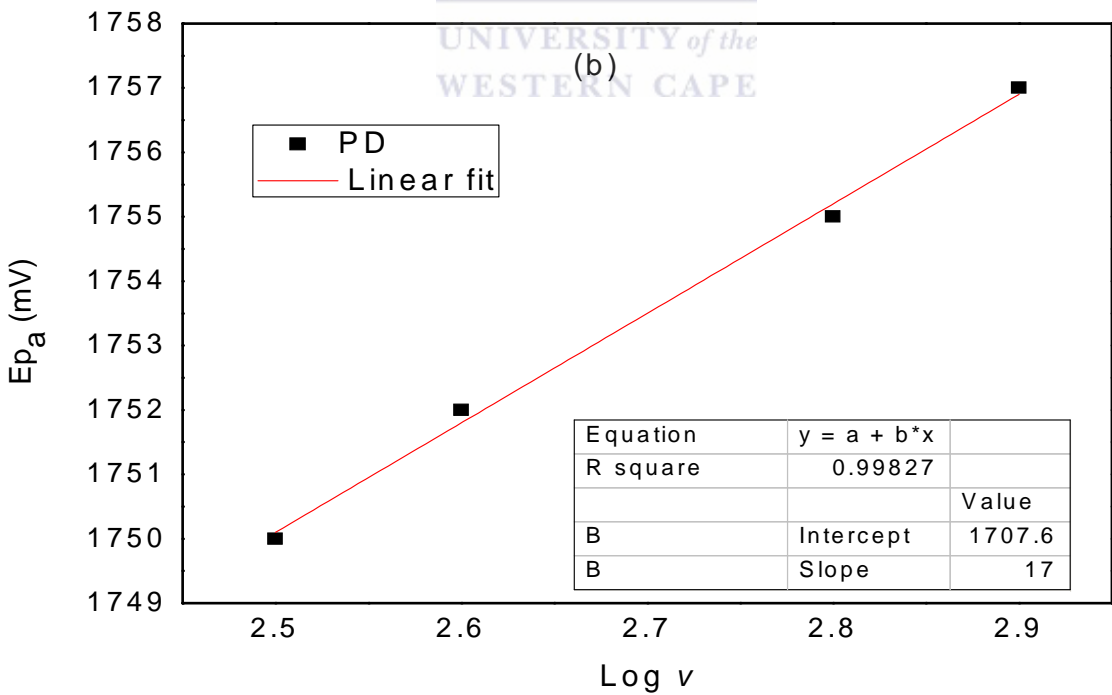


Figure 28: (b) A linear plot of anodic peak current versus log of scan rate of PD.

In the above figure **28(a)** the peak potential versus log of scan rate shows that there is an invariant factor due to the uncompensated solution resistance. It is observed that there is characteristic of irreversibility even though the results show there is another process taking place at the surface of the electrode. The linear plot of PD as observed in figure **28(b)** there is a linear regression of 0.99827 at a higher scan rate which can be used to calculate the number of electrons and the α value with the use of a slope of 17, the following equation will

be used for reactions at 25 °C is as follows; $Slope = \frac{30}{\alpha n_{\alpha}}$

$n = 3.52 \approx 4$ and $\alpha = 0.441 \approx 0.4$.

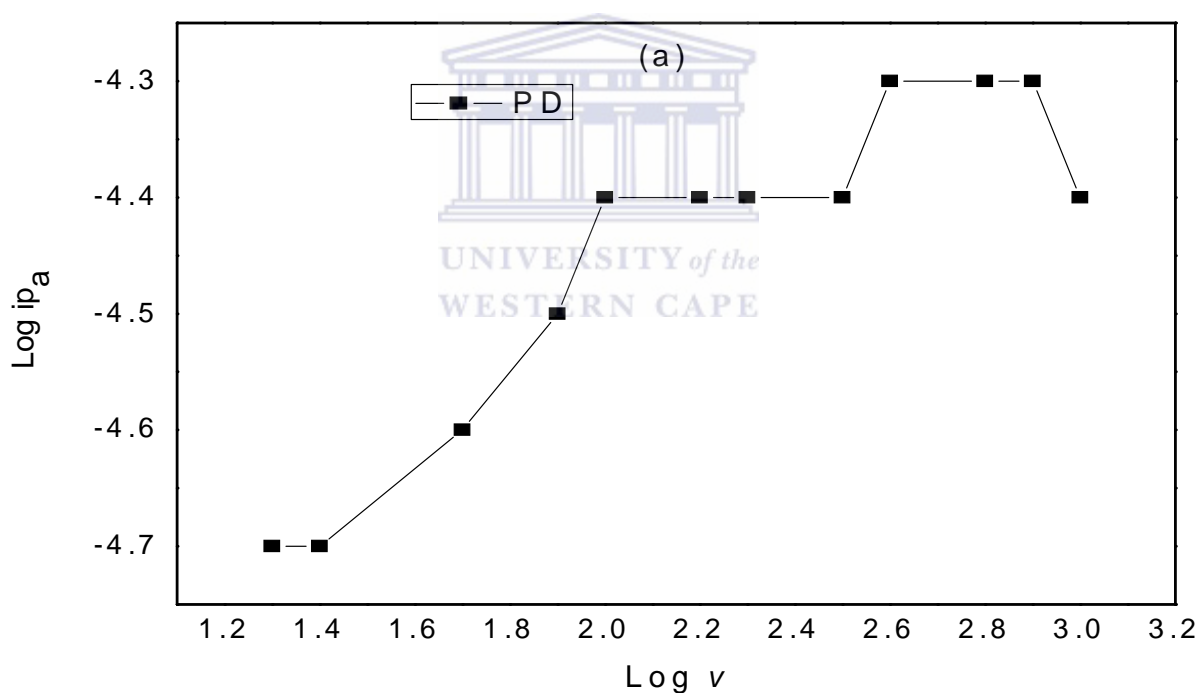


Figure 29: (a) A plot of log of anodic peak current versus log of scan rate of PD.

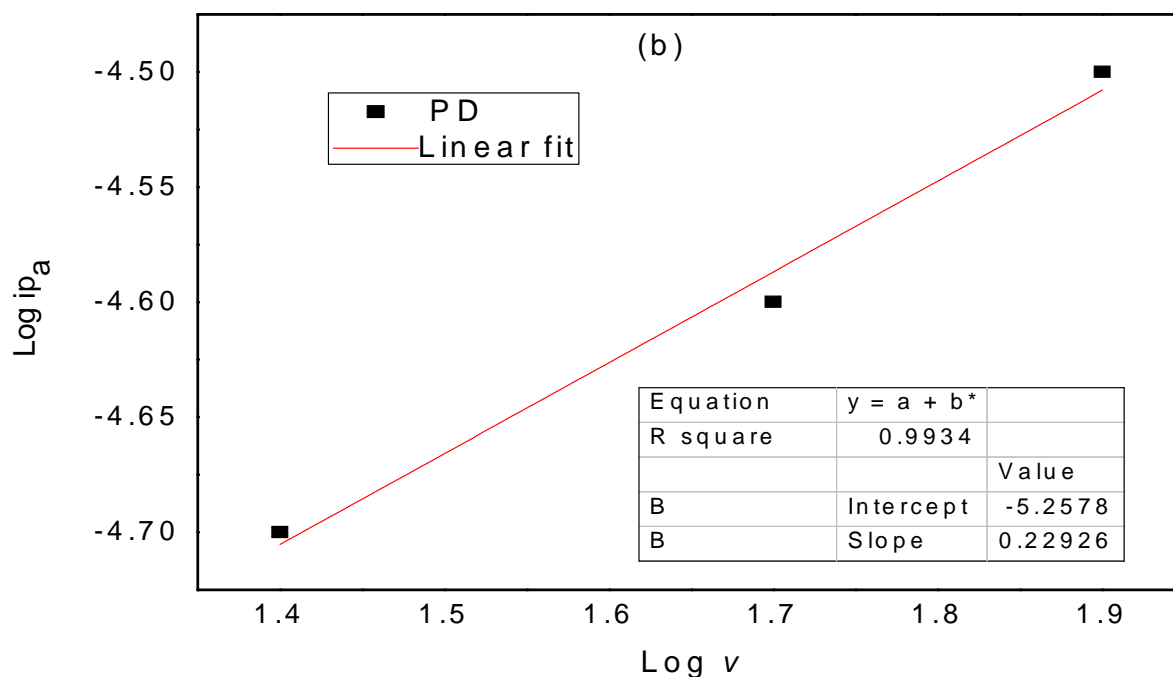


Figure 29: (b) A linear plot of log of anodic peak current versus log of scan rate of PD.

In the above figure **29(a)** the logarithmic anodic peak current increases with logarithmic of scan rate at lower scan rate, as the scan rate increases it can be observed that current becomes constant with an increase in scan rate. It shows that there was a factor that was interfering with the experiment. In figure **29(b)** a good linear regression of 0.9934 is reported at higher log of scan rate with a slope = 0.22926 which proves that the reaction is diffusion controlled. This explains the constant peak current at some scan rate and an increase in some others.

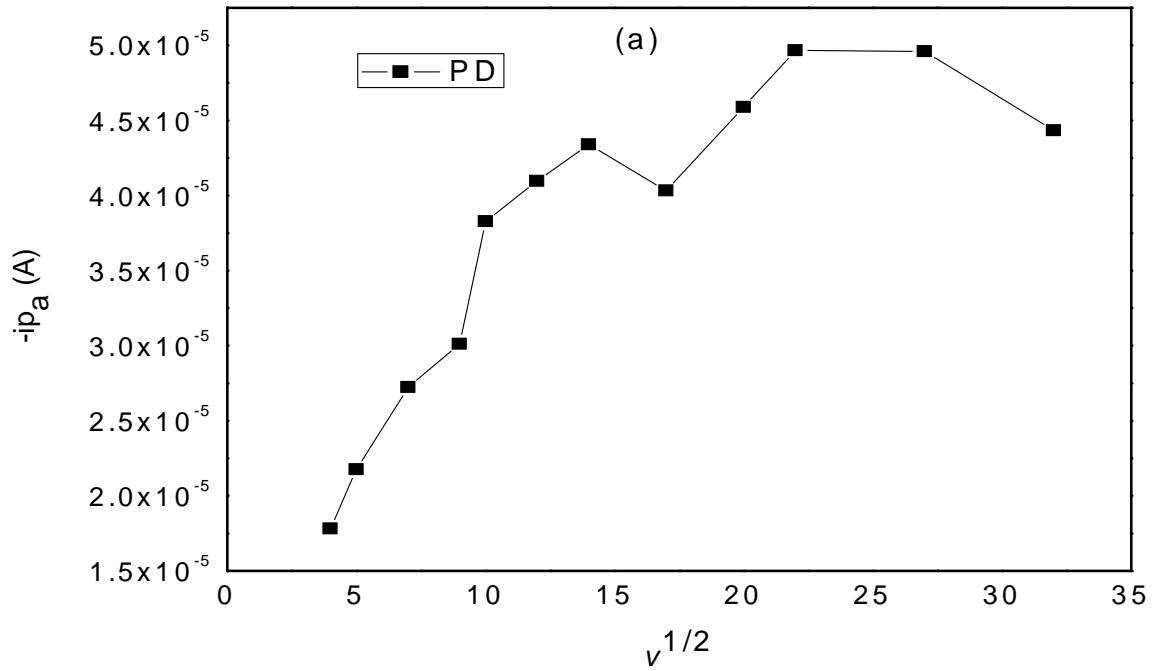


Figure 30: (a) A plot of anodic peak current versus square root of scan rate of PD.

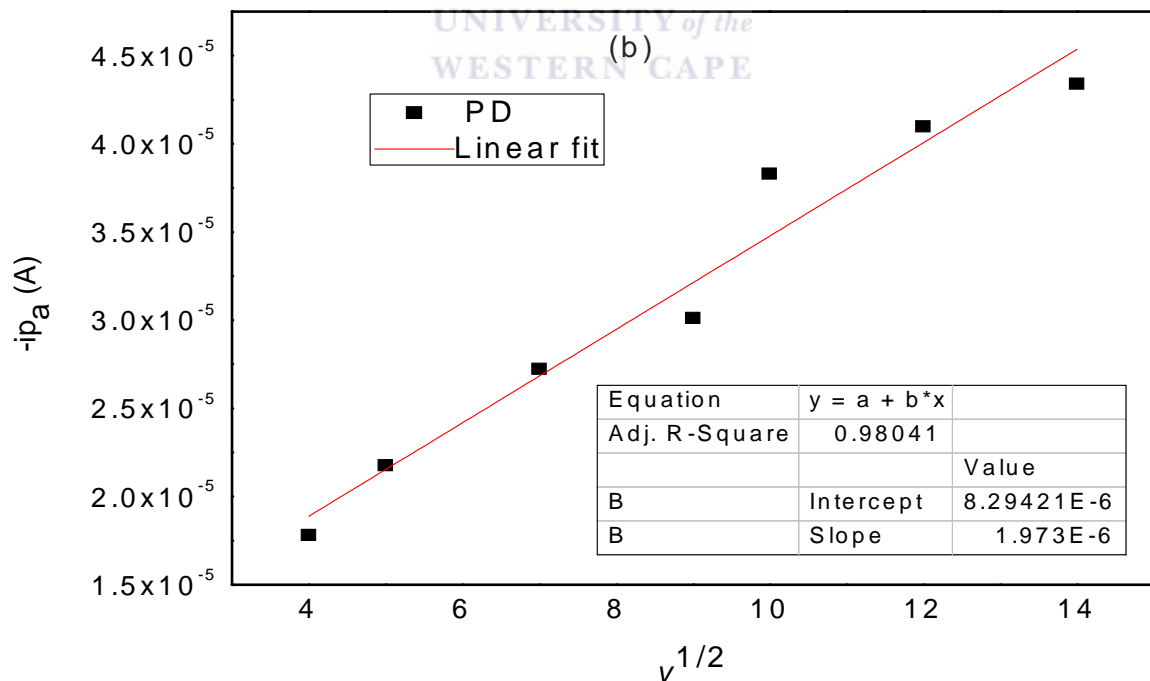


Figure 30: (b) A linear plot of anodic peak current versus square root of scan rate of PD.

In the above figure **30(a)** there is an increase in peak current with increase in square root of scan rate, at higher scan rate it can be observed there are some areas where peak current decreases which show characteristics of slight fouling at the electrode surface. A linear plot in figure **30(b)** a good linear regression of 0.98041 which is an indication there is linearity. The slope of 1.973E-6 will be used to calculate the diffusion coefficient D_{ox} of PD. The following equation will be used;

$$i_{p_a} = 2.99 \times 10^5 n_{\alpha}^{3/2} \alpha^{1/2} A D_{ox}^{1/2} C_{ox} \nu^{1/2}$$

$$\text{Area of Pt electrode} = 0.0201 \text{ cm}^2$$

$$\text{Constant} = 2.99 \times 10^5 \text{ C mol}^{-1} \text{ V}^{1/2}$$

$$\text{Number of electrons} = 4$$

$$\text{Concentration} = 2 \times 10^{-10} \text{ mol/cm}^3$$

$$\text{Slope} = 1.973 \text{E-}6 \text{ mV}^{-1/2} \text{ s}^{1/2} = 6.24 \times 10^{-5} \text{ C} \cdot \text{V}^{-1/2} \text{ s}^{-1/2}$$

$$D_{ox}^{1/2} = \text{Slope} / 2.99 \times 10^5 n_{\alpha}^{3/2} \alpha^{1/2} A C_{ox}$$

$$\text{With a } D_{ox} = 3.20 \text{ cm}^2/\text{s}$$



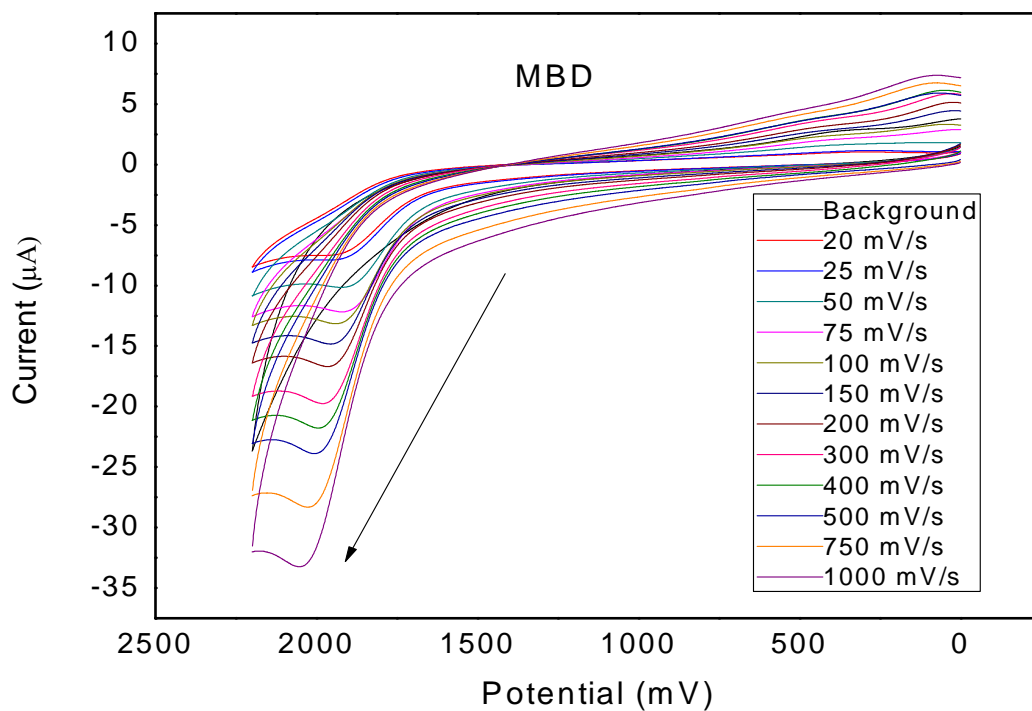
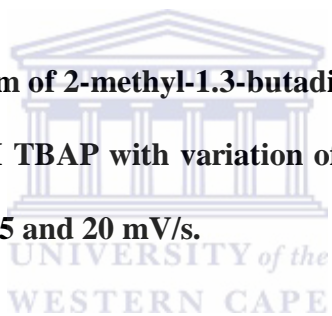


Figure 31: Cyclic voltammogram of 2-methyl-1,3-butadiene with a Pt working electrode in acetonitrile containing 1.0 M TBAP with variation of scan rate from 1000, 750, 500, 400, 300, 200, 150, 100, 75, 50, 25 and 20 mV/s.



In the above figure 31 oxidation peaks are observed, a decrease in scan rate results in a decrease in peak current. The experiment was repeated three times to ensure reproducibility and the experiment was reproducible which indicates there is no or less fouling occurring at the electrode surface.

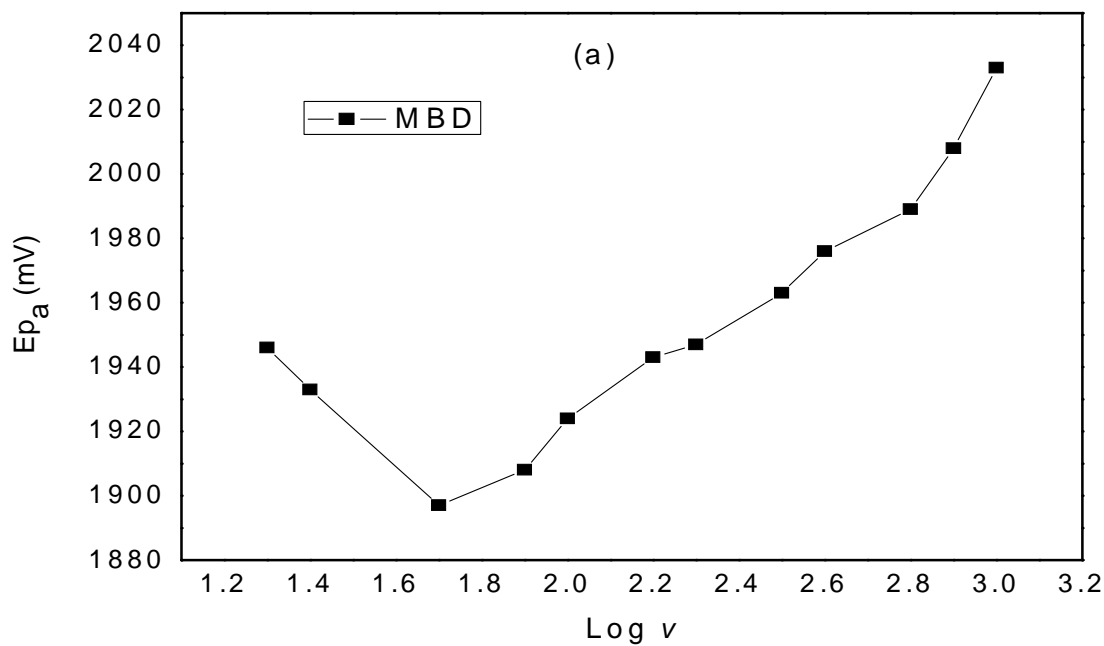


Figure 32: (a) A plot of anodic peak potential versus log of scan rate of MBD.

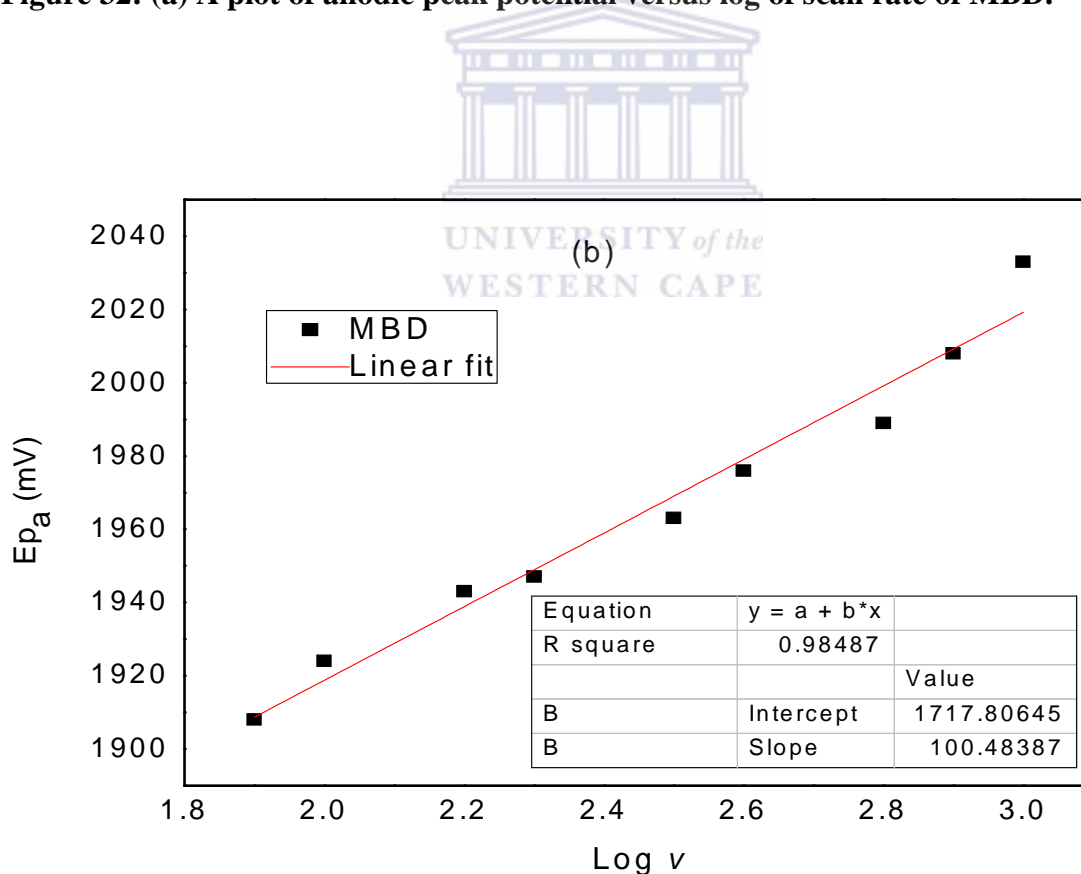


Figure 32: (b) A linear plot of anodic peak potential versus log of scan rate of MBD.

The above figure **32(a)** anodic peak current shows a quasi-reversible characteristic, at a low scan rate reversibility is observed and at higher scan rate irreversibility is observed. From the figure **32(a)** it can be observed that irreversibility is a dominating factor due to the linearity which is from higher scan rate as illustrated in figure **32(b)**. A linear regression of 0.98487 and a slope of 100.48 which will be used to calculate the number of electrons and α value

with the following equation; $Slope = \frac{30}{\alpha n_{\alpha}}$

$n = 0.59 \approx 1$ and $\alpha = 0.506 \approx 0.5$

The suggested mechanism at the electrode surface is $MBD \rightarrow MBD^{+} + e^{-}$ which is an oxidation process illustrated in figure **31**.

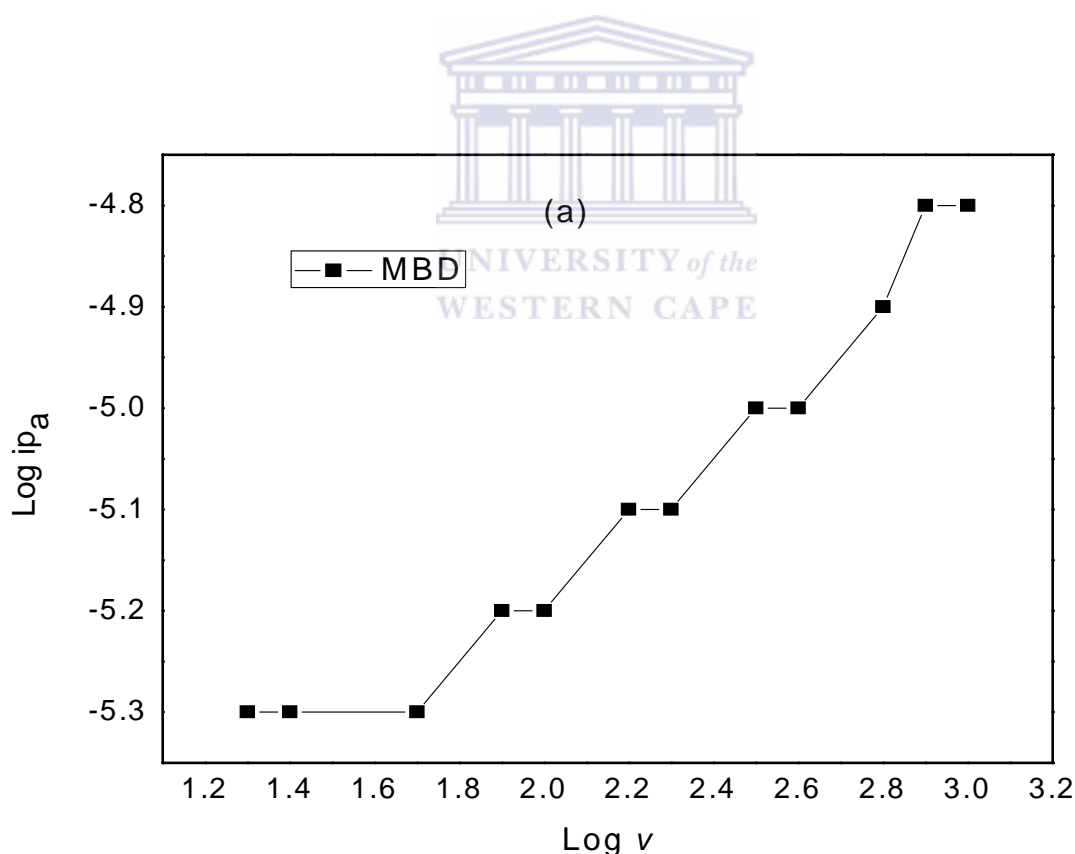


Figure 33: (a) A plot of log of anodic peak current versus log of scan rate of MBD.

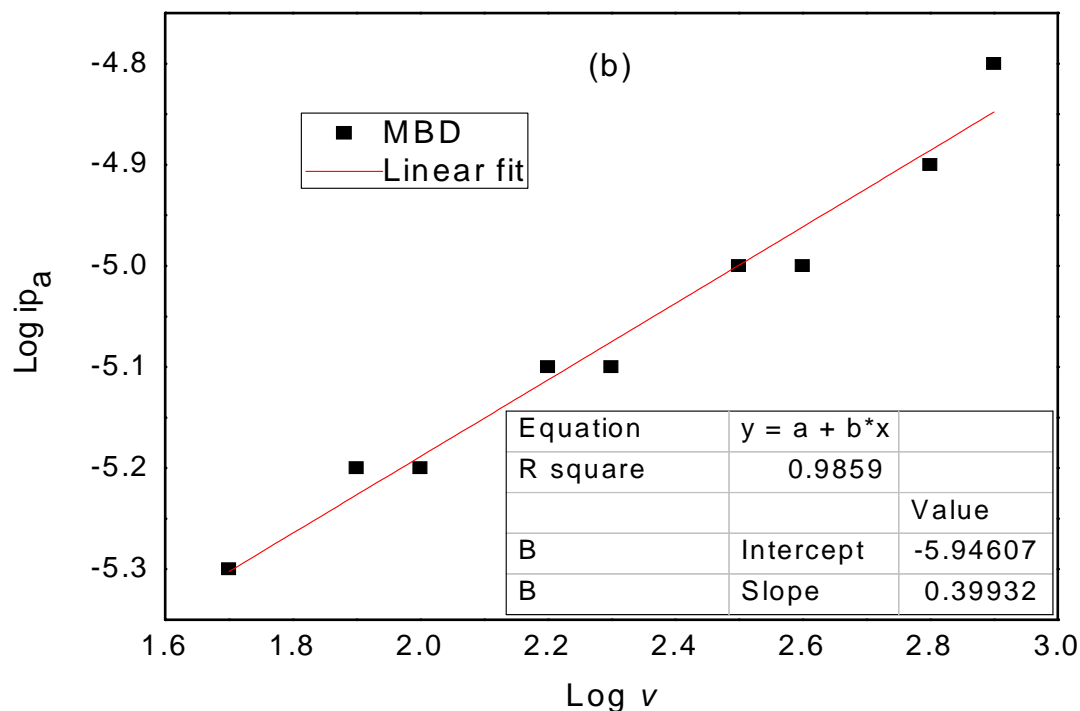
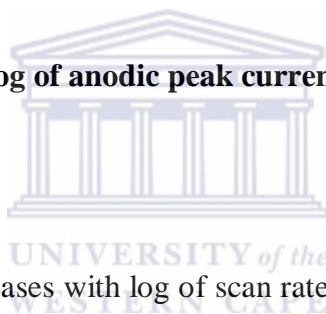


Figure 33: (b) A linear plot of log of anodic peak current versus log of scan rate of MBD.



The log anodic peak current increases with log of scan rate in figure 33(a) it can be observed at certain scan rates there is constant anodic peak current which is an indication there is an extra activity at the electrode surface which is an indication there might be a slight fouling at the electrode surface. The linear plot in figure 33(b) has a linear regression of 0.9859 and a slope of 0.399 which is an indication that the reaction is diffusion controlled. Diffusion is the sole means for the electro active species MDB to approach the electrode.

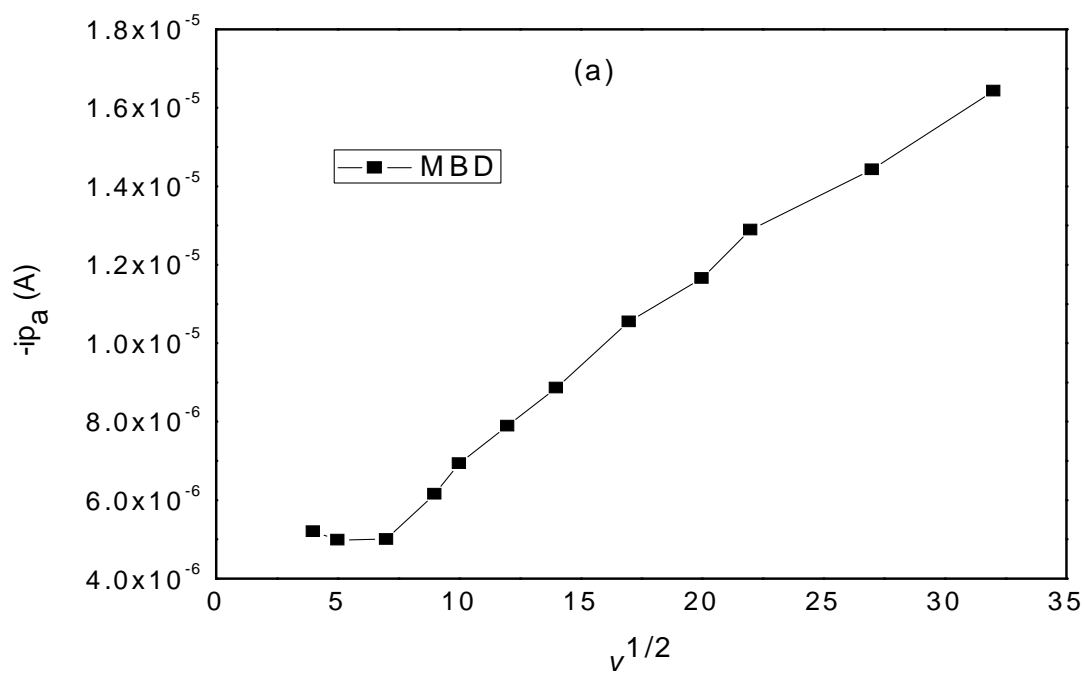


Figure 34: (a) A plot of anodic peak current versus square root of scan rate of MBD.

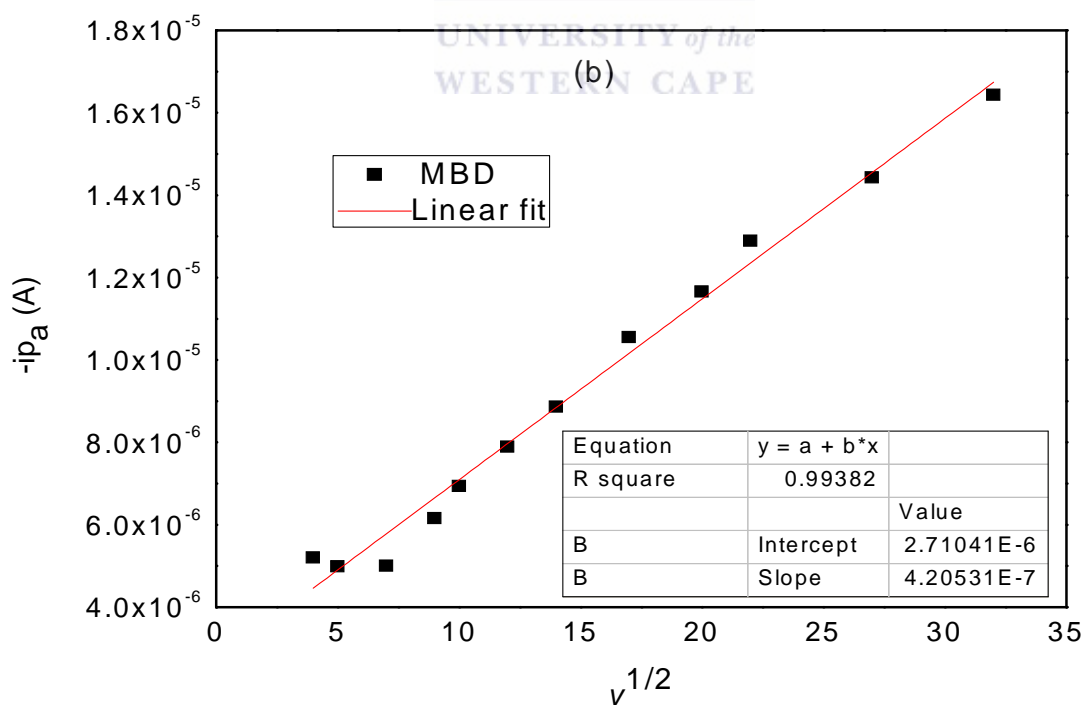


Figure 34: (b) A linear plot of anodic peak current versus square root of scan rate of MBD.

In figure **34(a)** there is a gradual increase of anodic peak current with the square root of scan rate, where linearity is observed in figure **34(b)** with a good linear regression of 0.99382. The slope of 4.205E-7 will be used to calculate the diffusion coefficient by using the following equation;

$$ip_a = 2.99 \times 10^5 n_a^{3/2} \alpha^{1/2} A D_{ox}^{1/2} C_{ox} v^{1/2}$$

$$\text{Area of Pt electrode} = 0.0201 \text{ cm}^2$$

$$\text{Constant} = 2.99 \times 10^5 \text{ C mol}^{-1} \text{ V}^{1/2}$$

$$\text{Number of electrons} = 1$$

$$\text{Concentration} = 2 \times 10^{-10} \text{ mol/cm}^3$$

$$\text{Slope} = 4.205 \text{E-}7 \text{ mV}^{-1/2} \text{ s}^{1/2} = 1.33 \times 10^{-5} \text{ C. V}^{-1/2} \text{ s}^{-1/2}$$

$$D_{ox}^{1/2} = \text{Slope} / 2.99 \times 10^5 n_a^{3/2} \alpha^{1/2} A C_{ox}$$

$$\text{With a } D_{ox} = 3.96 \text{ cm}^2/\text{s}$$

Further calculations have been done to calculate the effective area of the electrode surface on the glassy carbon electrode due to the observed fouling that occurred at the electrode surface. Several working electrode has been used to minimize the effect of fouling there are as follows; boron doped diamond electrode, gold electrode, titanium electrode and Pt working electrode. It was found that Pt working electrode gave better results and was able to minimize the effect of fouling. Use of the ferrocene oxidation process to provide both reference electrode potential calibration and a simple measurement (via semi integration) of the uncompensated resistance in cyclic voltammetric studies in high-resistance organic solvents. The effective area will help to determine how much of the conjugated diene covered the

glassy carbon electrode surface which it can be useful for future studies. The actual area of GCE is $7.707 \times 10^{-2} \text{ cm}^2$.

Table 3: GCE Kinetics of conjugated dienes (CHD, COD, PD and MBD)

GCE				
Conjugated Dienes	Effective Area(A) cm^2	Number of electrons(n)	Diffusion coefficient (D_{ox}) cm^2/s	α
CHD	7.14×10^{-5}	1	5.51×10^{-3}	0.5
COD	6.14×10^{-5}	1	6.81×10^{-3}	0.49
PD	7.00×10^{-4}	1	1.84×10^{-5}	0.48
MBD	9.35×10^{-4}	3	3.5×10^{-8}	0.5

In the above table 3 it is clear that there was fouling on the electrode surface because the effective area proves that there is a decrease in the electrode area surface. When these results are compared to the Pt working electrode there was no significant change in the effective area. This proves beyond a doubt Pt working electrode has been able to minimize the effect of fouling. There is some inconsistency when it comes to the number of electron transferred on the electrode surface which is an indication of the uncompensated solution resistance which can result to such an error.

4.7. SNIFTIR

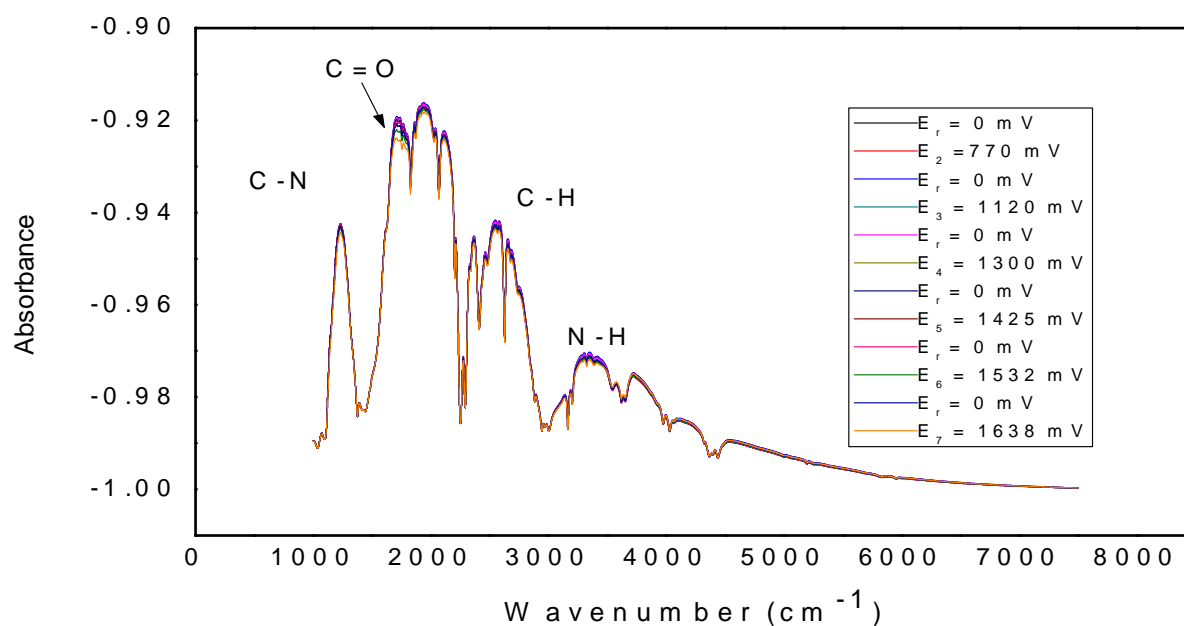


Figure 35: SNIFTIR of acetonitrile containing 0.1 M TBAP electrolyte with positive potential steps starting at $E_{\text{ref}2} = 0 \text{ mV}$, $E_2 = 770 \text{ mV}$; $E_{\text{ref}3} = 0 \text{ mV}$, $E_3 = 1120 \text{ mV}$; $E_{\text{ref}4} = 0 \text{ mV}$, $E_4 = 1300 \text{ mV}$; $E_{\text{ref}5} = 0 \text{ mV}$, $E_5 = 1425 \text{ mV}$; $E_{\text{ref}6} = 0 \text{ mV}$, $E_6 = 1532 \text{ mV}$; $E_{\text{ref}7} = 0 \text{ mV}$, and $E_7 = 1638 \text{ mV}$.

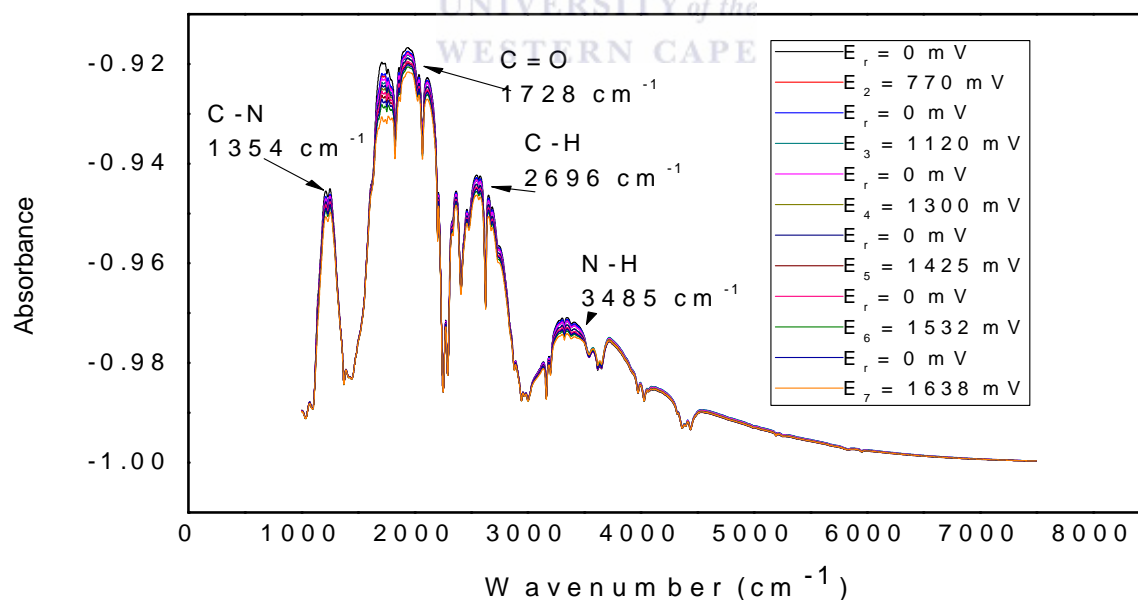


Figure 36: SNIFTIR of 0.1M 1.3-cyclohexadiene acetonitrile containing 0.1 M TBAP electrolyte with positive potential steps starting at $E_{\text{ref}2} = 0 \text{ mV}$, $E_2 = 770 \text{ mV}$; $E_{\text{ref}3} = 0 \text{ mV}$, $E_3 = 1120 \text{ mV}$; $E_{\text{ref}4} = 0 \text{ mV}$, $E_4 = 1300 \text{ mV}$; $E_{\text{ref}5} = 0 \text{ mV}$, $E_5 = 1425 \text{ mV}$; $E_{\text{ref}6} = 0 \text{ mV}$, $E_6 = 1532 \text{ mV}$; $E_{\text{ref}7} = 0 \text{ mV}$ and $E_7 = 1638 \text{ mV}$.

The formula used to plot the above graph is as follows; $Absorbance = \frac{A_{sample} - A_{reference}}{A_{reference}}$,

Knowing the spectroscopic behaviour of 1,3-cyclohexadiene, its oxidation product and peaks from the electrolyte alone without any analyte allows the SNIFTIR of 1,3-cyclohexadiene to be measured and understood. In the above figure **35** it is a spectrum of only the electrolyte and supporting electrolyte with the applied steps of positive potential to easily differentiate when the analyte is added to the solution. It can be clearly observed that there is more positive absorbance change and less negative absorbance change. The spectrum is generated by the presence of TBAP as supporting electrolyte. In figure **36** the electro-oxidation of 1,3-cyclohexadiene in acetonitrile containing 0.1 M TBAP solution for positive potential from $E_1 = 770$ mV to $E_2 = 1638$ mV. An intense peak appeared at 1354 and 1728 cm^{-1} as the potential was stepped to $E_7 = 1638$ mV. An apparent intense broad band is observed at 2696 and 3485 cm^{-1} when $E_2 < 770$. The 1,3-cyclohexadiene products dominate the spectrum which is found at 1354 cm^{-1} . The above spectrum shows that there is a product formed at the electrode surface. There is no much evidence that there is electro-reduction observed at the electrode surface due to the absence or little evidence of negative absorbance change. There is much evidence that electro-oxidation is happening at the electrode surface due to positive absorbance change. The potential step as it is applied an increase in absorption change is observed, the peaks are more intense. At 2696 cm^{-1} it can be observed that there are new C-H bonds that are formed from the aromatic ring of CHD as the potential is increased.

4.8. Ultra-violet visible spectroscopy

The UV-Vis spectroscopy of four conjugated dienes

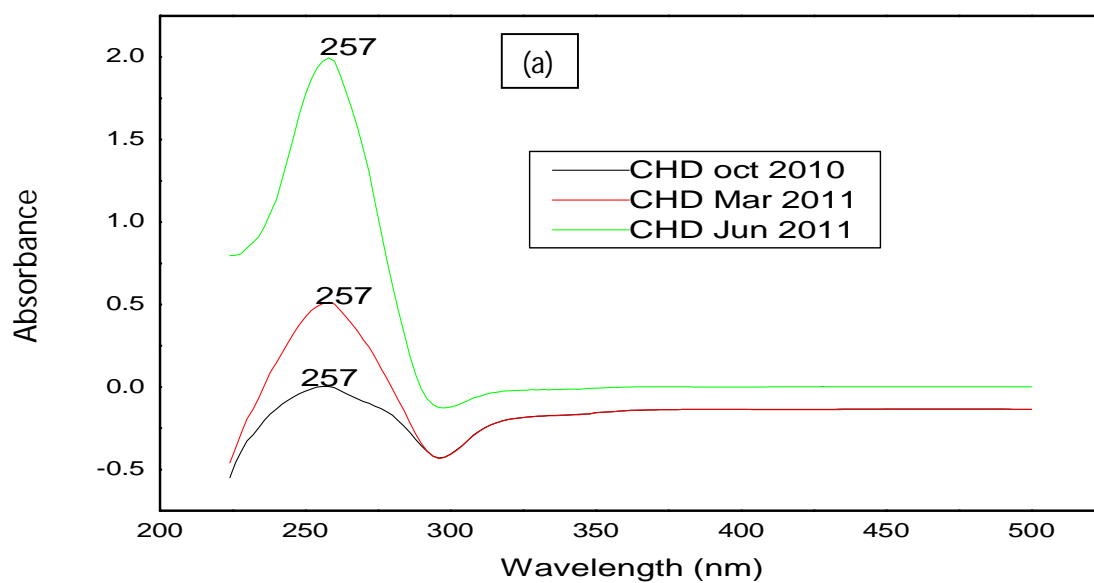


Figure 37: (a) UV-vis spectroscopy of 1,3-cyclohexadiene variation of period.

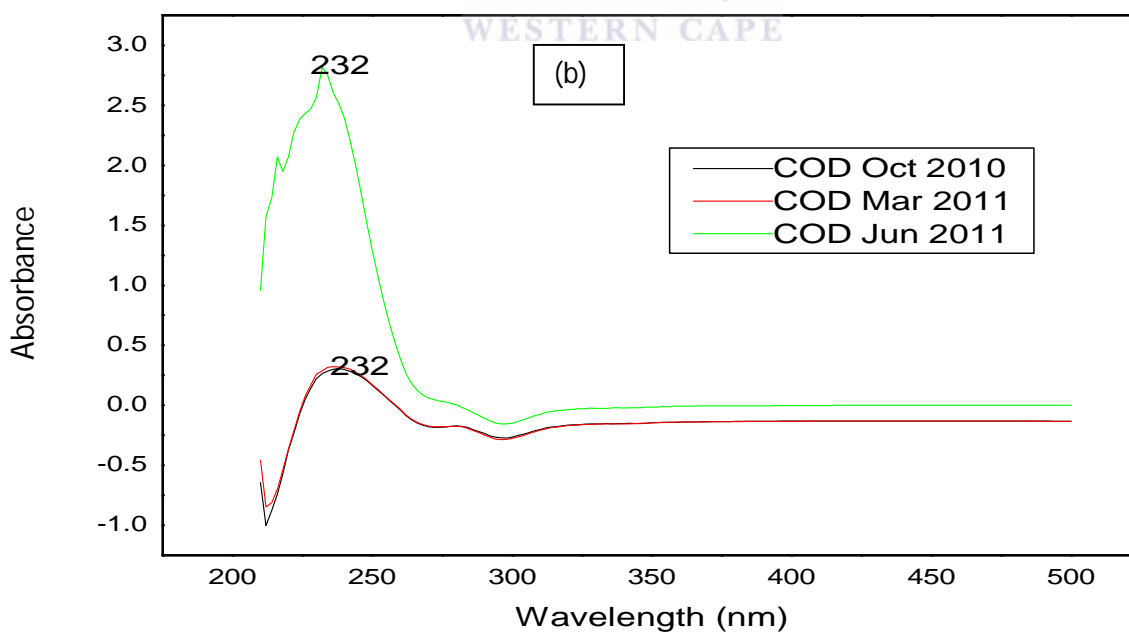


Figure 37: (b) UV-vis spectroscopy of 1,3-cyclooctadiene variation of Period.

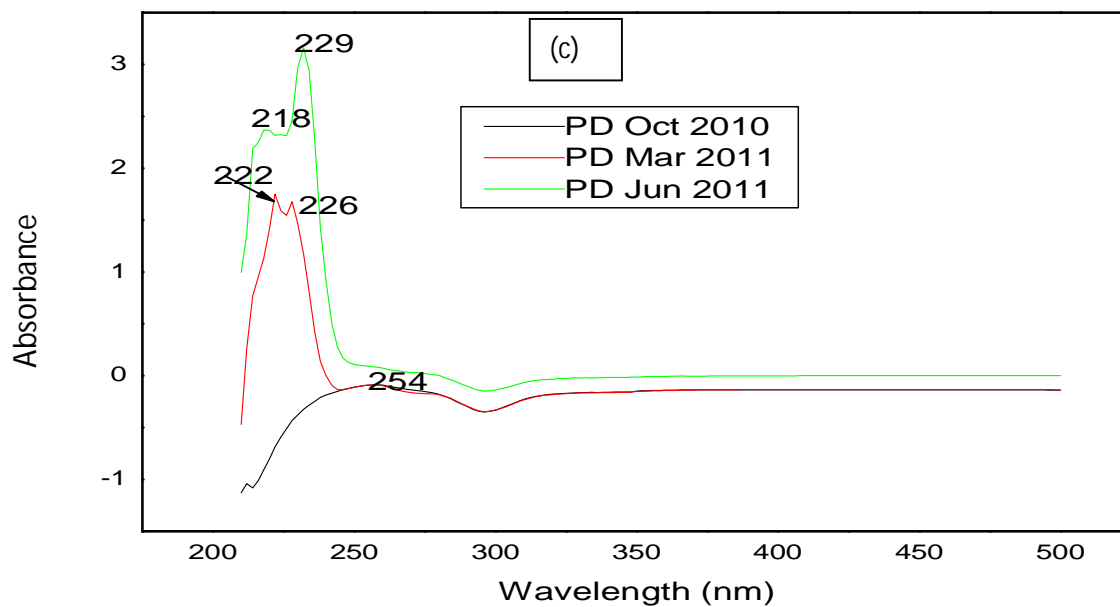


Figure 37: (c) UV-vis spectroscopy of trans-1.3-pentadiene variation of period.

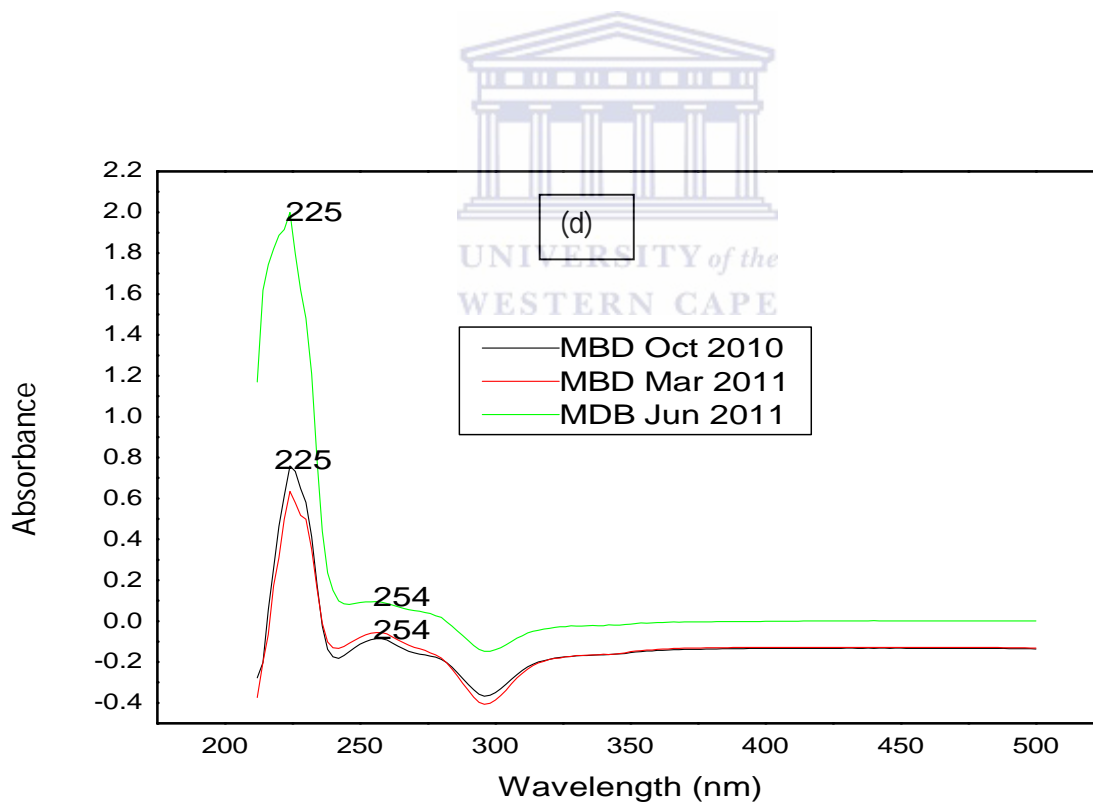


Figure 37: (d) UV-vis spectroscopy 2-methyl-1.3-butadiene variation of period.

In the above figure **37(a)** CHD shows that time does not affect the wavelength but it affects the absorption peak. The wavelength where CHD can be observed is 257 nm which is attributed by $\pi\text{-}\pi^*$ transition of conjugated six membered cyclic ring. In figure **37(b)** there is a wavelength of 232 nm which is also attributed by $\pi\text{-}\pi^*$ transitions of conjugated eight membered rings. During the month of June 2011 it can be shown that the conjugated diene was giving rise to a new peak at 210 nm which proves that the longer the conjugated diene is stored the more it develops a tendency to polymerise. COD was stored in the refrigerator around 8 °C to prevent polymerization because during storage of gasoline it is stored in the car gasoline tank which is subjected to warm temperatures. This is an indication how fast the conjugated dienes can polymerise even at cooler temperatures. In figure **37(c)** it can be observed that PD 2010 October gave a wavelength at 254 nm, June 2011 gave a wavelength of 229 and 218 nm with a strong absorption peak and March 2011 gave a wavelength of 226 and 222 nm. It can be observed from the spectrum there have been a significant shift in the wavelength with the period. This shows that PD is one of the conjugated dienes that easily polymerise even when stored at cool and dry surroundings. In figure **37(d)** it can be observed that MBD gave a wavelength of 254 and 225 nm for all the periods, it proves that MBD is much more stable the only difference is in the absorption peak. This study of the uv-vis spectrum has illustrated how fast conjugated dienes can be polymerized and also the stability of the conjugated dienes during storage.

4.9. Interference studies

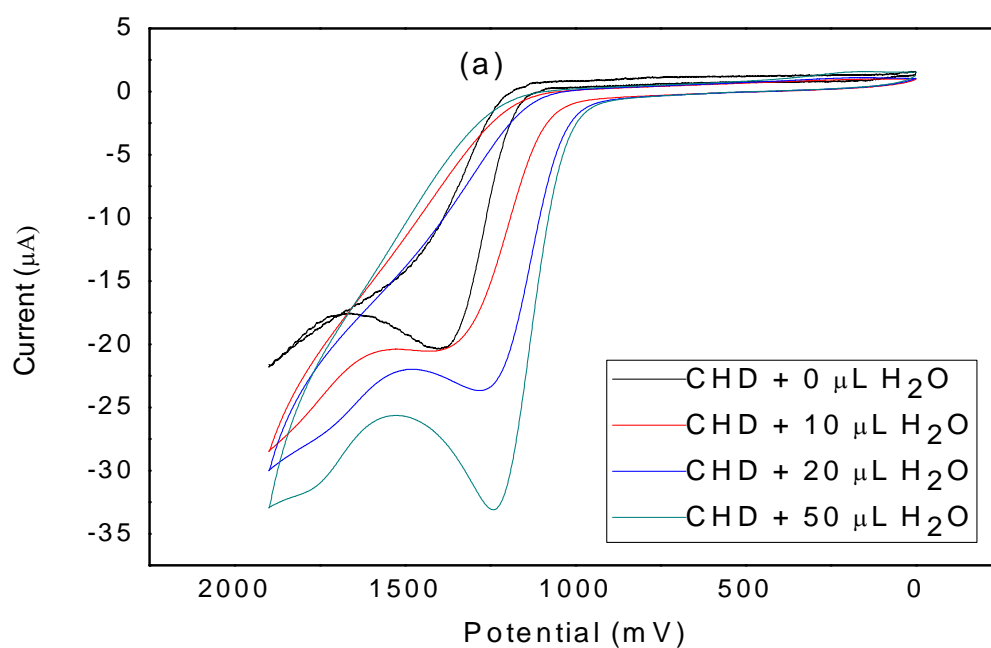


Figure 38: (a) CHD cyclic voltammogram of 0.0025 M of conjugated dienes in acetonitrile containing 0.1 M TBAP at room temperature for inference studies with water in increments of 10, 20 and 50 μL .

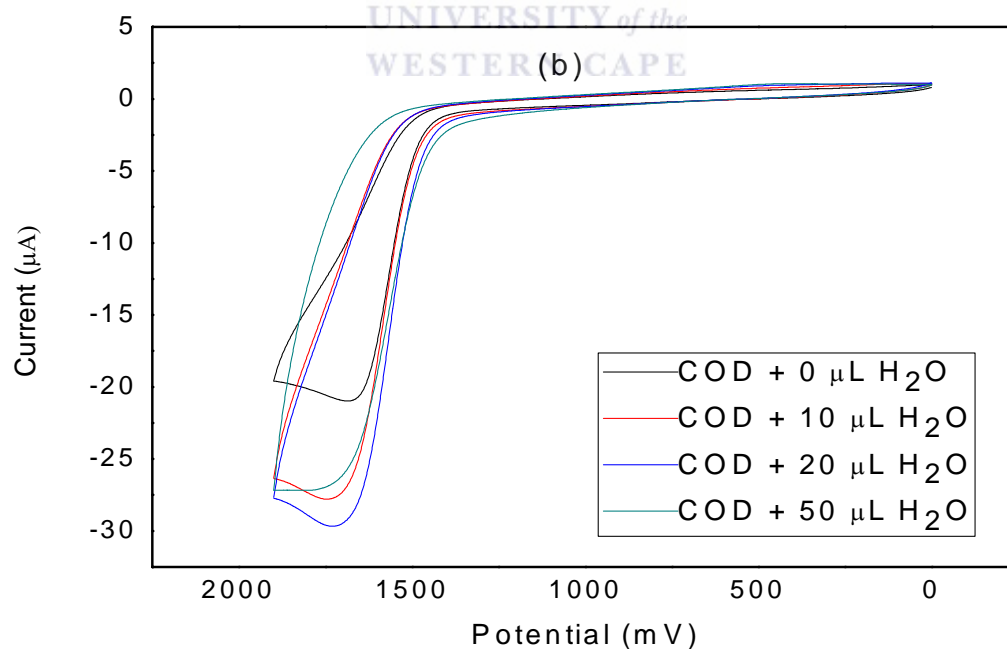


Figure 38: (b) COD cyclic voltammogram of 0.0025 M of conjugated dienes in acetonitrile containing 0.1 M TBAP at room temperature for inference studies with water in increments of 10, 20 and 50 μL .

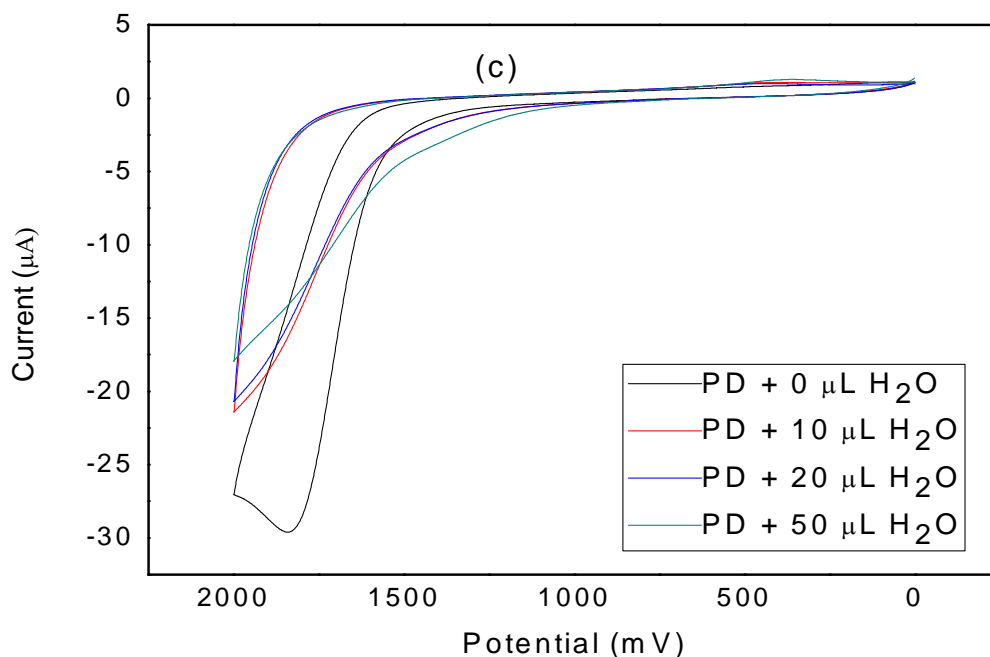


Figure 38: (c) cyclic voltammogram of 0.0025 M of conjugated dienes in acetonitrile containing 0.1 M TBAP at room temperature for inference studies with water in increments of 10, 20 and 50 μL .

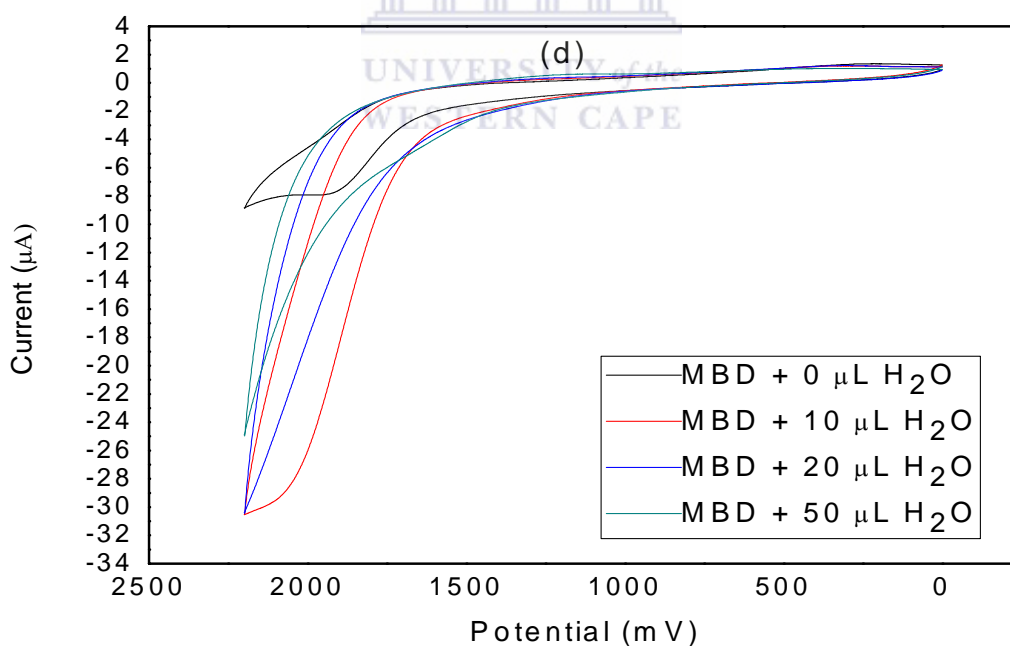


Figure 38: (d) cyclic voltammogram of 0.0025 M of conjugated dienes in acetonitrile containing 0.1 M TBAP at room temperature for inference studies with water in increments of 10, 20 and 50 μL . (a) CHD, (b) COD, (c) PD and (d) MBD.

Conjugated dienes have been identified as interfering factors in the stability of gasoline, in this study it was investigated what factors can cause conjugated dienes interfere with the stability of gasoline. It has been previously reported that ethanol can cause interference to an extent that gum can be formed in the gasoline tank. The experiments reported above were done at room temperature where there is availability of moisture, light, motions etc. water was used as an interfering factor since it could easily dissolve in acetonitrile and also determine how much of the water present in the electrolyte can affect the experiment or results. In figure **38(a)** the concentration of CHD was kept constant with the addition of water, as the water was added in the electrolyte it can be observed that there is an increase in the peak current and also a shift in the peak potential. In figure **38(b)** the concentration of COD was kept constant; it was observed as the volume of water increased in the electrolyte it caused fouling which resulted in the peak current of 50 μL of water to be less than other peaks. In Figure **38(c)** the concentration of PD was kept constant, it was observed as the water was added to the electrolyte there peak current of PD was decreasing with every addition. In figure **38(d)** as the concentration of MBD was kept constant it was observed that every addition of water resulted in the decrease in current and caused fouling at the Pt working electrode. The above results show clearly that water is indeed interference; during the experiment water can be represented by a form of moisture. The longer the experiment is exposed to the moisture it can result in incorrect readings and results.

4.10 Steady state amperometry

The organic sensor lifetime was evaluated from steady state amperometry experiment performed at -1404 mV, a Pt organic sensor was used as a working electrode in an air saturated acetonitrile containing 0.1 M TBAP and solution was stirred at 500 rpm.

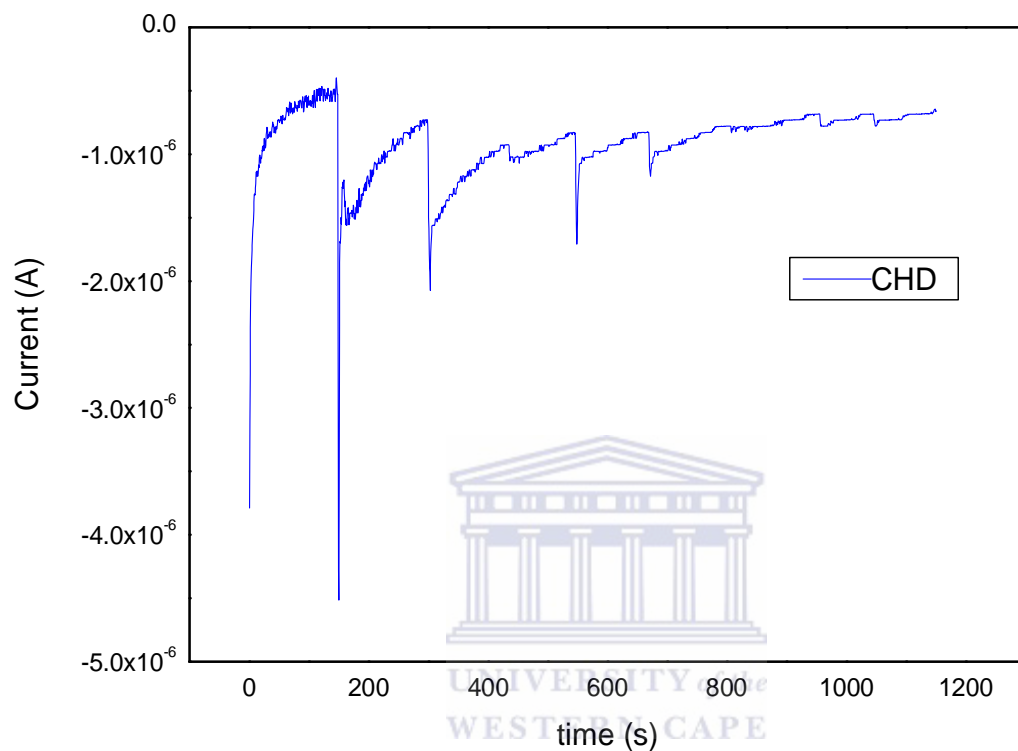


Figure 39: A plot of current versus time response of organic sensor of 1,3-cyclohexadiene in Acetonitrile containing 0.1 M TBAP.

In the above figure **39** it can be observed that in the first 160 s a response was observed when 0.00005 M CHD was added followed by a second addition of 0.00005 M CHD. The concentration was then increased to 0.0004 M, 0.0005 M and 0.001 M which resulted in a decrease in the response current. The concentration of the conjugated diene could not be kept constant due to the fact that there was no response observed when the third 0.00005 M CHD added. As the concentration was increased there was a response that was observed till the

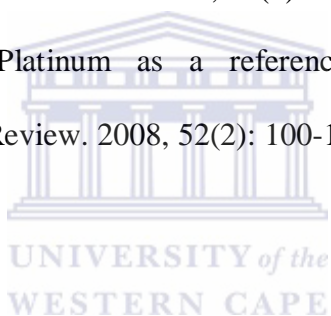
steady state was reached. The online application of a bare Pt electrode sensor has shown that there is an extra activity happening at the electrode surface which could not be observed during cyclic voltammetry experiment because the results were reproducible and there was linearity observed with variation of concentration. The product formed at the electrode surface does not dissolve in the electrolyte it is deposited at the electrode surface which is fouling, from the above figure **39** it is clearly illustrated.



4.11. References

- [1] Kang Y, Choi S, Gopatan A, Lee K, Kang H, Song YS. Tuning of morphology of Ag nanoparticles in the Ag/Polyaniline nanocomposite prepared by γ -ray irradiation. *Journal of Non-crystalline Solids*. 2006, 352(5): 463-468.
- [2] Song JH, Kim Y, Kim J. Synthesis of gold nanoparticles using N,N-dimethylacetamide: size shape control by reaction temperature. *Current Applied Physics*. 2006, 6(2): 216-218.
- [3] Bouazza S, Alonzo V, Hauchard D. Synthesis and characterization of Ag Nanoparticles–polyaniline composite powder material. *Synthetic Metals*. 2009, 159(15-16): 1612-1619.
- [4] Wang X, Wang X, Wu Y, Bao L, Wang H. Interfacial synthesis of polyaniline nanostructures induced by 5-Sulfosalicylic acid. *Materials Letters*. 2010, 64(17): 1865-1867.
- [5] Ansari R, Keivani MB. Polyaniline conducting electroactive polymers: Thermal and environmental stability studies. *Journal of Chemistry*. 2006, 3(13): 202-217.
- [6] Detsri E, Dubas ST. Interfacial polymerization of water-soluble polyaniline and its assembly using the layer-by-layer technique. *Journal of Metals, Materials and Minerals*. 2009, 19(1): 39-44.
- [7] Tang Y, Pan K, Wang X, Liu C, Luo S. Enhanced electrochemistry and electrocatalytic activities of polyaniline via co-doping with poly(Styrene sulfonate) and gold. *Journal of Electroanalytical Chemistry*. 2010, 639(1-2): 123-129.
- [8] Huang J.X, Kaner R.B. Polyaniline nanofibers: A unique polymer nanostructure for versatile applications. *Journal of American Chemistry Society*. 2004, 126(4): 851-855.
- [9] Sarma T.K, Chattopadhyay A. Nanoparticles of silver loaded on polyaniline and nylon *Journal of Physical Chemistry*. 2004, 108(1): 7482-7487.

- [10] Pillalamarri SK, Blum FD, Tokuhiko AT, Bertino MF. One-pot synthesis of polyaniline-metal nanocomposites. *Chemistry of Materials*. 2005, 17(3): 5941-5944.
- [11] Muchindua M, Waryo T, Arotiba O, Kazimierska E, Morrin A, Killard AJ, Malcolm R. Smyth MR, Jahed N, Kgarebe B, Baker PGL, Iwuoha EI. Electrochemical nitrite nanosensor developed with amine- and sulphate-functionalised polystyrene latex beads self-assembled on polyaniline. *Electrochimica Acta*. 2010, 55(14): 4274–4280.
- [12] Ganne RR, Carl A, Lisensky GC. Ferrocene as an internal standard for electrochemical measurements. *Inorganic Chemistry*. 1980, 19(9): 2854-2855.
- [13] Pitts MR. Safer, faster and cleaner reactions using encapsulated metal catalysts and microwave heating. *Platinum Metal Review*. 2008, 52(2): 64-70.
- [14] Kasem K.K, Jones S. Platinum as a reference electrode in electrochemical measurements. *Platinum Metals Review*. 2008, 52(2): 100-106.



CHAPTER FIVE

**CONCLUSIONS AND
RECOMMENDATIONS**



UNIVERSITY *of the*
WESTERN CAPE

5.1. Conclusions

This thesis opens a whole new approach to the study of conjugated dienes with interesting findings on the electrochemical behaviour which is far more different from findings reported in literature, this give basic useful information which can be applied for the study of other conjugated dienes. Electroactive films of polyaniline-polystyrene sulfonic acid composite (PANi-PSSA) electrodeposited or drop-coated on the GCE, with and without gold nanoparticles, were also tested for the same application. The PANi-PSSA and PANi-PSSA/AuNP composites, prepared by the interfacial polymerization method and characterized by cyclic voltammetry, HRTEM, and UV-vis spectroscopy, were found to be of nanofibril structure, and the spherical gold nanoparticles were dispersed uniformly. However, the dienes exhibited no redox peaks between -1.0 V and +1.5 V, beyond which PANi would otherwise be overoxidized and loss its electroactivity. Furthermore, the drop-coated films did not give reproducible and steady background voltammogram as a result of which they could not be tested further for electrochemical sensing of the dienes. This proved that beyond a doubt that PANi and its composites could not be applicable for this study due to no redox peaks exhibited at potentials where dienes are more active. The main focus of the study is on the development of an electrochemical sensor in organic medium, interference from the liquid junction in Ag/AgCl as reference electrode was avoided by replacing with pseudo platinum wire reference electrode. Ferrocene was used as an internal reference, due to the extensive knowledge on its electrochemical behaviour, it is found that oxidation of ferrocene in acetonitrile is quasi-reversible independent of the nature of working electrode used. Ferrocene was used to report the real peak of the analyte by subtracting the peak of ferrocene. First, preliminary studies were carried out to see if these dienes were electroactive at glassy carbon electrode (GCE), platinum (Pt), boron doped diamond (BDD), gold (Au), and titanium (Ti) electrodes in tetrabutylammonium perchlorate/ acetonitrile solution. The

dienes also did not exhibit any electroactivity at BDD and Ti electrodes even though very wide polarization windows were used -1.5V to 2.0 V. For the Au electrode, which was polarized between -2.5 V to 2.0 V, the dienes exhibited multiple anodic ($E_{pa} = -829$ mV, 265 mV, 1610 mV) and cathodic peaks ($E_{pc} = 867$ mV, 1213 mV) which were, however, non-reducible and were not pursued further. For the GCE, single oxidation peaks were observed at 1500 mV, 1200 mV, 1100 mV, and 1400 mV in the presence of MBD, PD, CHD and COD, respectively. The available studies reported that conjugated dienes give reduction peak no study has reported oxidation peaks. However, since the CVs were not reproducible, possibly as a result of fouling processes, the studies with this electrode involved repeated polishing between each cyclic voltammogram. Reproducible CVs were observed only at the platinum electrode without any polishing after each cycle; platinum electrode successfully minimized the effect of fouling and gave better results as compared to GCE. Both Pt and GCE electrode were used for the investigation of the electrode kinetics and voltammetric-amperometry of MBD, PD, CHD and COD which was successfully studied. Water was used for interference studies which resulted in an increase in the peak current. The UV-vis spectrum was done on the conjugated dienes which proved some degrade on standing where a second peak starts to emerge with time. That kind of behaviour was observed with trans-1,3-pentadiene and 1,3-cyclooctadiene which proves that there conjugated dienes are polymerized in the gasoline tank of cars. This thesis has provided useful information that will contribute in the minimization of air pollution, lifetime of engines in cars and better quality of gasoline. Will be of great benefit for future studies because the kinetics have been well researched and different electrode have been exploit.

5.2. Recommendation

- This thesis has bridged the gap between synthetic chemistry and electrochemistry when it comes to the petrochemical industry and opens a whole new approach on the study of conjugated dienes with novelty on the electrochemical behaviour which is far more different from findings reported in literature.
- Sensor surface can be Pt/AuNP, Pt/PANi, Pt/Over Oxidized PANi, Pt/PANi/AuNp and Pt/over oxidized PANi/AuNP to optimise the detection of conjugated dienes in organic medium.
- Electrochemical impedance spectroscopy can be used to study the solution resistance by using ferrocene as a probe due to the electrochemistry of conjugated dienes being irreversible.

